

FIGURE 3.4.1; FINITE ELEMENT MODEL OF MPC-24

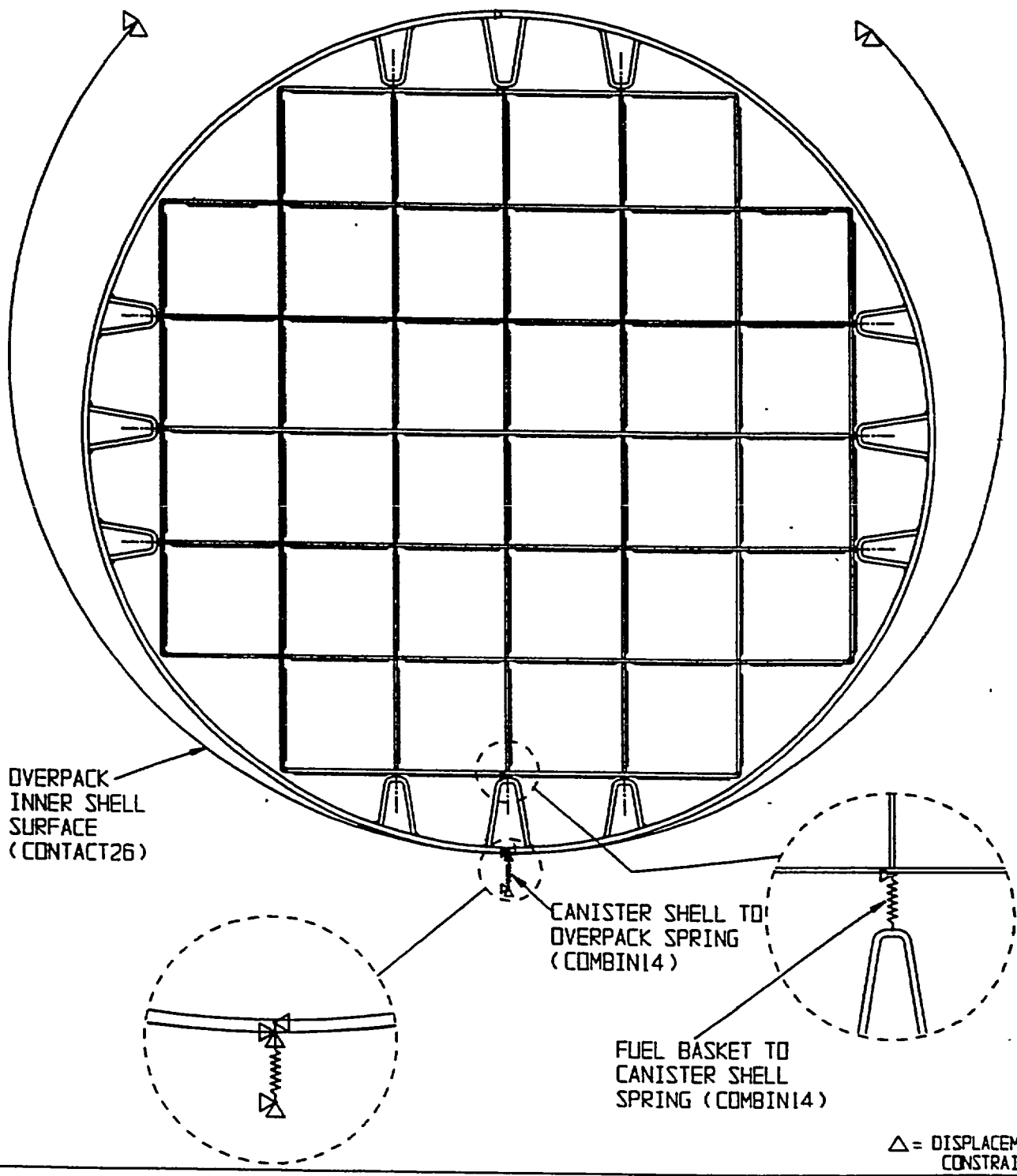


FIGURE 3.4.2; FINITE ELEMENT MODEL OF MPC-32

(0 DEGREE DROP MODEL)

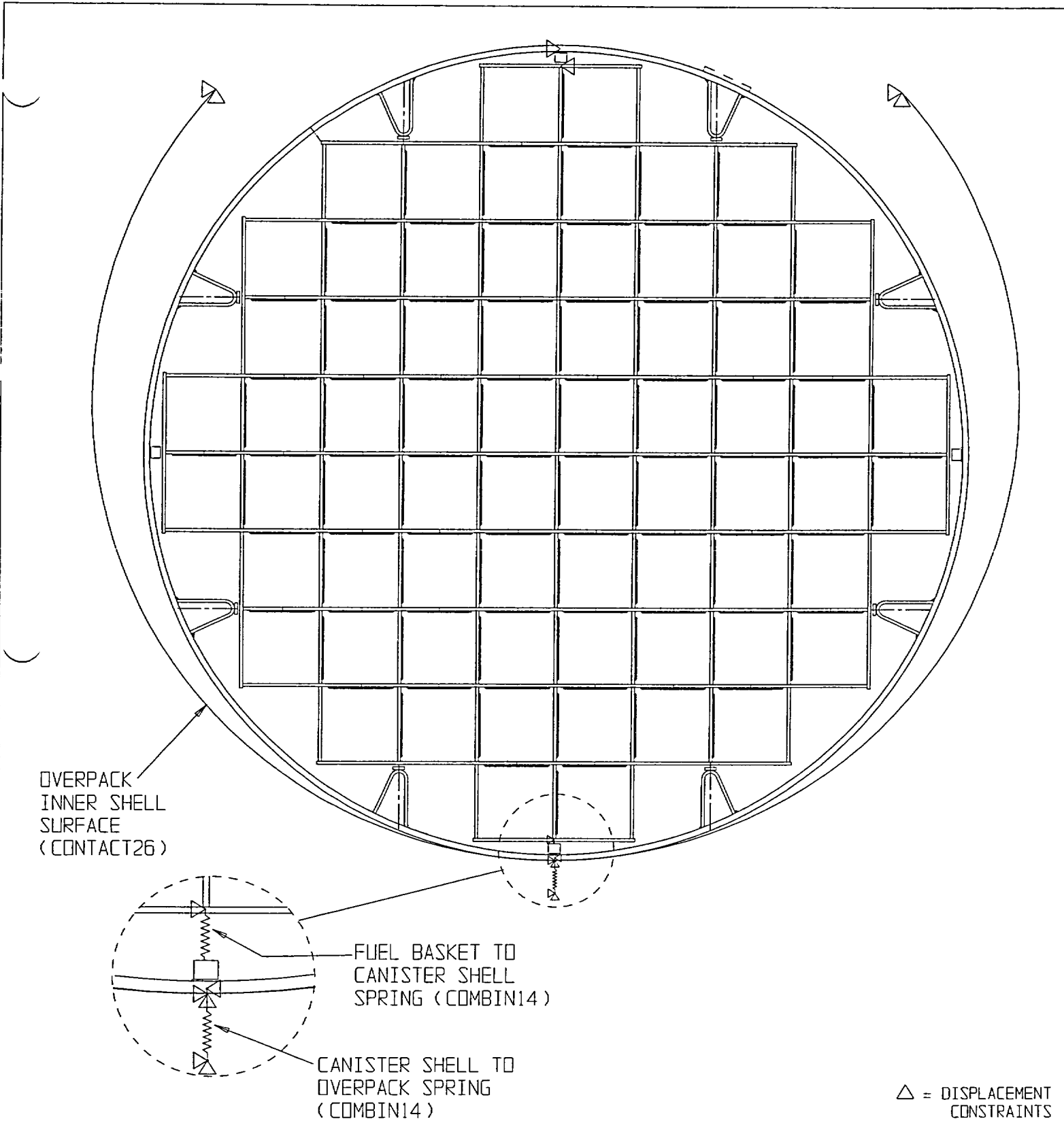


FIGURE 3.4.3; FINITE ELEMENT MODEL OF MPC-68

(0 DEGREE DROP MODEL)

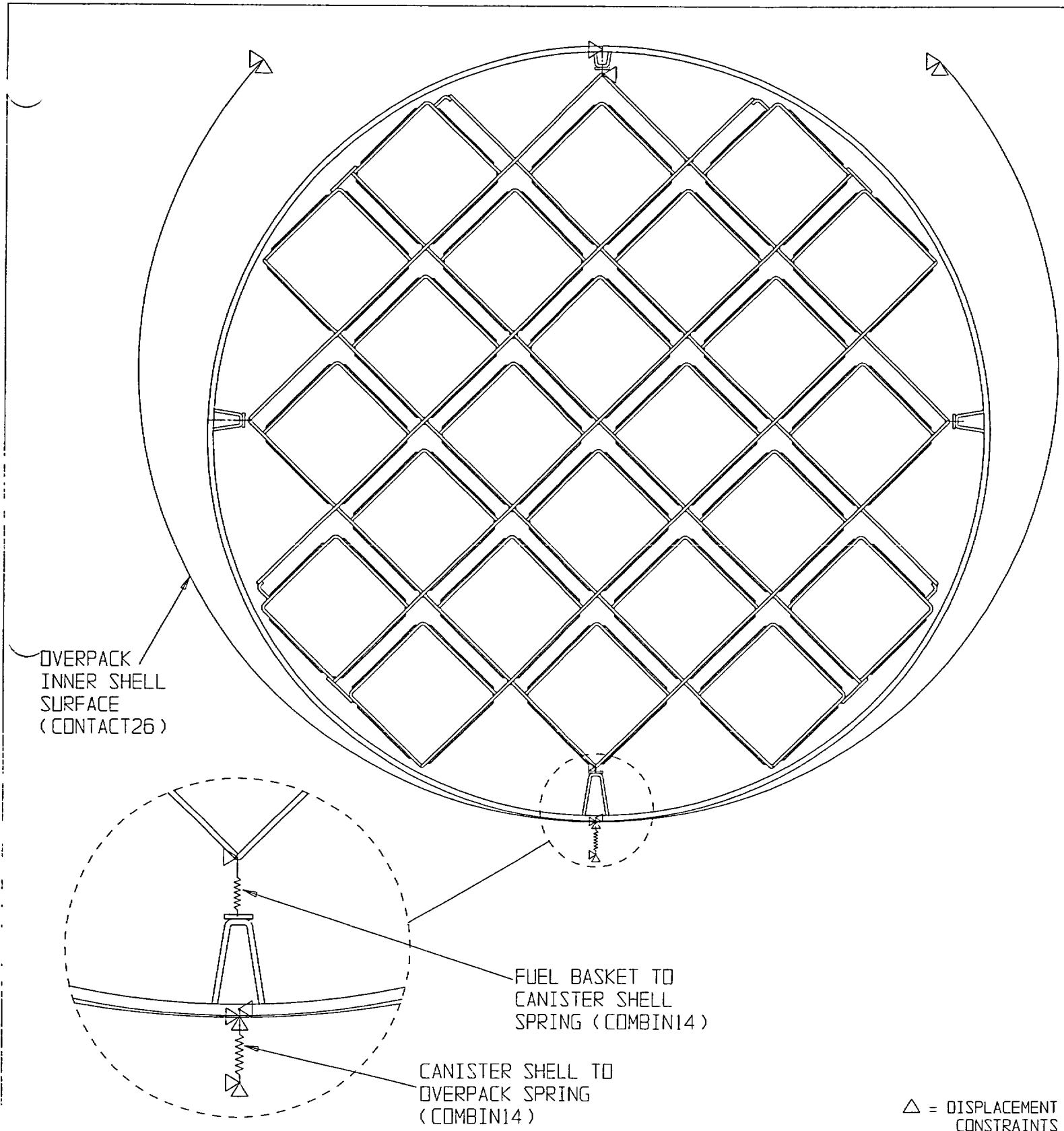


FIGURE 3.4.4; FINITE ELEMENT MODEL OF MPC-24

(45 DEGREE DROP MODEL)

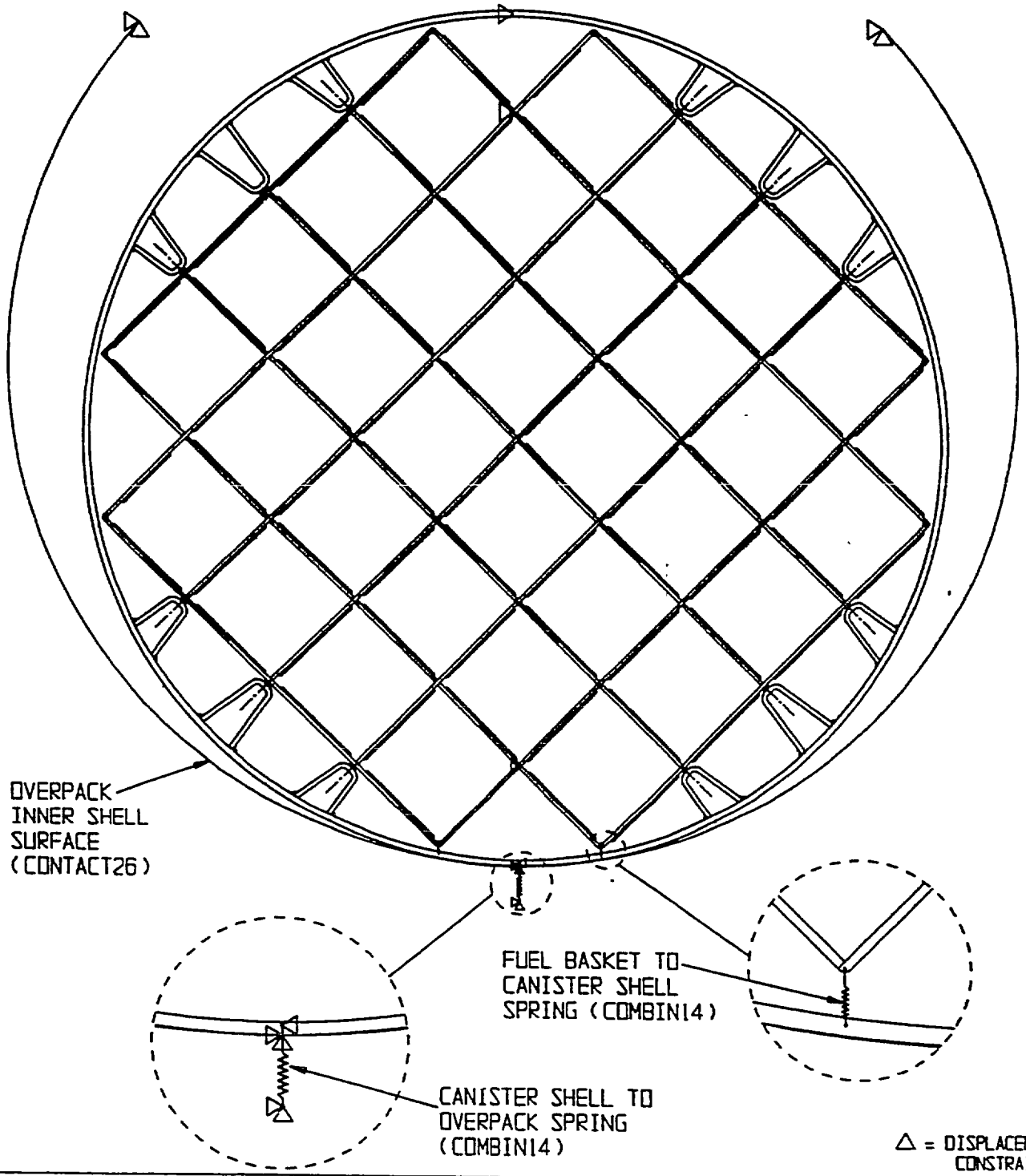


FIGURE 3.4.5; FINITE ELEMENT MODEL OF MPC-32

(45 DEGREE DROP MODEL)

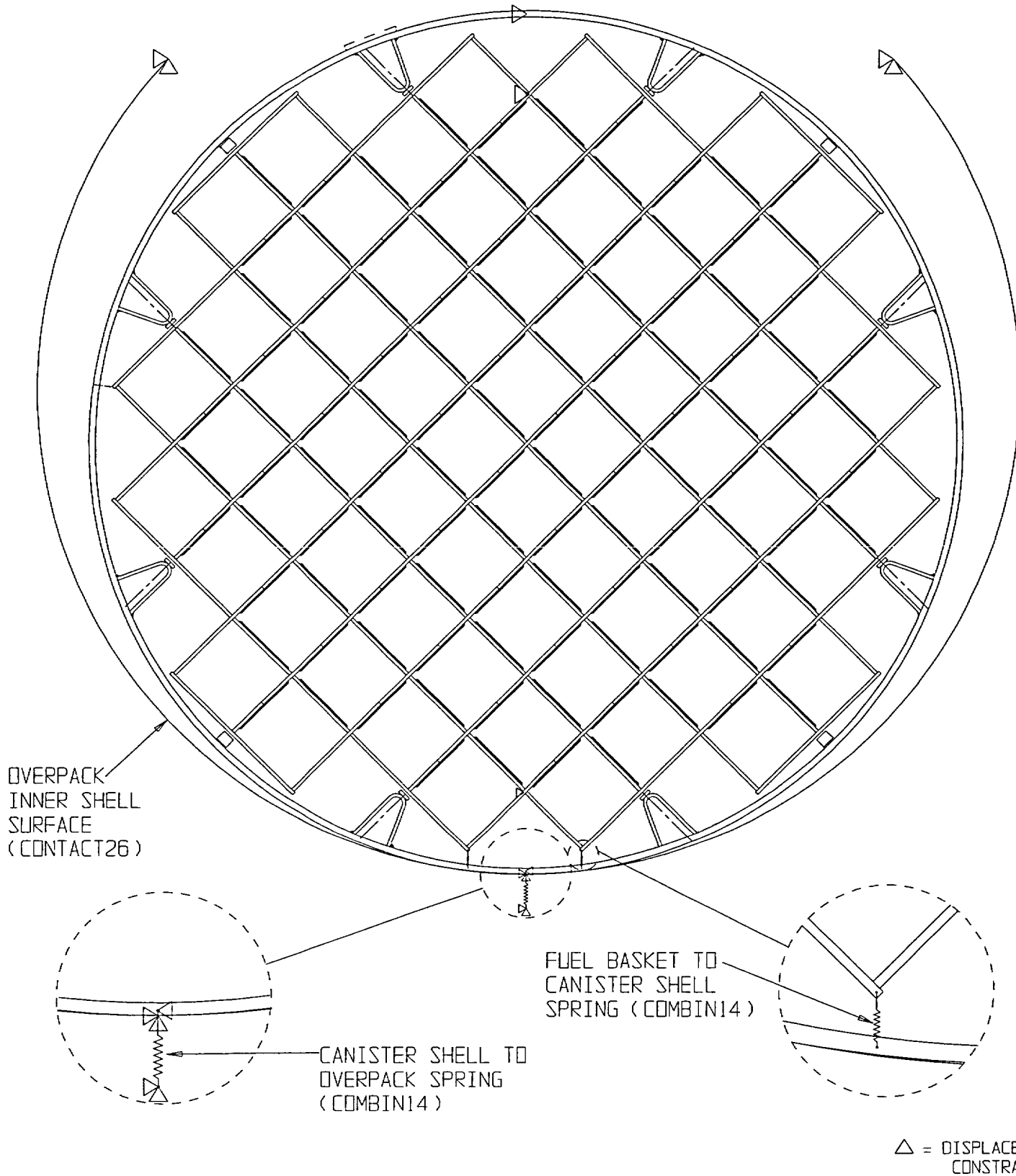


FIGURE 3.4.6; FINITE ELEMENT MODEL OF MPC-68

(45 DEGREE DROP MODEL)

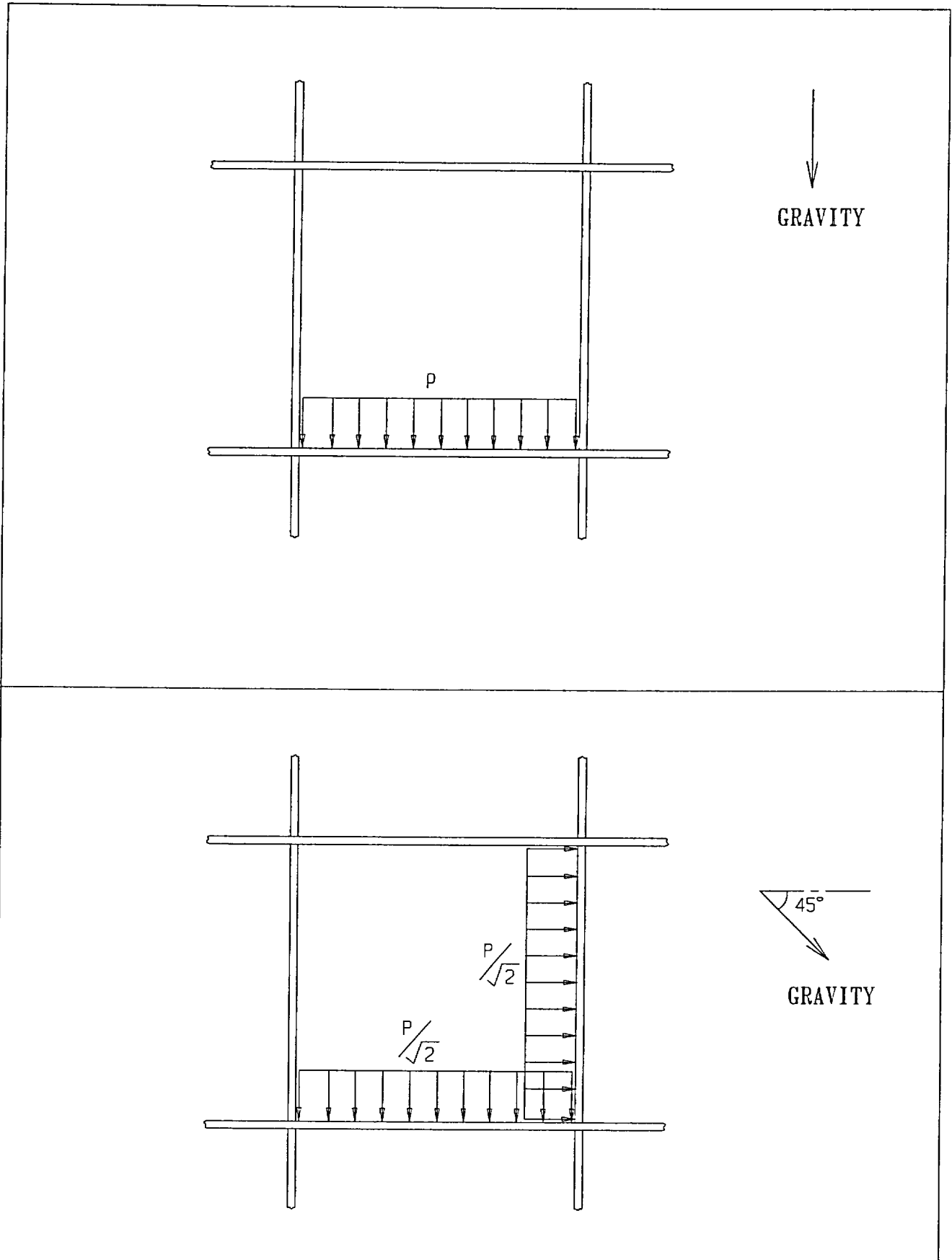


FIGURE 3.4.7; DETAIL OF FUEL ASSEMBLY PRESSURE  
LOAD ON MPC BASKET

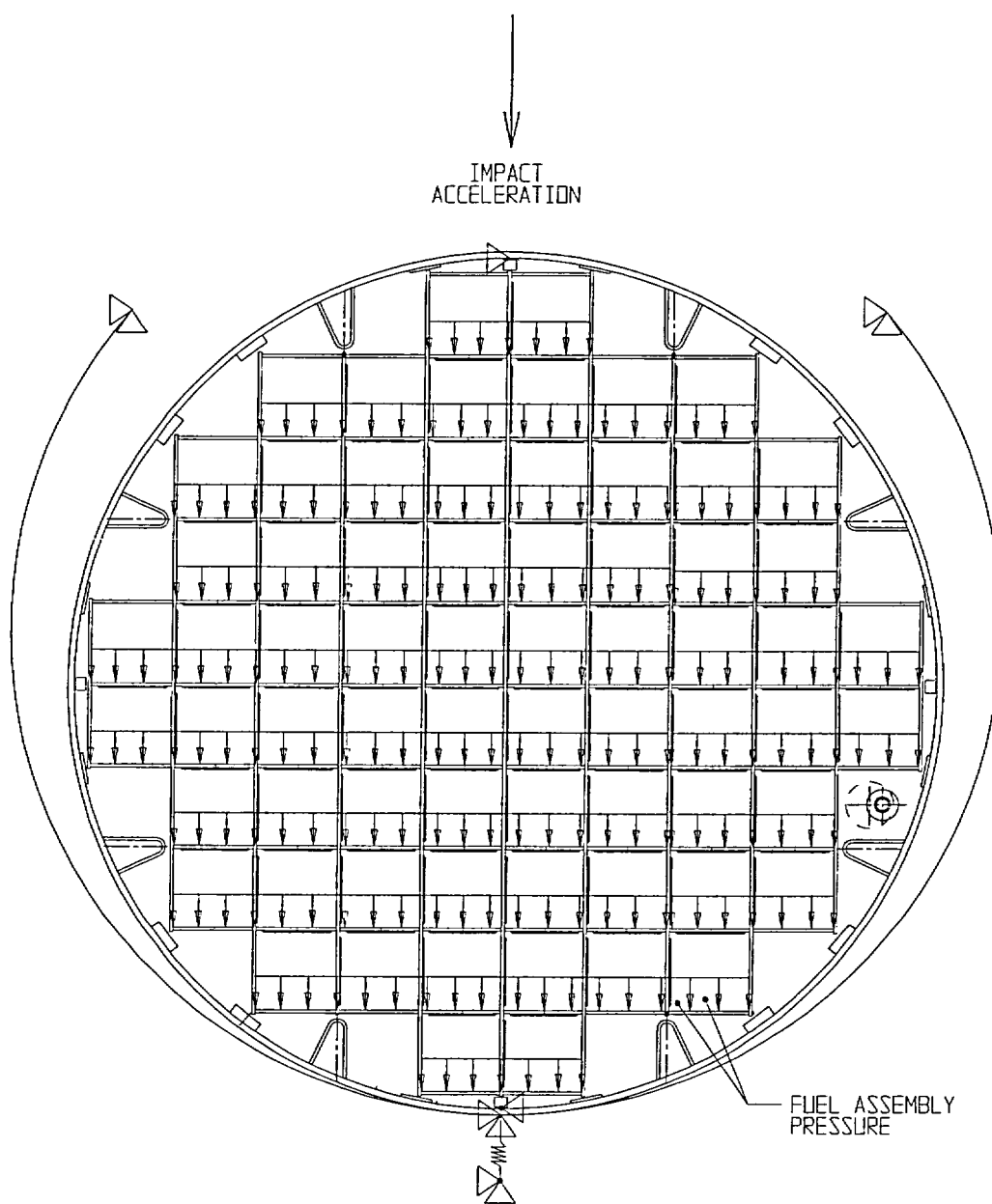


FIGURE 3.4.8; 0 DEGREE SIDE DROP OF MPC



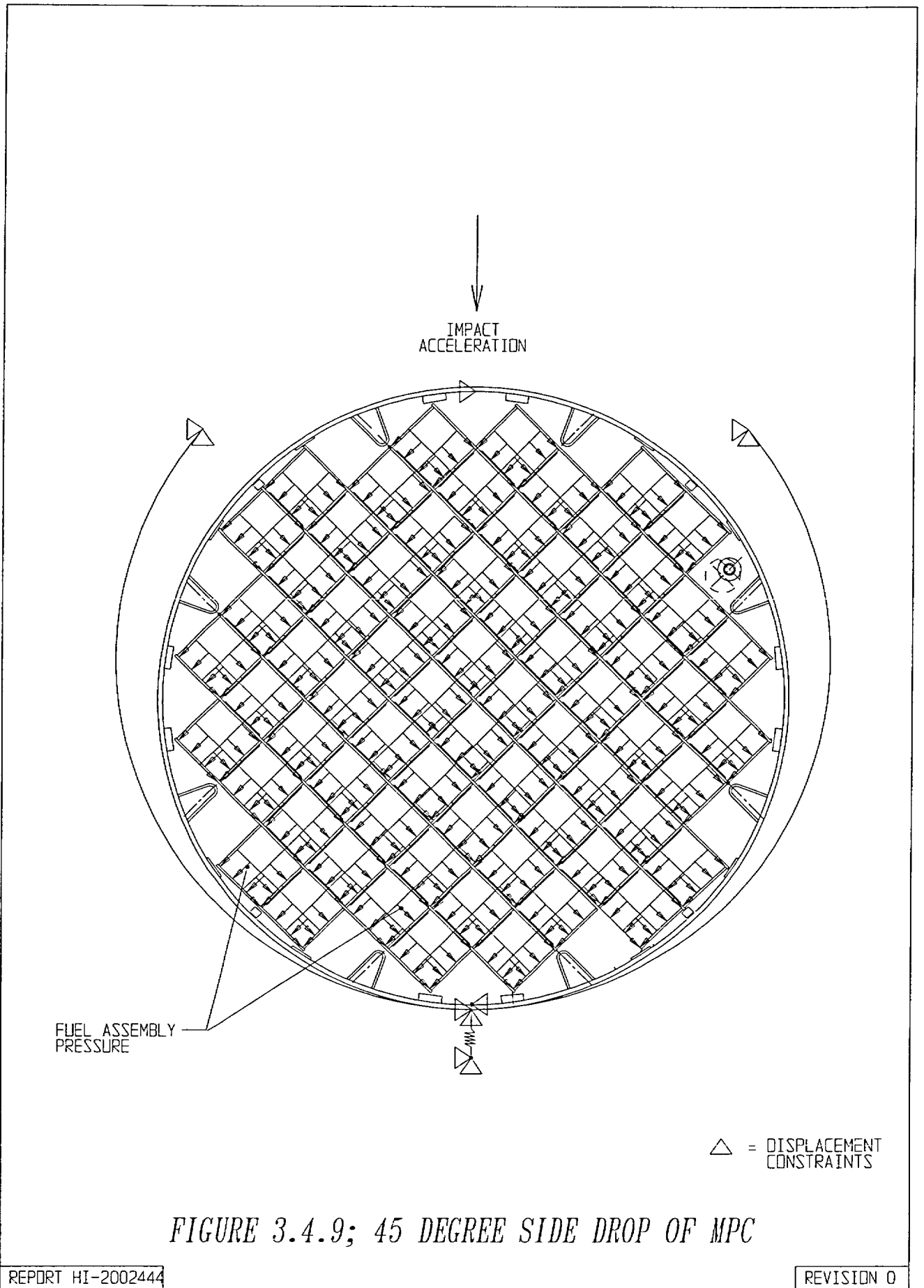
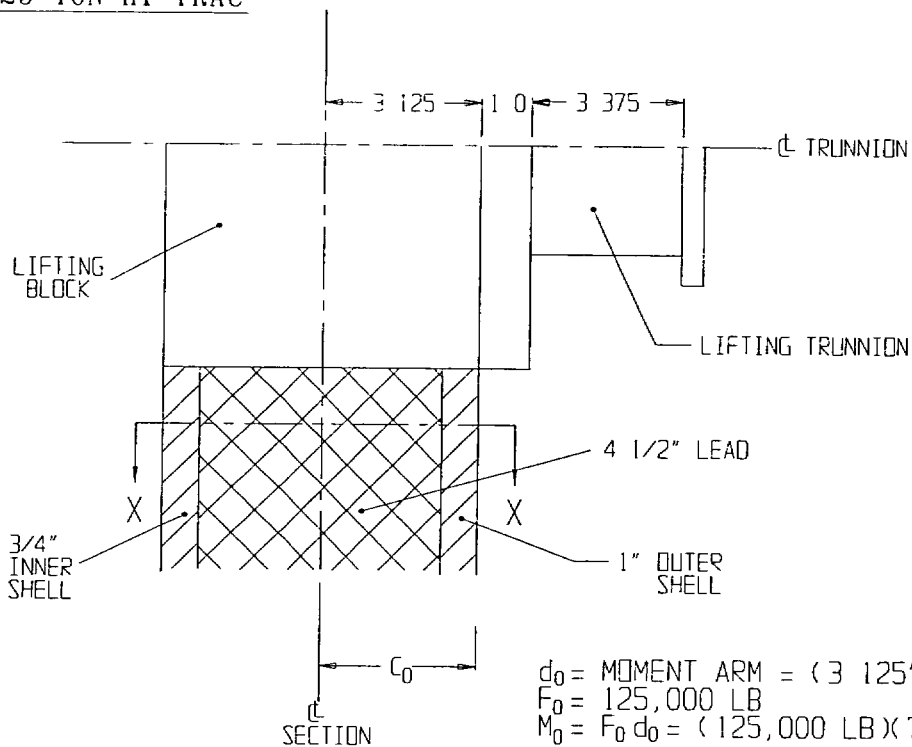


FIGURE 3.4.9; 45 DEGREE SIDE DROP OF MPC

125 TON HI-TRAC

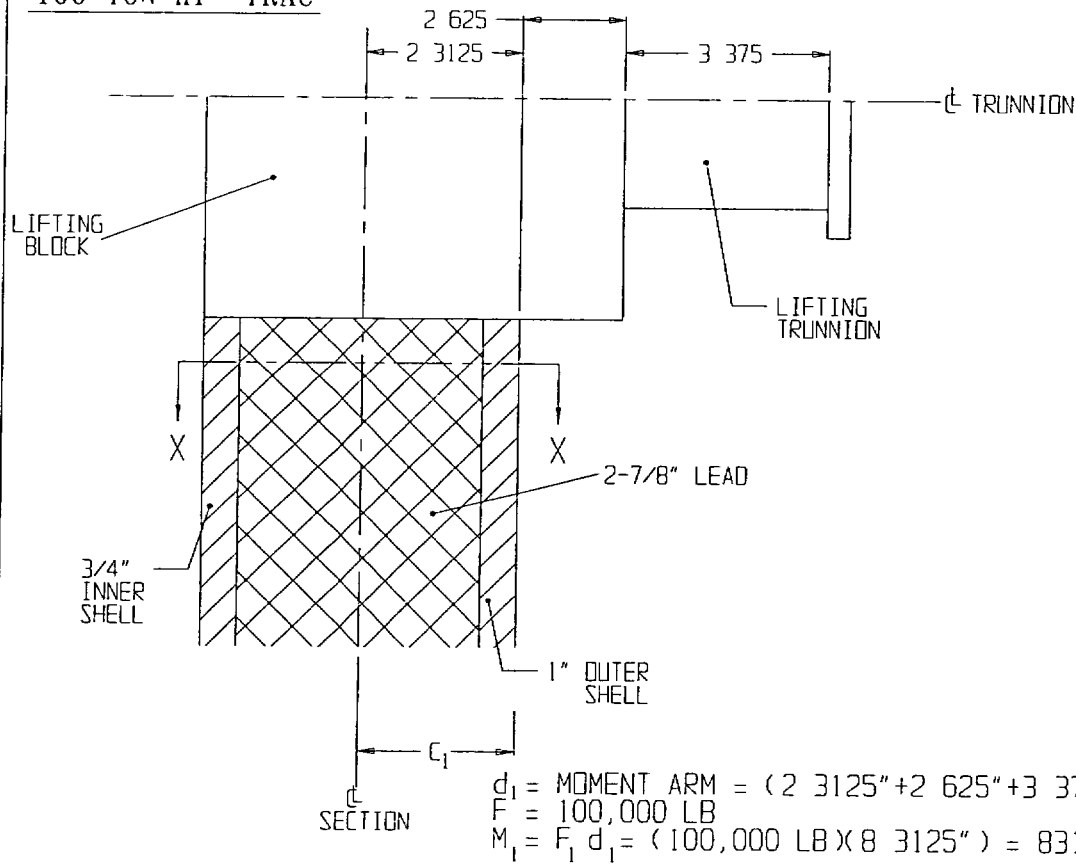


$$d_0 = \text{MOMENT ARM} = (3.125" + 1.0" + 3.375") = 7.5"$$

$$F_0 = 125,000 \text{ LB}$$

$$M_0 = F_0 d_0 = (125,000 \text{ LB} \times 7.5") = 937,500 \text{ LB. IN}$$

100 TON HI-TRAC



$$d_1 = \text{MOMENT ARM} = (2.3125" + 2.625" + 3.375") = 8.3125"$$

$$F_1 = 100,000 \text{ LB}$$

$$M_1 = F_1 d_1 = (100,000 \text{ LB} \times 8.3125") = 831,250 \text{ LB IN}$$

FIGURE 3.4.10; COMPARISON OF 125 TON AND 100 TON HI-TRAC LIFTING TRUNNION CONNECTION

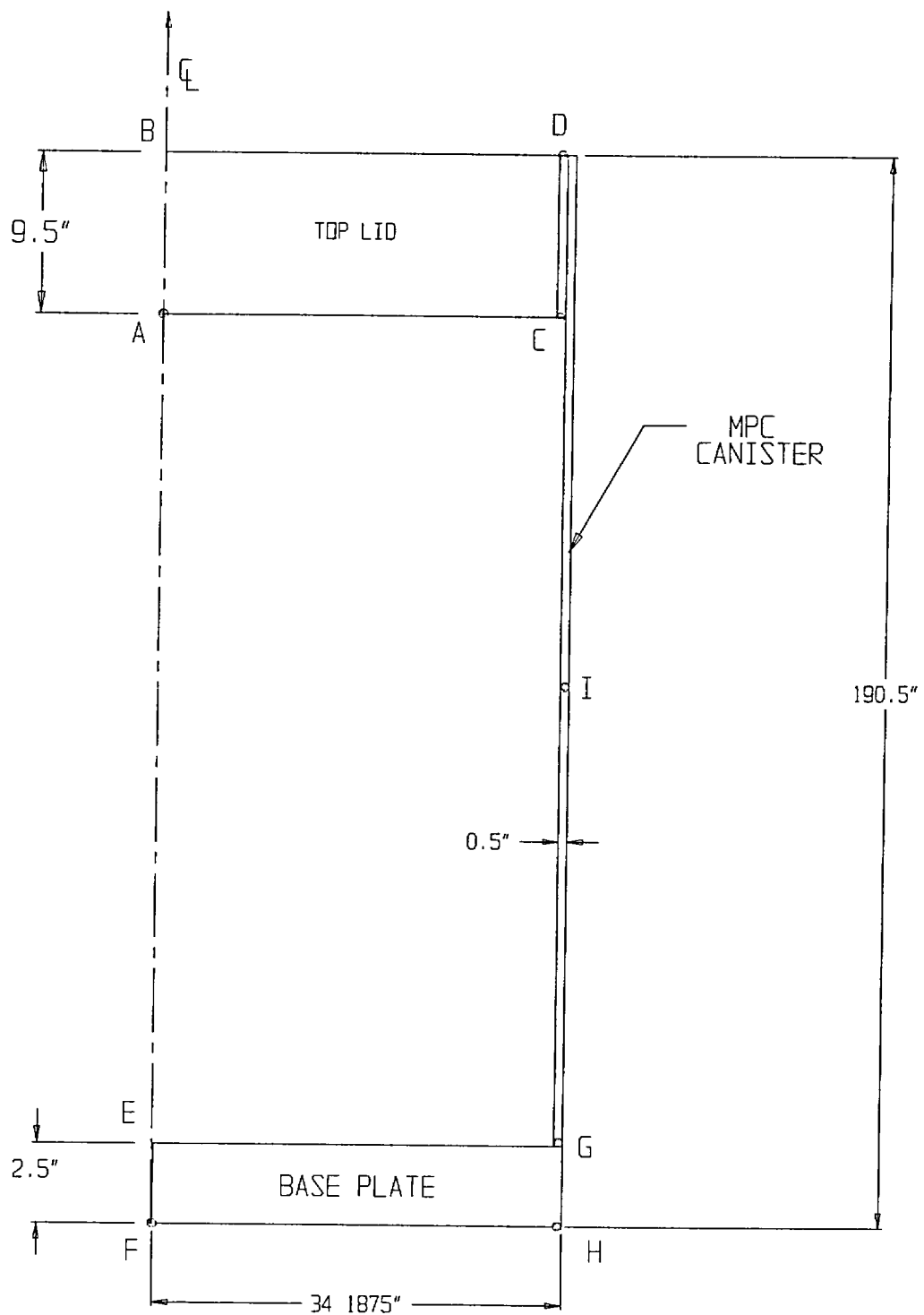


FIGURE 3.4.11 CONFINEMENT BOUNDARY MODEL SHOWING TEMPERATURE DATA POINTS

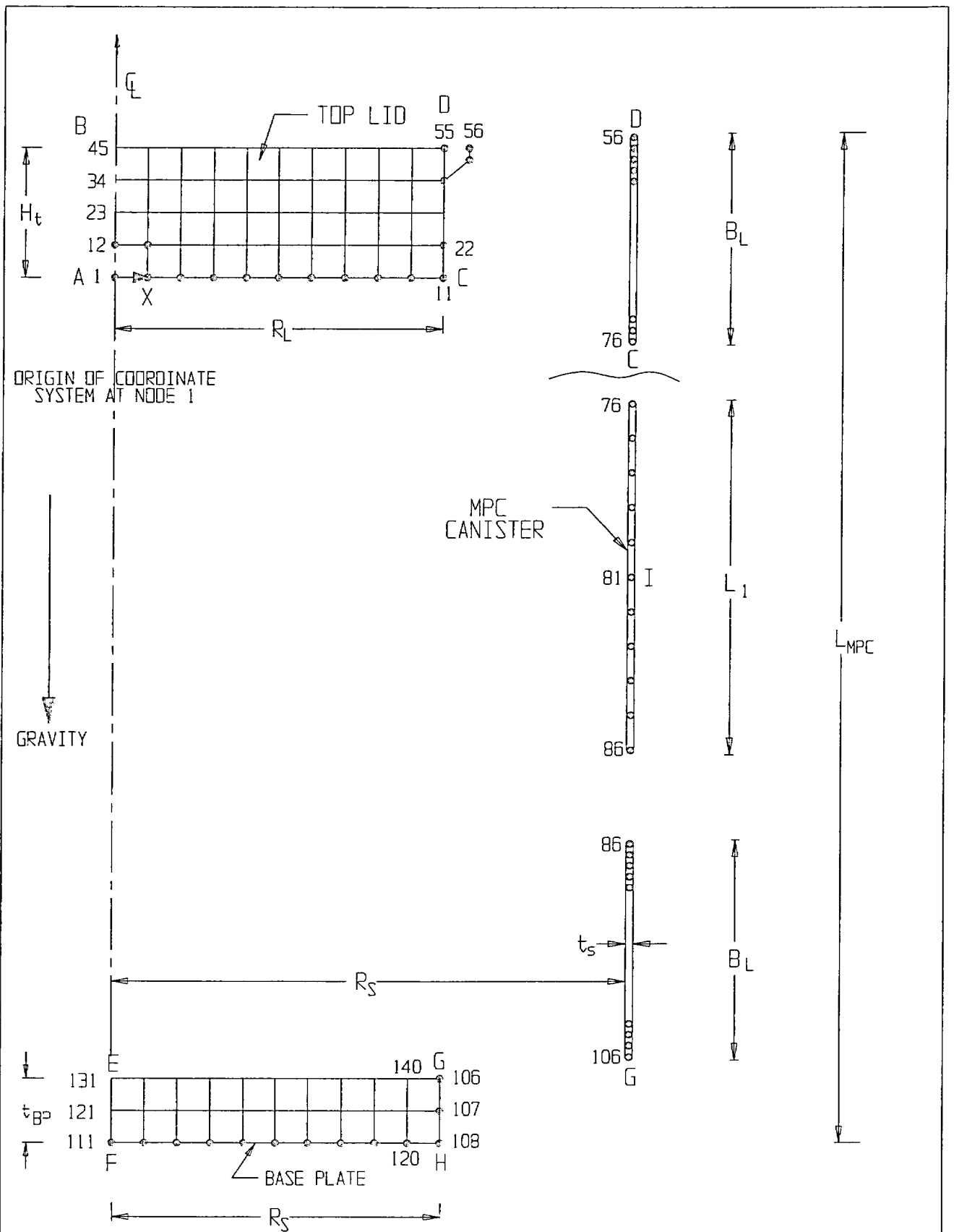


FIGURE 3.4.12 MPC - CONFINEMENT BOUNDARY  
FINITE ELEMENT GRID (EXPLODED VIEW)

HISTORM DEFORMABLE TIP OVER 1.5 RAD/SE  
STEP 80 TIME = 7.9997852E-002  
MAX\_VONMISES

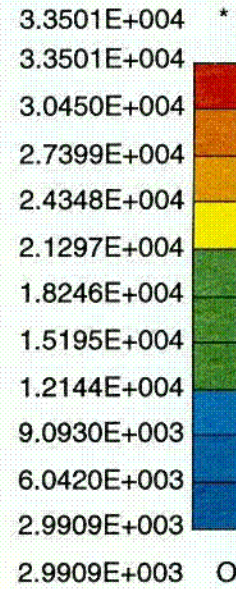
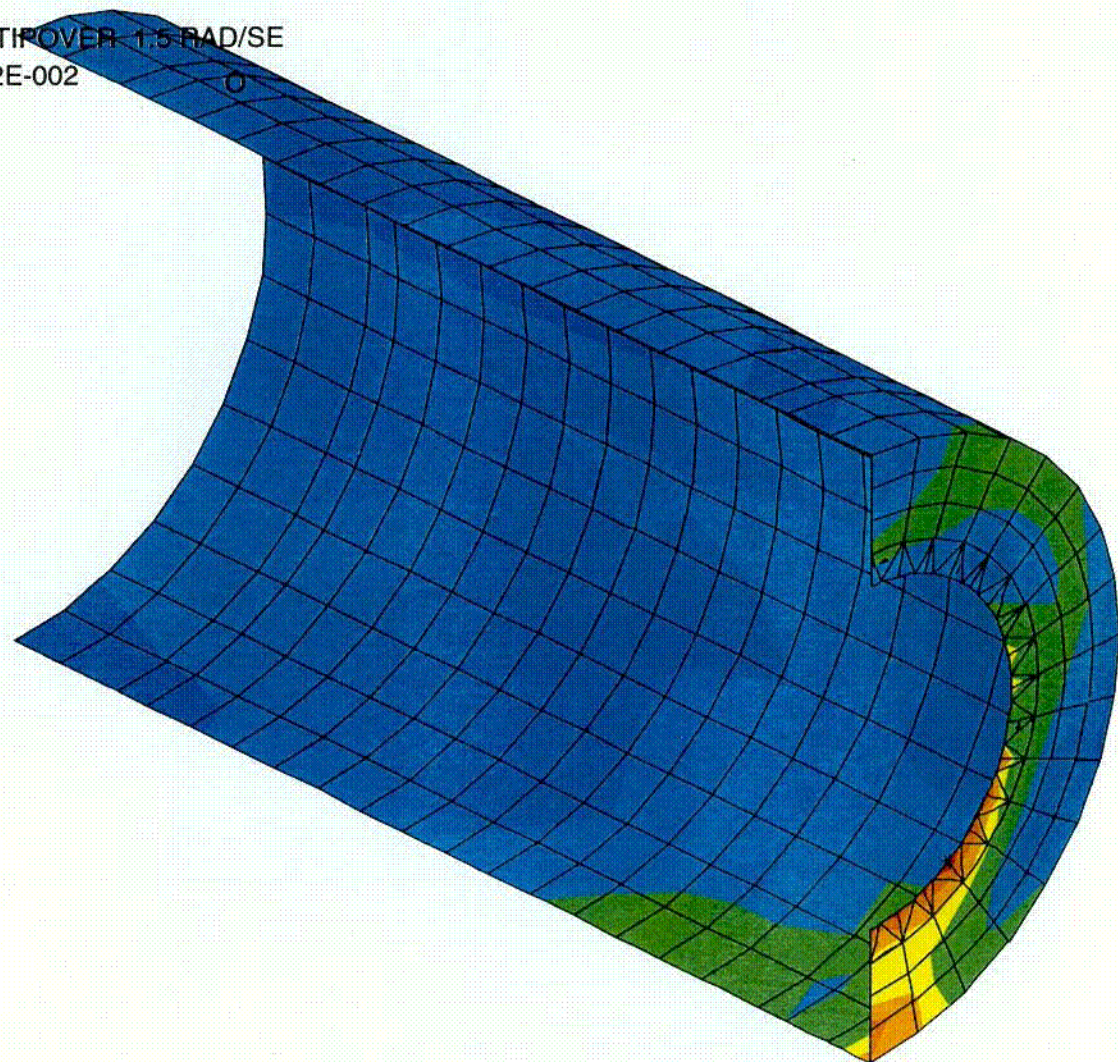
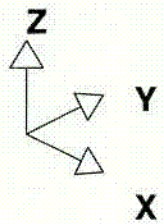
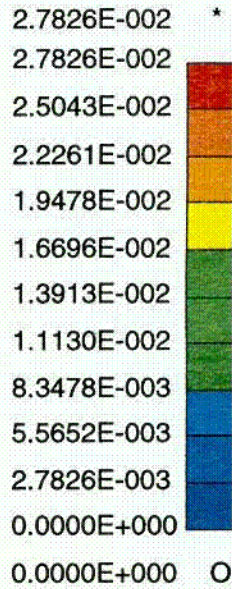
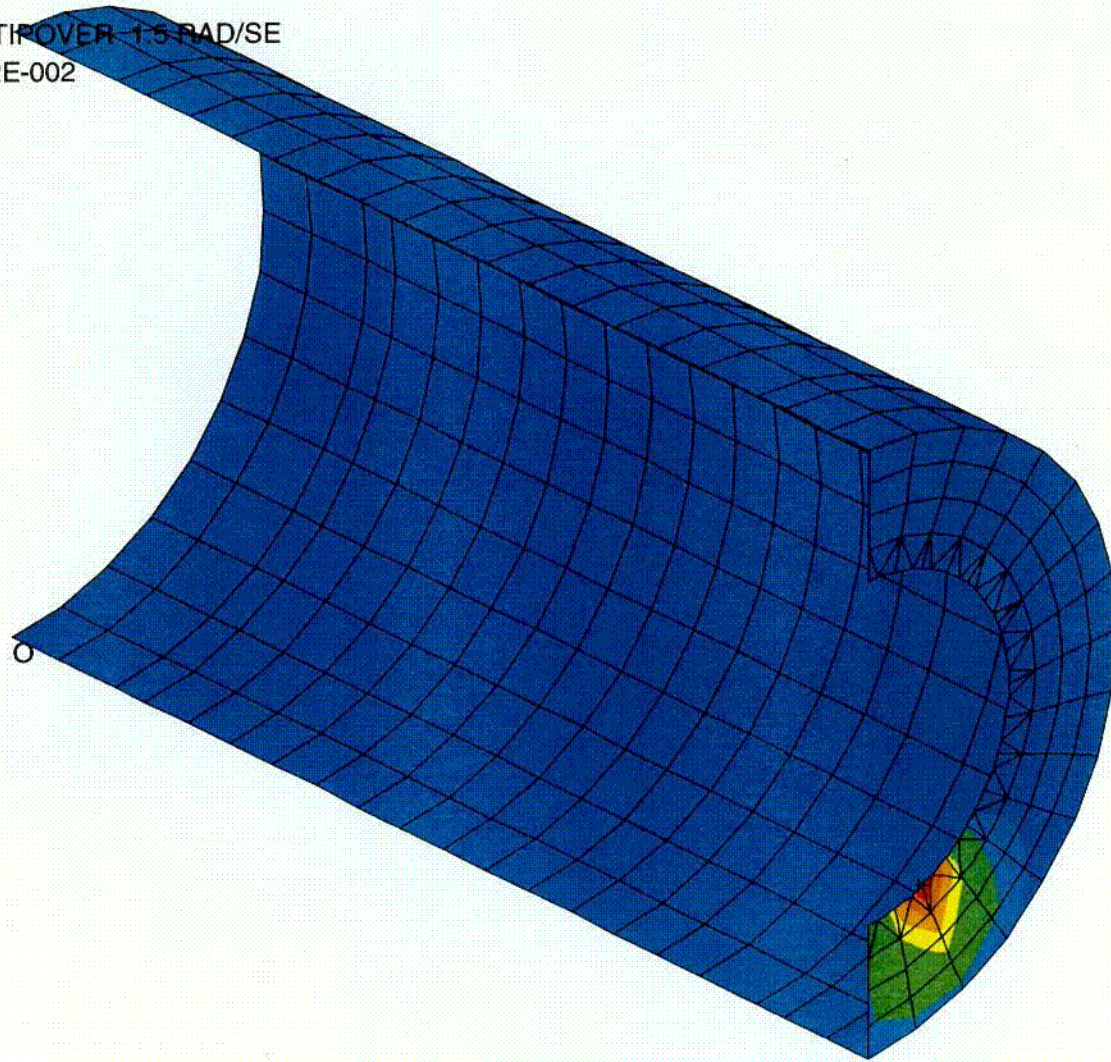
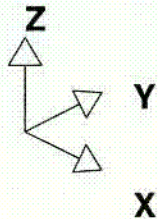


Fig. 3.4.13 Von Mises Stress Outer Shell



HISTORM DEFORMABLE TIPOVER 1.5 RAD/SE  
STEP 80 TIME = 7.9997852E-002  
PSTN(TOP)



HI-2002444  
HI-STORM FSAR

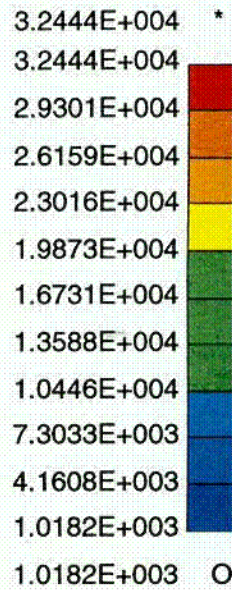
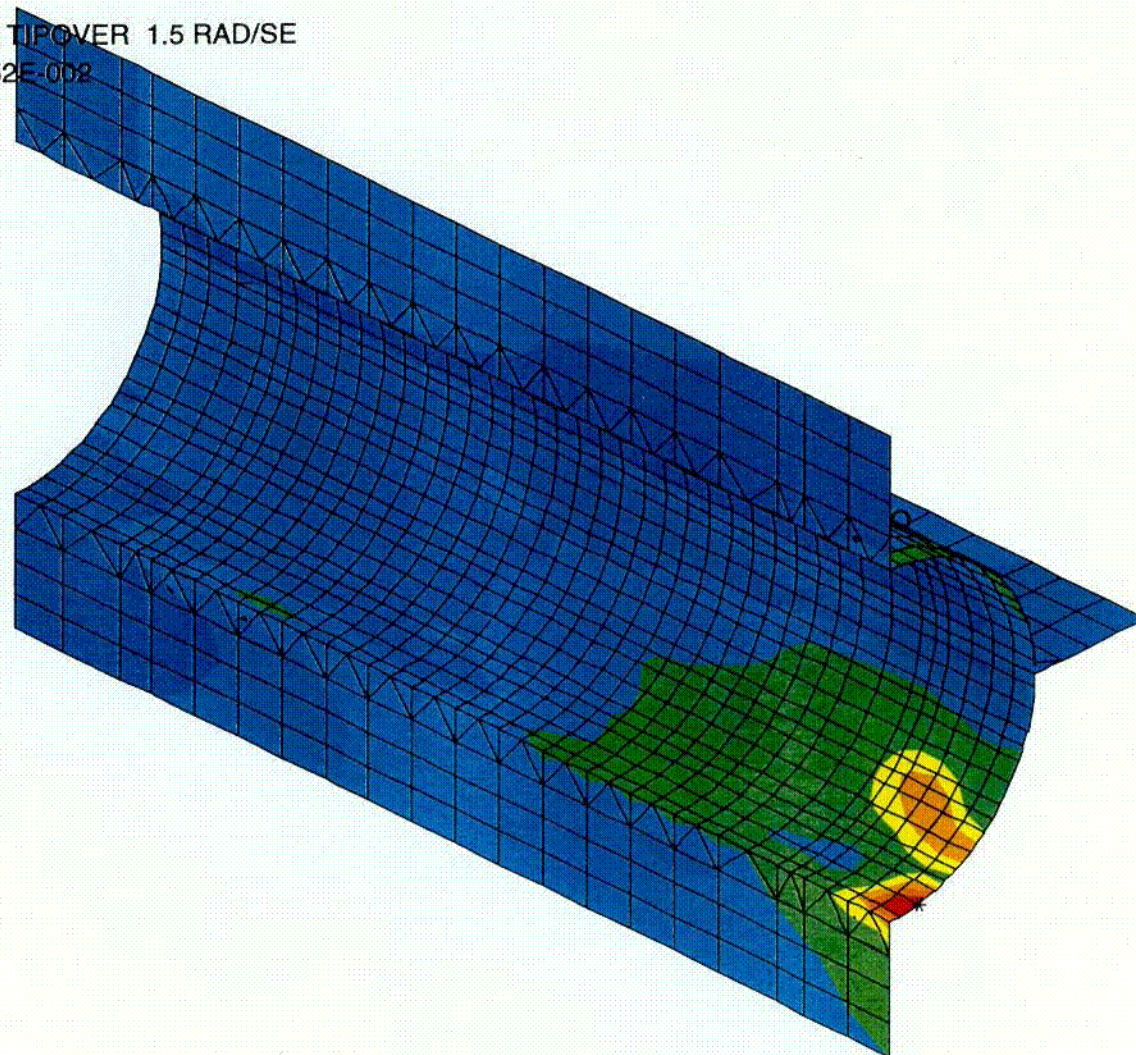
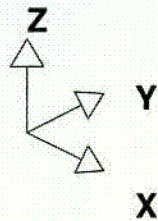
Fig. 3.4.14 Plastic Strain Outer Shell

Rev. 0

C02



HISTORM DEFORMABLE TIPOVER 1.5 RAD/SE  
STEP 80 TIME = 7.9997852E-002  
MAX\_VONMISES



HI-2002444

Fig. 34.15 Von Mises Stress - Inner Shell

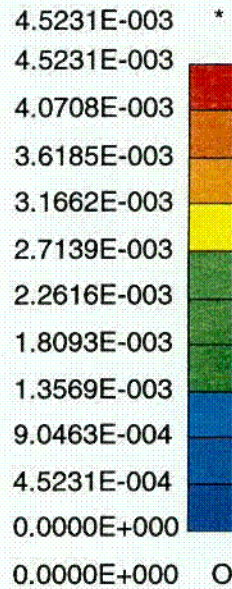
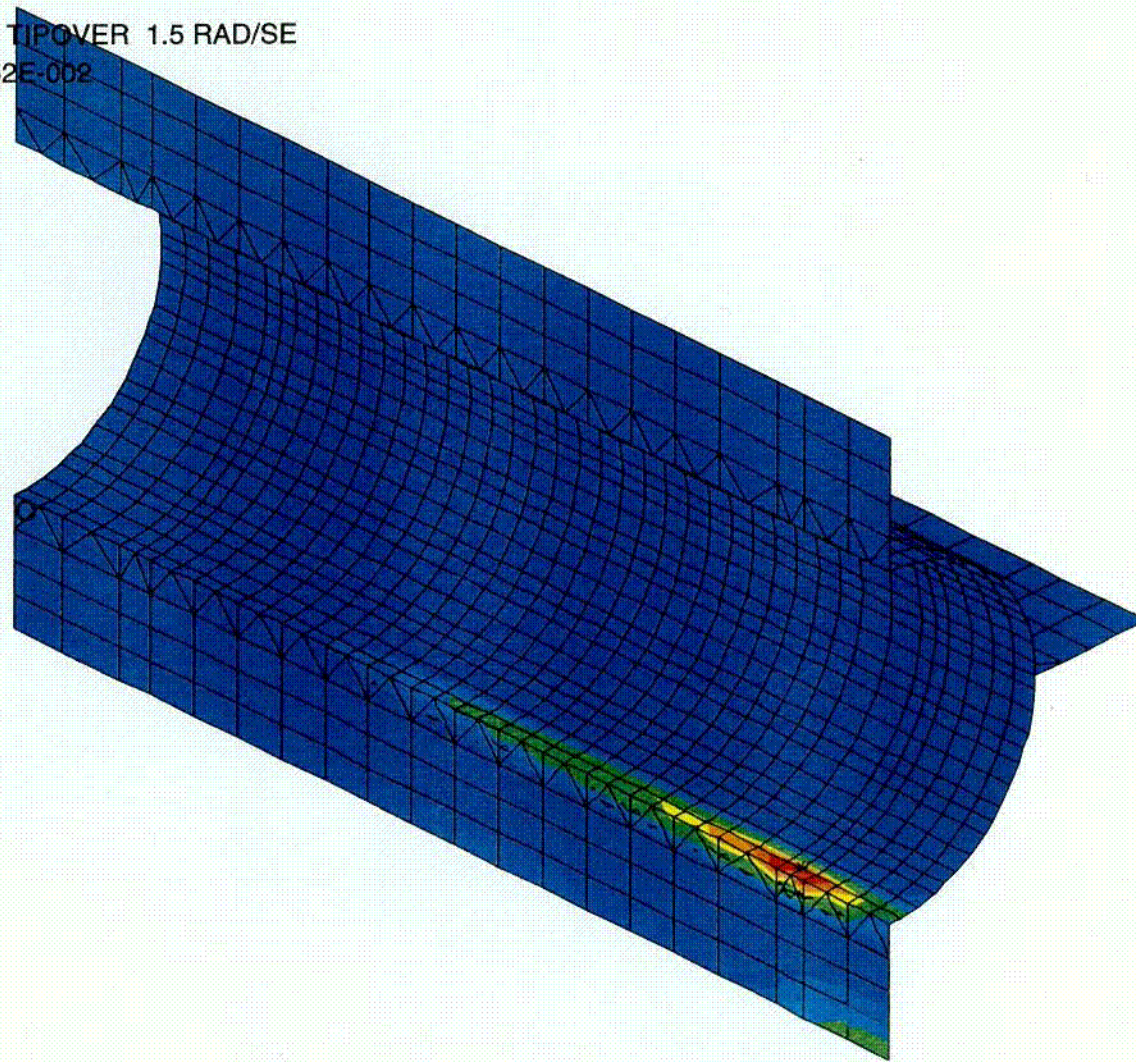
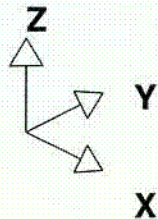
REV. 0

HI-STORM FSAR

C03



HISTORM DEFORMABLE TIPOVER 1.5 RAD/SE  
STEP 80 TIME = 7.9997852E-002  
PSTN(TOP)



HI-2002444  
HI-STORM FSAR

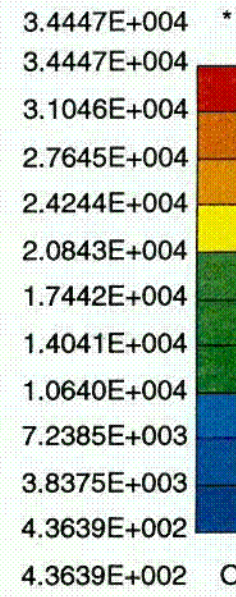
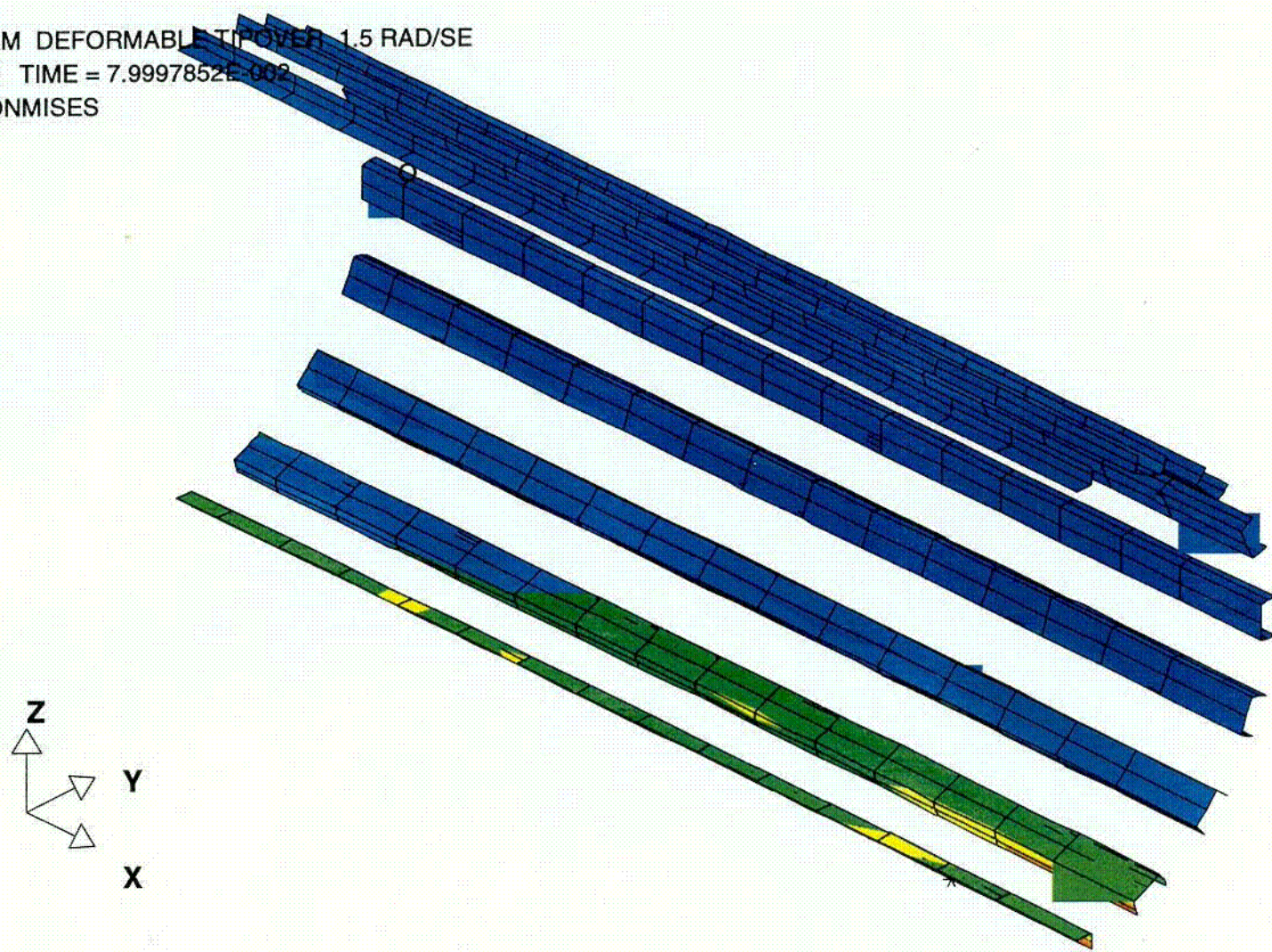
Fig. 3.4.16 Plastic Strain Inner Shell

Rev. 0

COF



HISTORM DEFORMABLE TIP OVER 1.5 RAD/SE  
STEP 80 TIME = 7.9997852E-002  
MAX\_VONMISES



HI-2002444  
HI-STORM FSAR

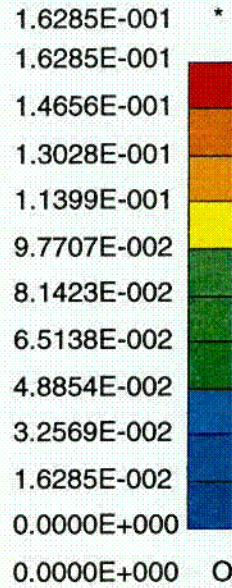
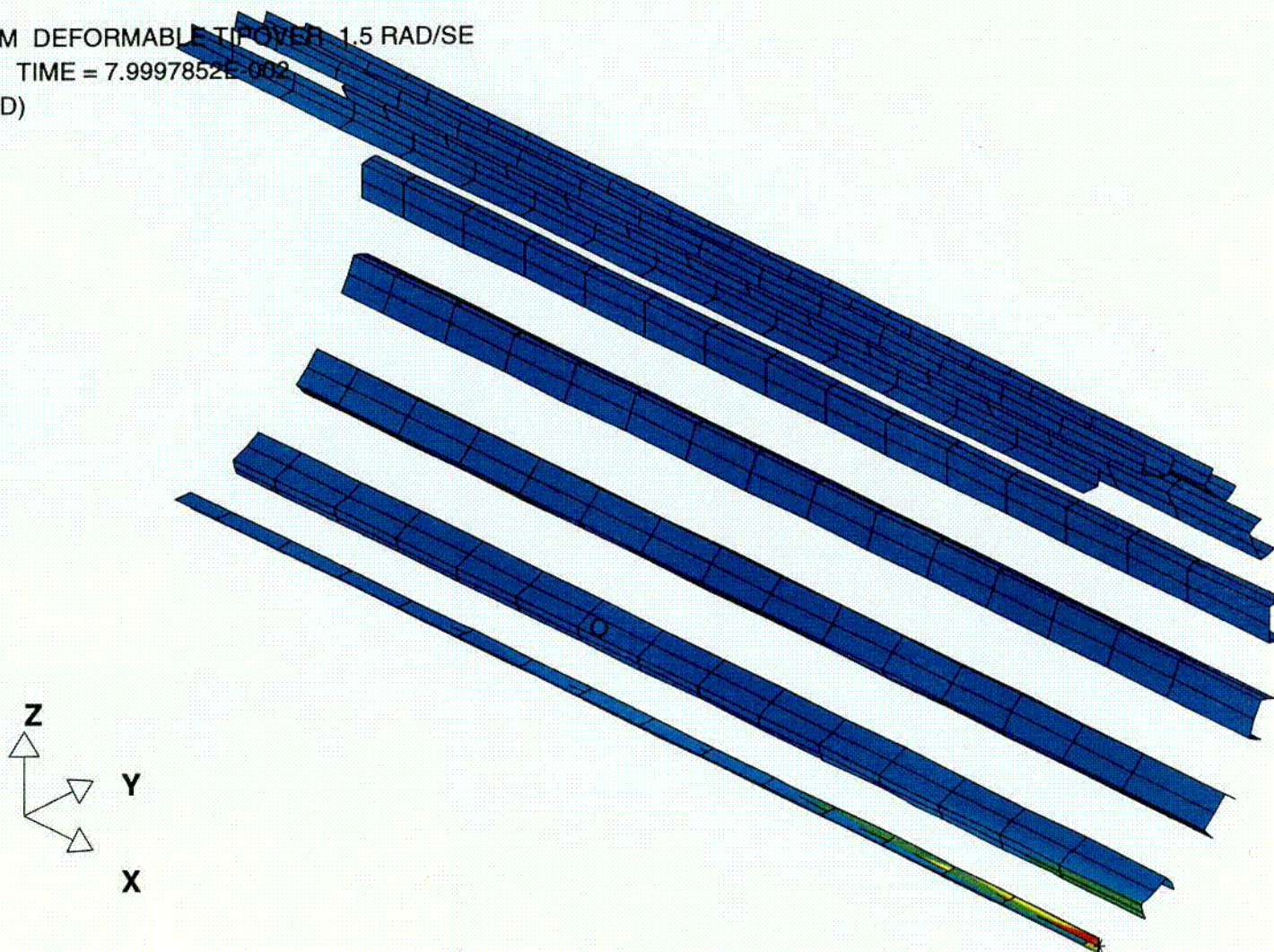
Fig. 3.4.16a Von Mises Stress - Channel

REV. 0

C05



HISTORM DEFORMABLE TIP OVER 1.5 RAD/SE  
STEP 80 TIME = 7.9997852E-002  
PSTN(MID)



HI-2002444  
HI-STORM FSAR

Fig. 3.4.16b Plastic Strain - Channel

REV. 0

606

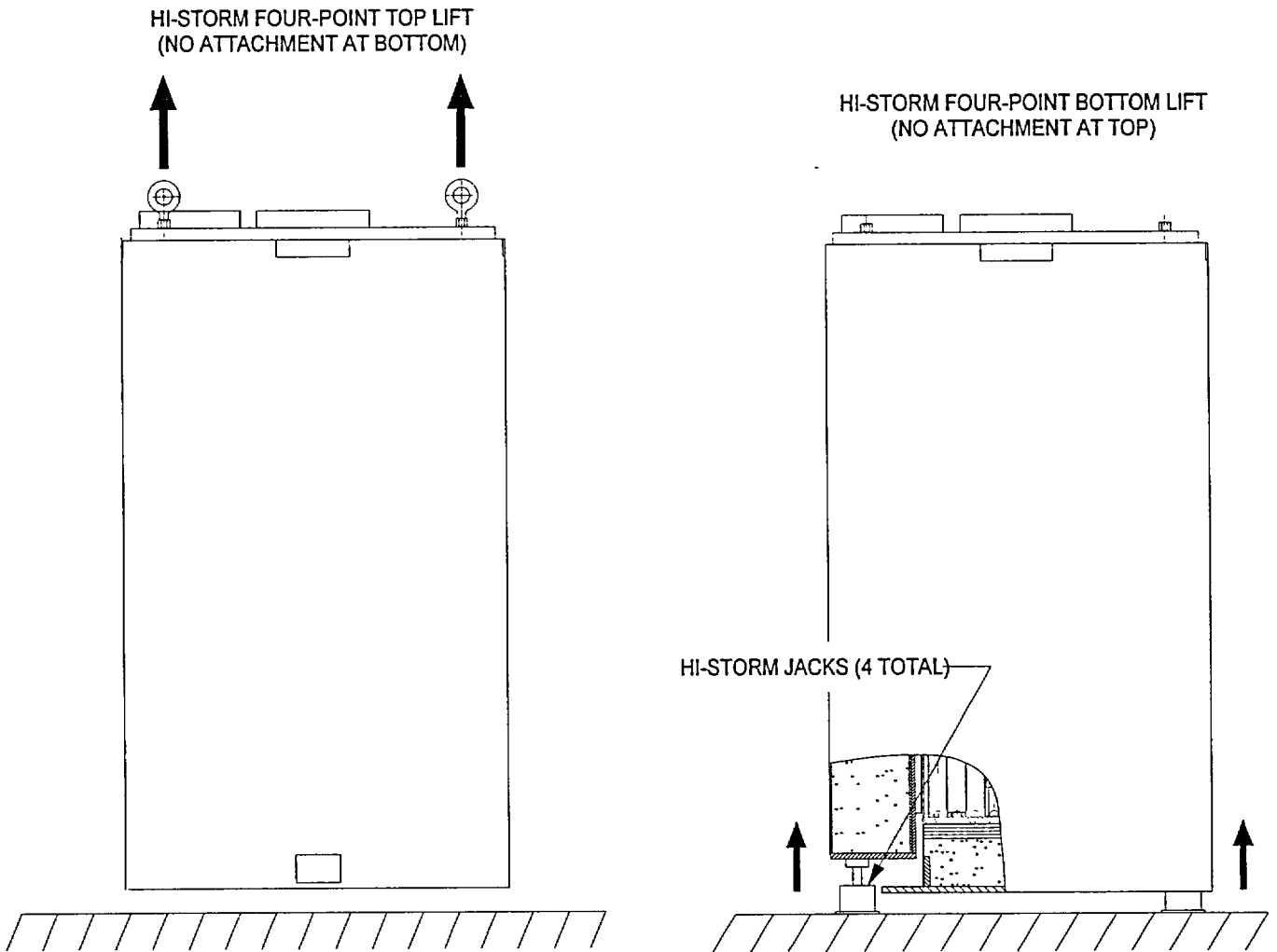


**Figure 3.4.17; Top and Bottom Lifting of the Loaded HI-STORM 100**

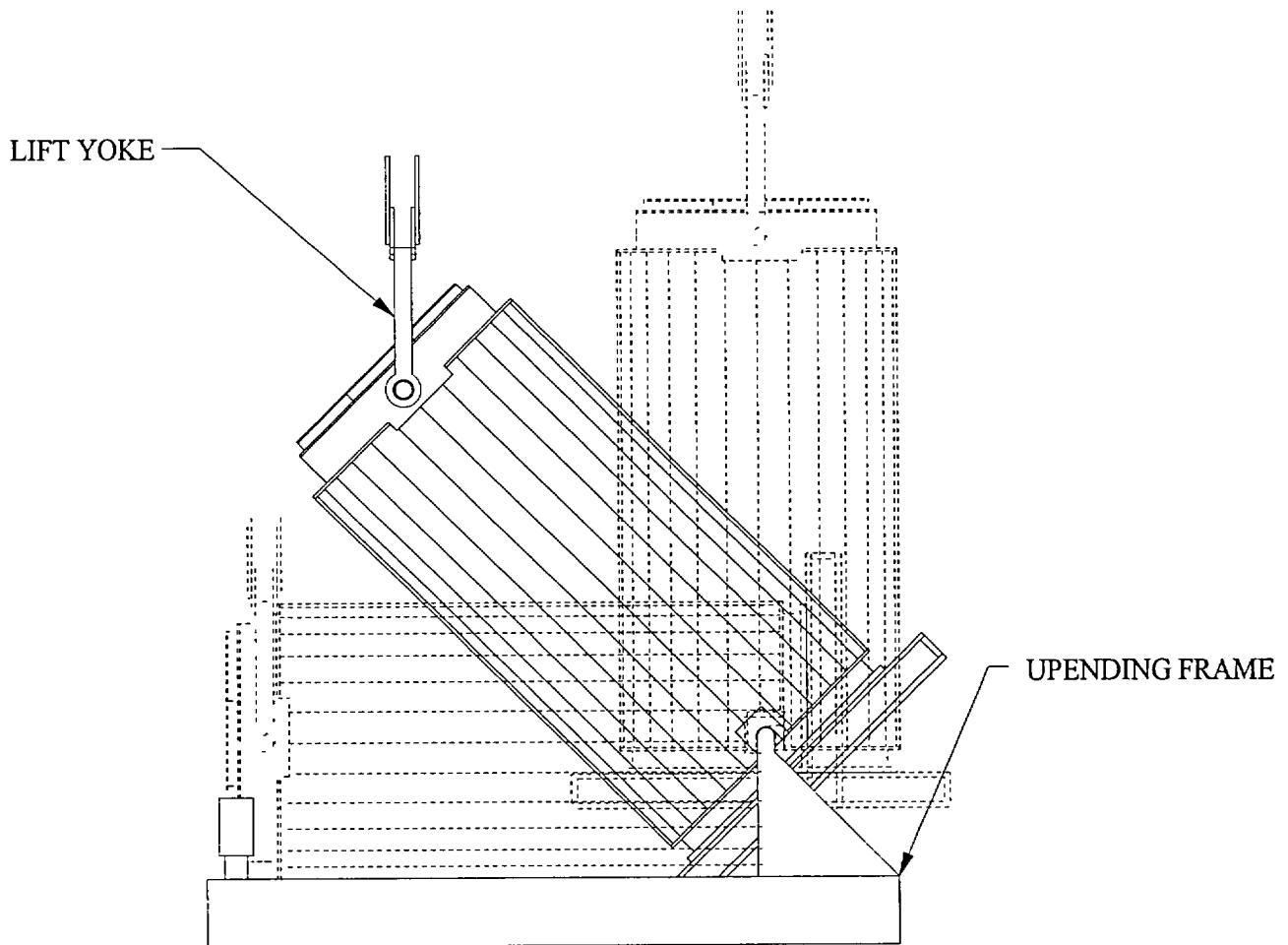


**Figure 3.4.18; HI-TRAC Upending in the Upending Frame**

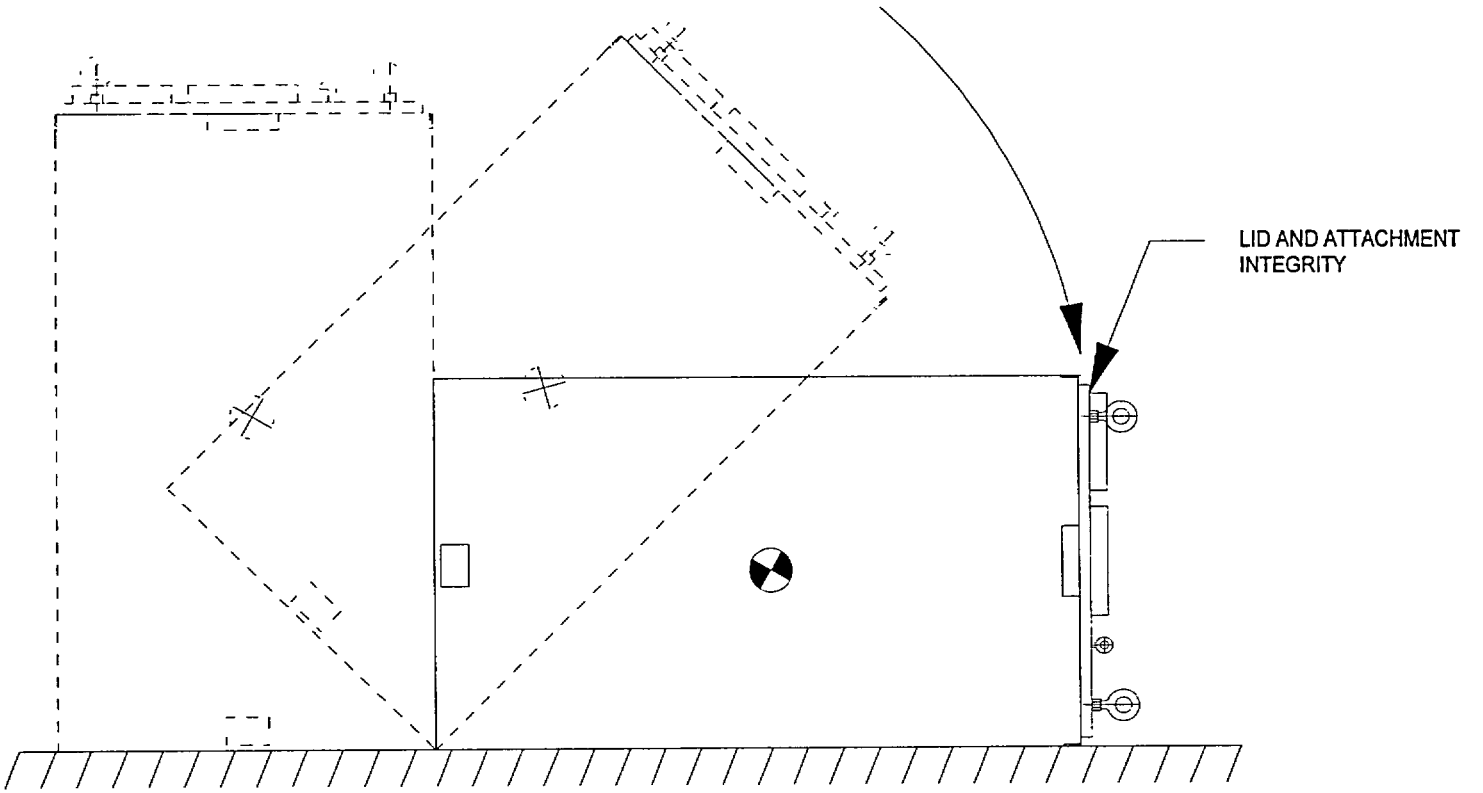


**Figure 3.4.19; HI-STORM 100 Tip-Over Event**

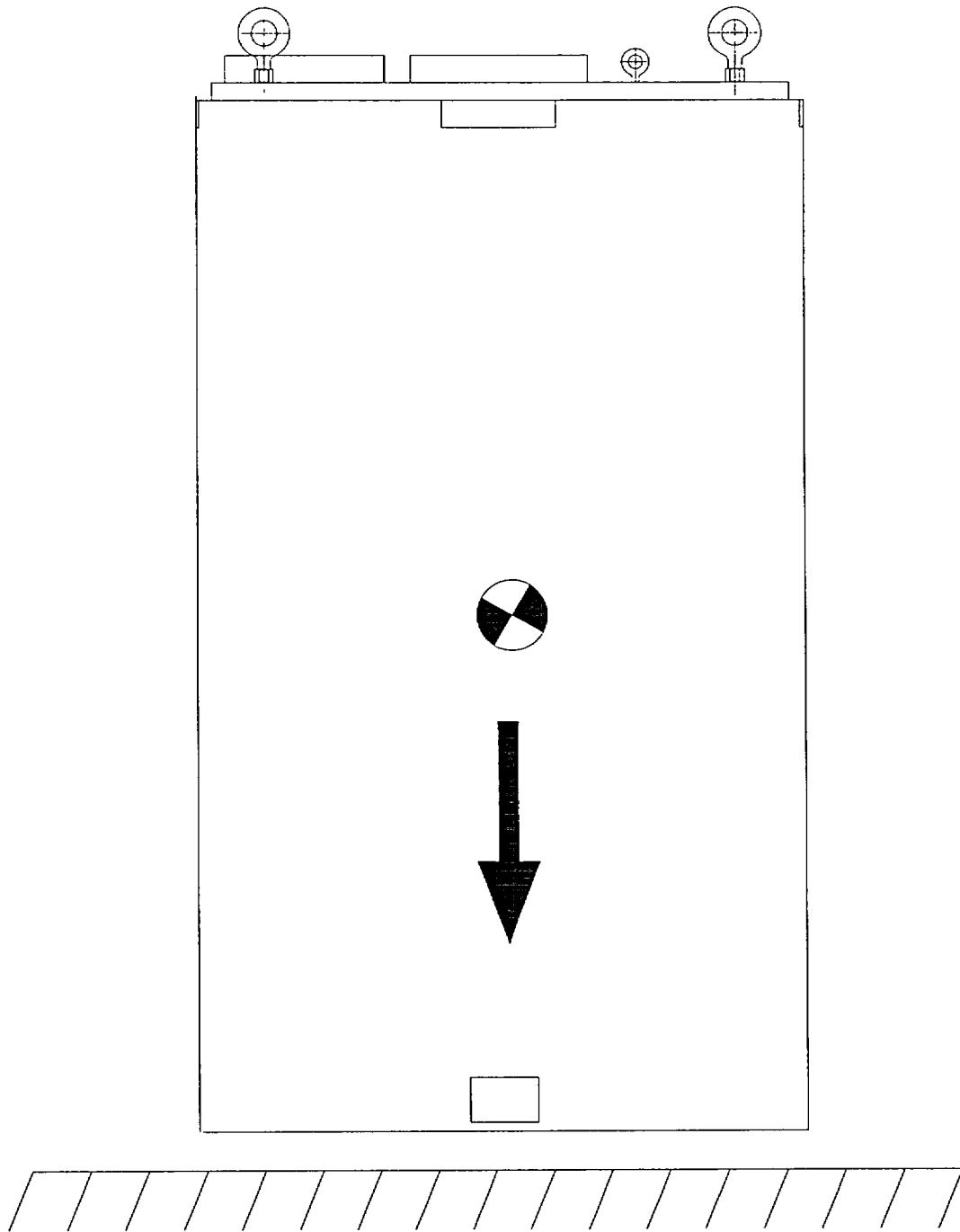
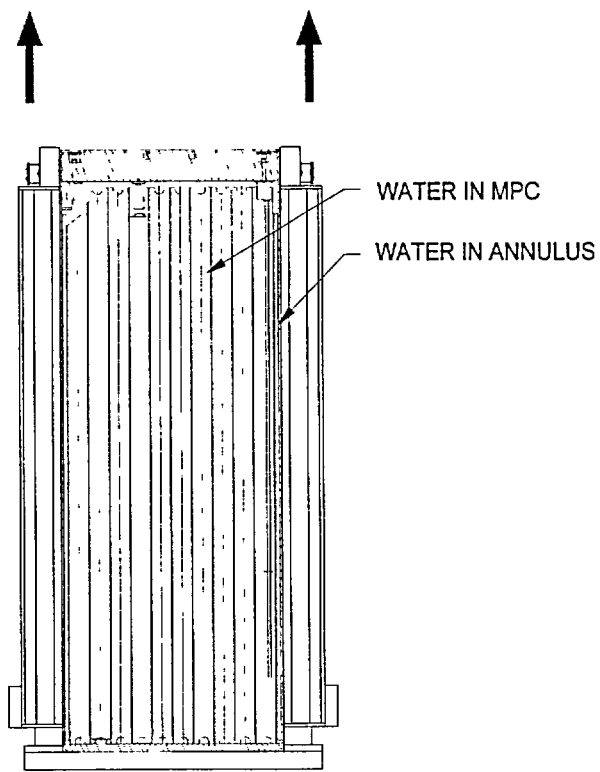
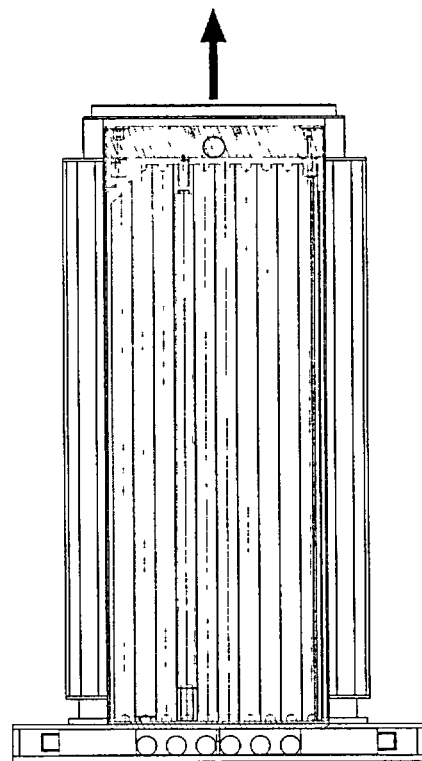


**Figure 3.4.20; HI-STORM 100 End Drop Event**



HI-TRAC LIFTING WITH  
THE POOL LID



HI-TRAC LIFTING WITH  
THE TRANSFER LID

**Figure 3.4.21; HI-TRAC Lifting with the Pool and Transfer Lids**

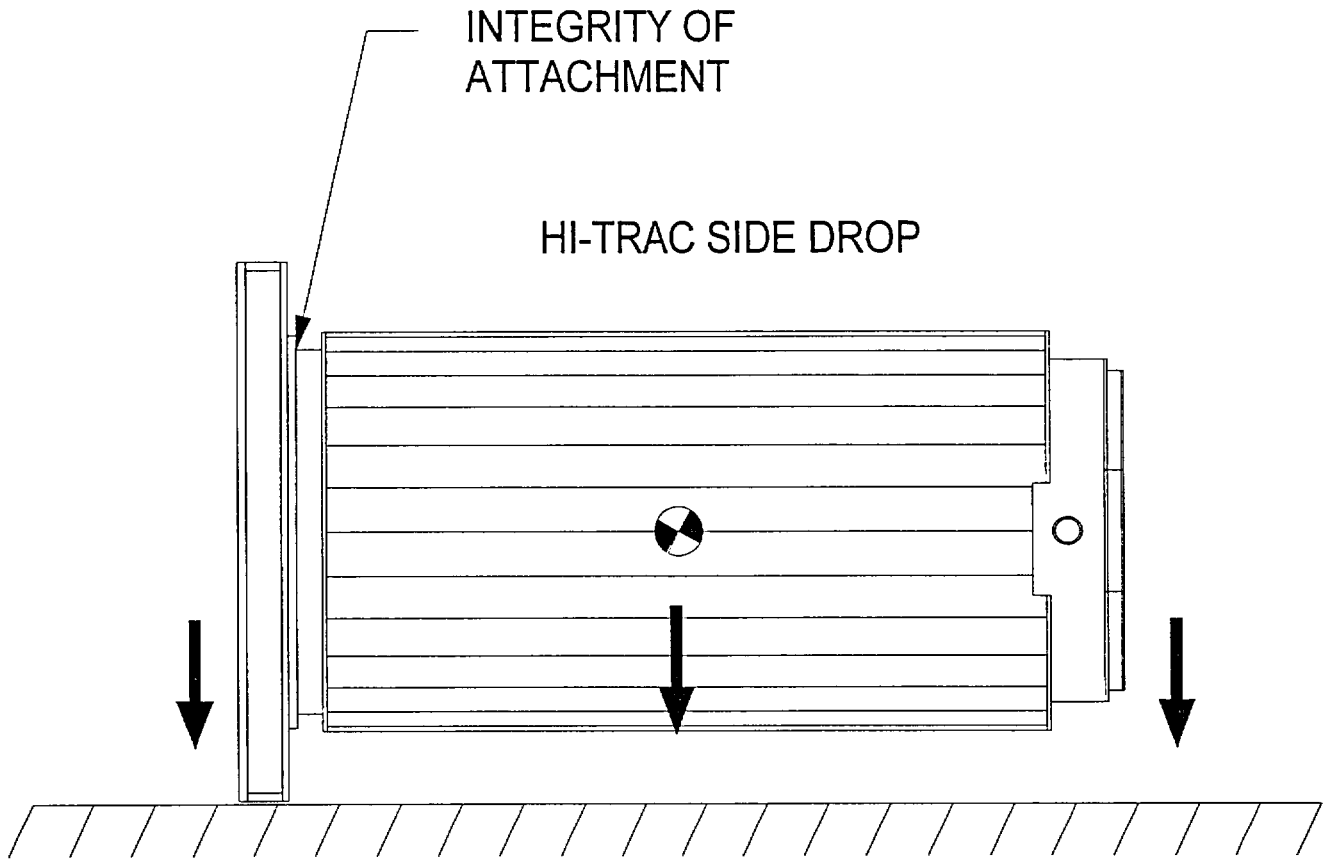


**Figure 3.4.22; HI-TRAC Side Drop Event**



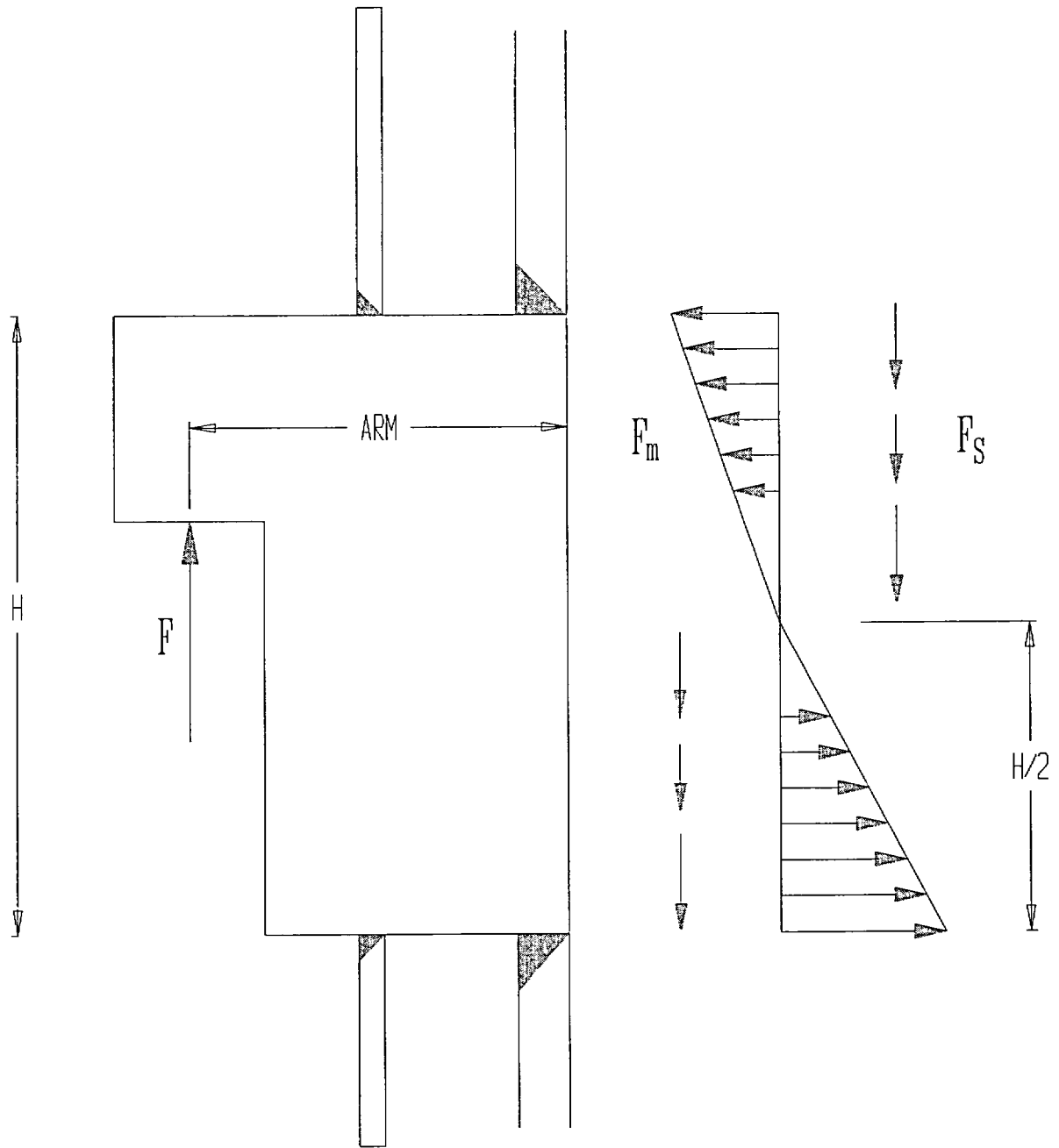


FIGURE 3.4.23 FORCES AND MOMENTS ON  
125 TON ROTATION TRUNNION WELD

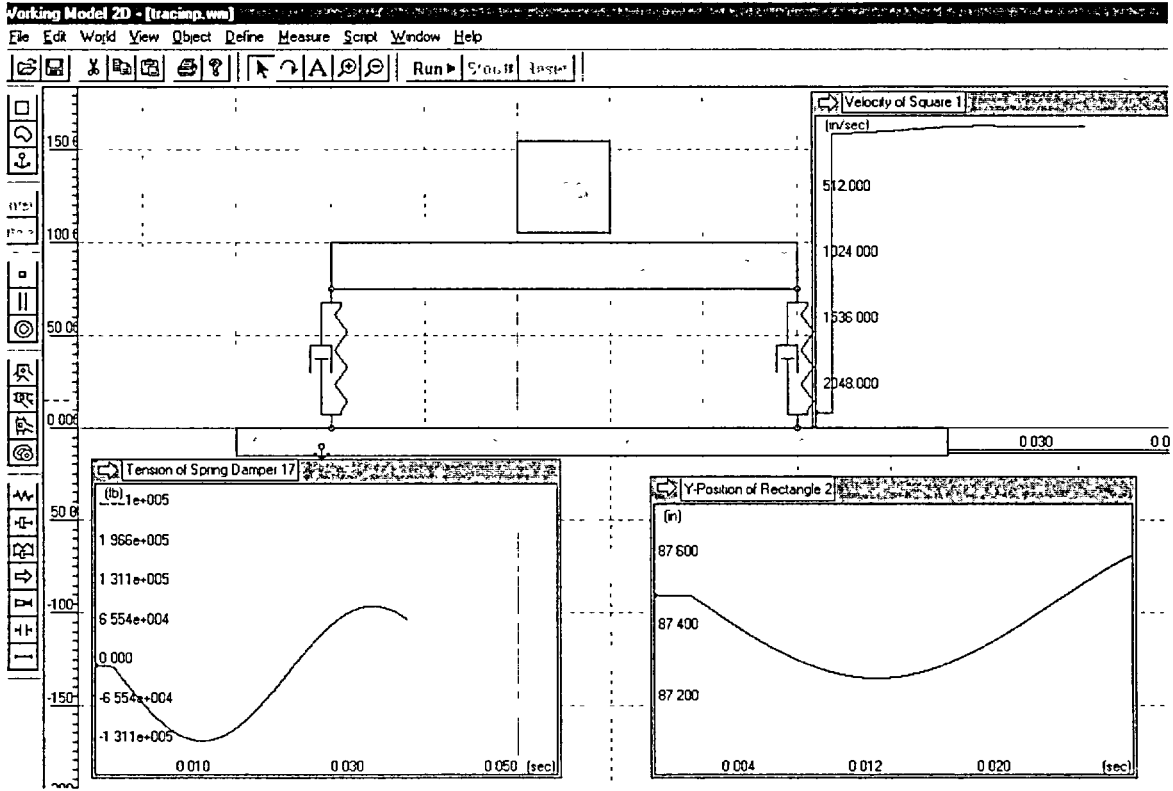


FIGURE 3.4.24 WORKING MODEL SOLUTION FOR IMPACT FORCE ON HI-TRAC 100 TRANSFER CASK OUTER SHELL

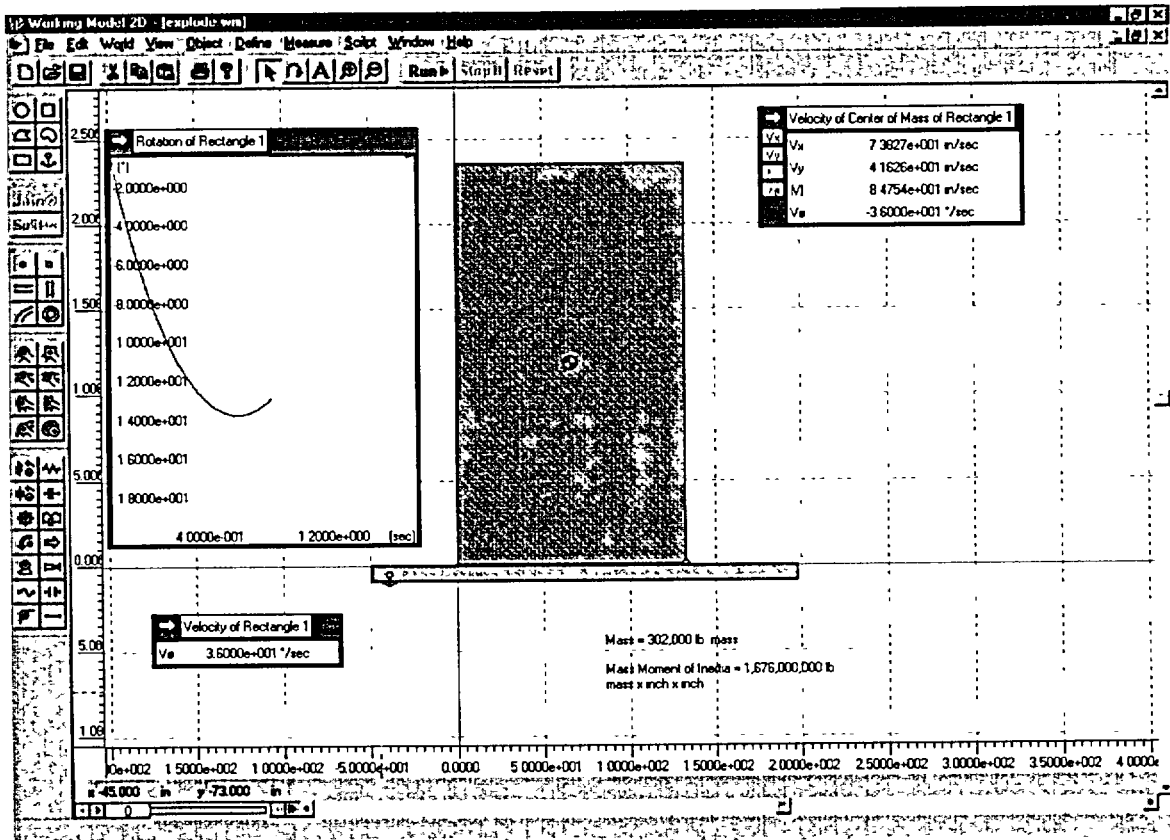


FIGURE 3.4.25: HI-STORM 100 OVERTURNING SCENARIO - INITIAL ANGULAR VELOCITY = 0.628 RADIANS/SECOND ASSUMED CAUSED BY A PRESSURE PULSE

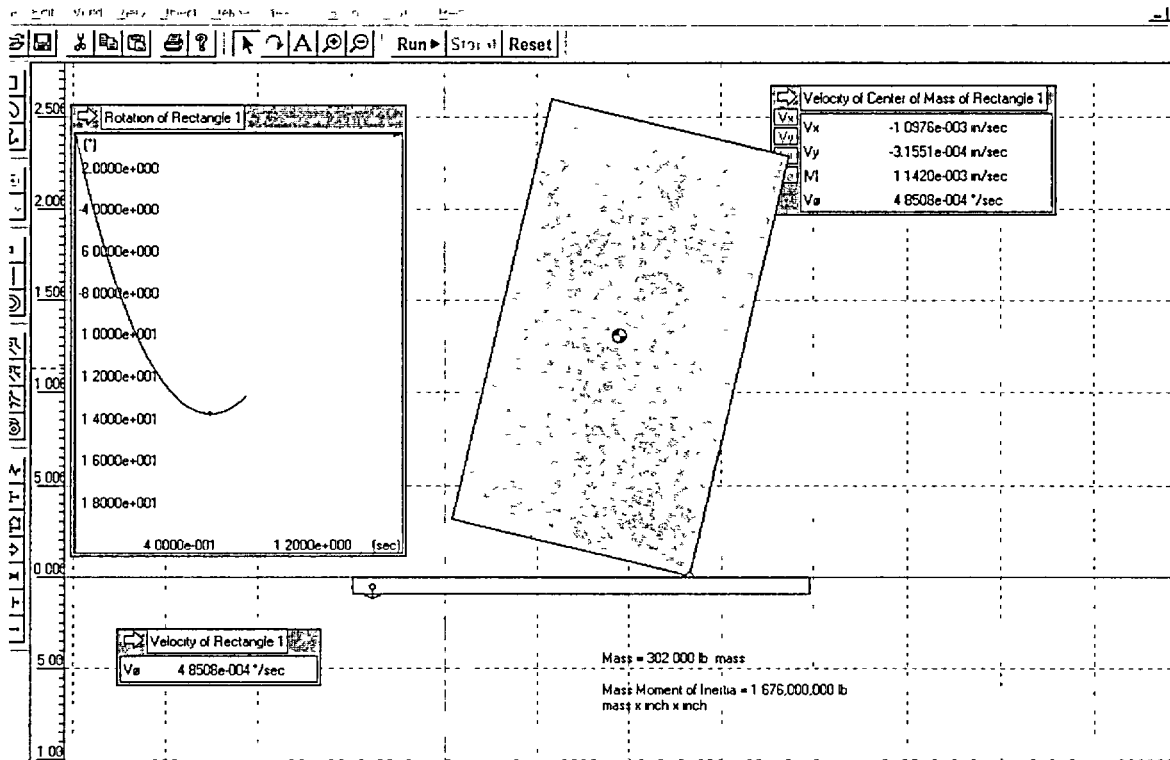
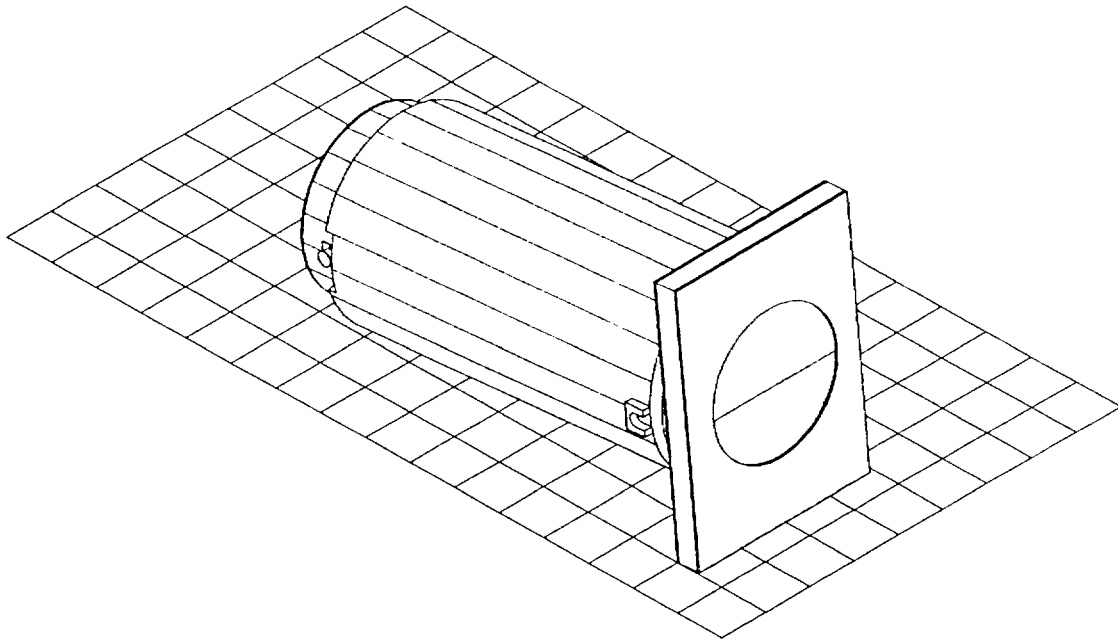
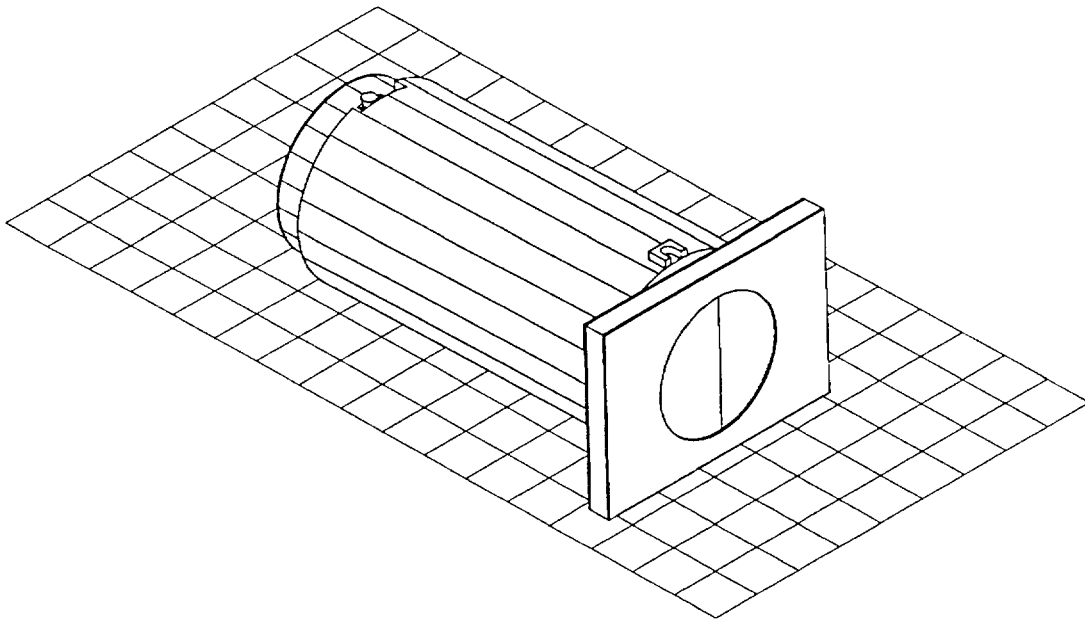


FIGURE 3.4.26: HI-STORM 100 OVERTURNING SCENARIO - INITIAL ANGULAR VELOCITY = 0.628 RADIANS/SECOND MAXIMUM ANGULAR EXCURSION



**FIGURE 3.4.27; HI-TRAC TRANSFER CASK IN SHORT-SIDE IMPACT  
(CASK RESTS AT A POSITION OF  $-5^{\circ}$  FROM HORIZONTAL)**



**FIGURE 3.4.28; HI-TRAC TRANSFER CASK IN LONG-SIDE IMPACT  
(CASK RESTS AT A POSITION OF  $-1^{\circ}$  FROM HORIZONTAL)**

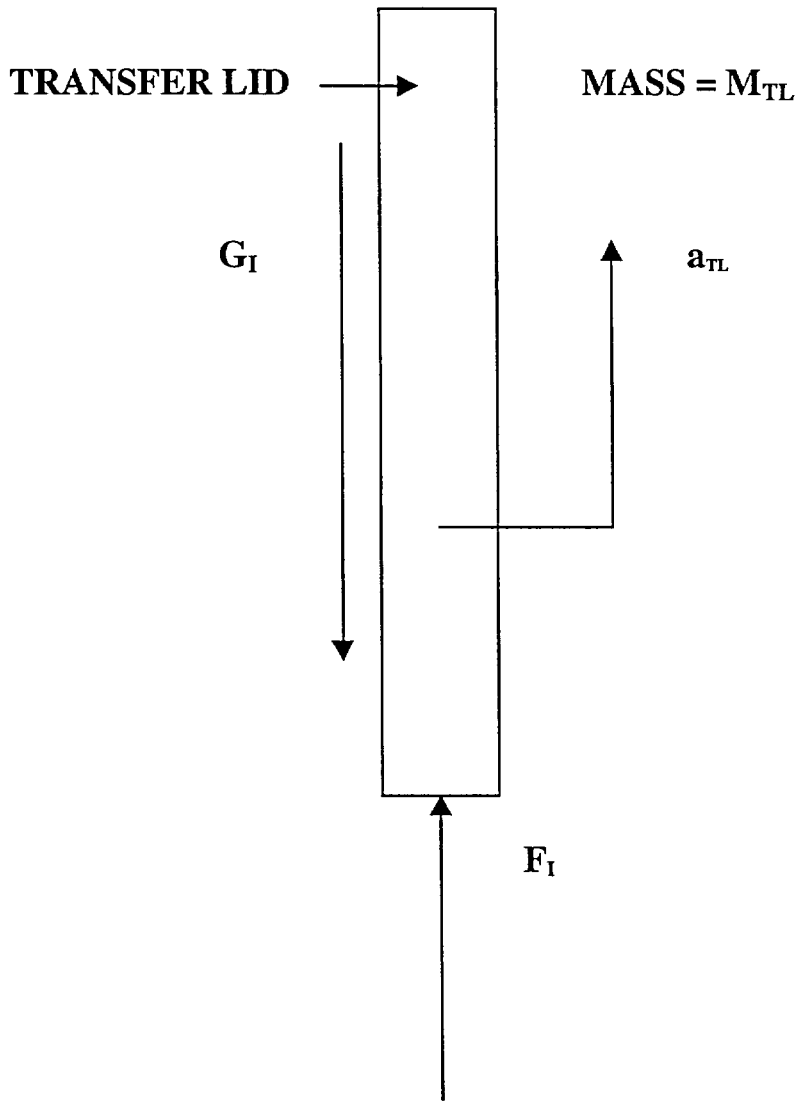


**FIGURE 3.4.29; FREE-BODY OF TRANSFER LID DURING PRIMARY IMPACT WITH TARGET**



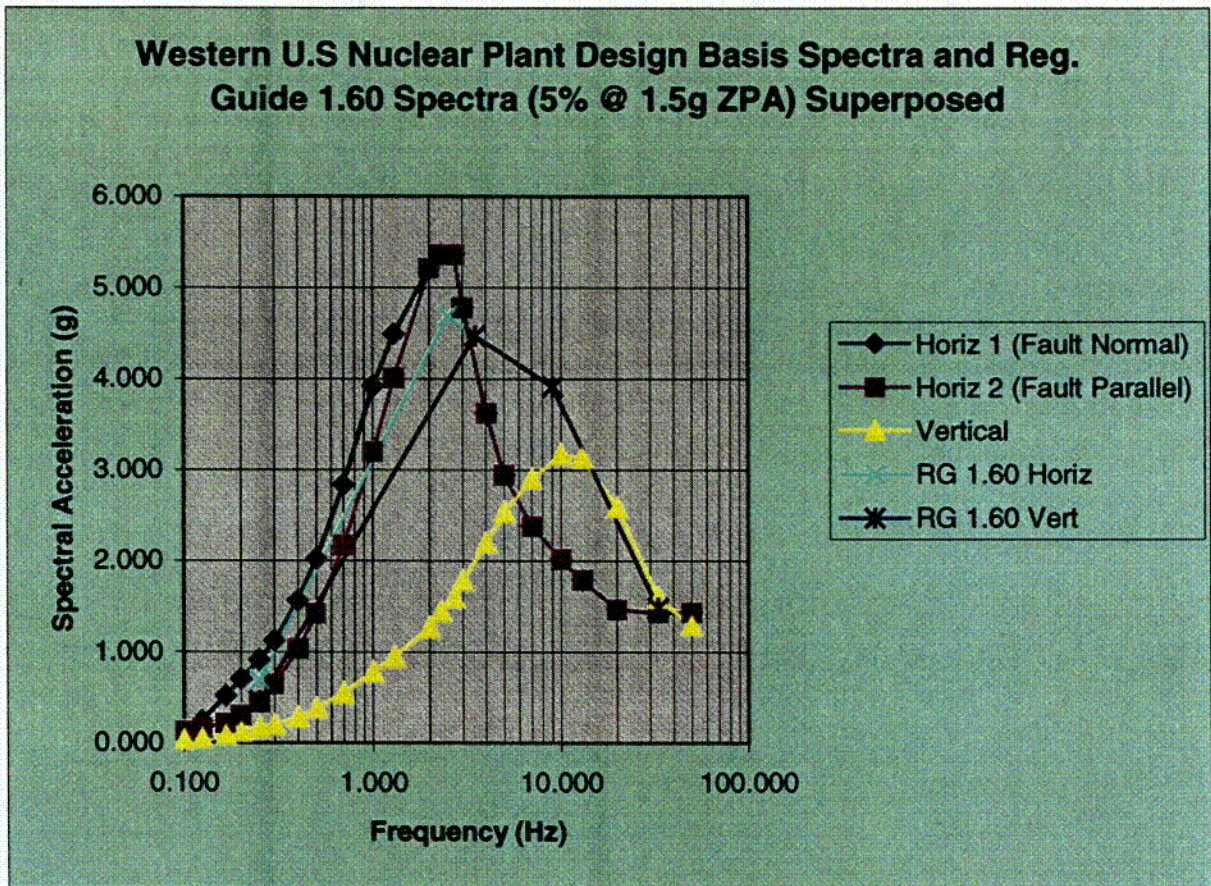


FIGURE 3.4.30 SEISMIC SPECTRA SETS USED FOR TIME HISTORY ANALYSIS OF HI-STORM 100A ON ISFSI PAD



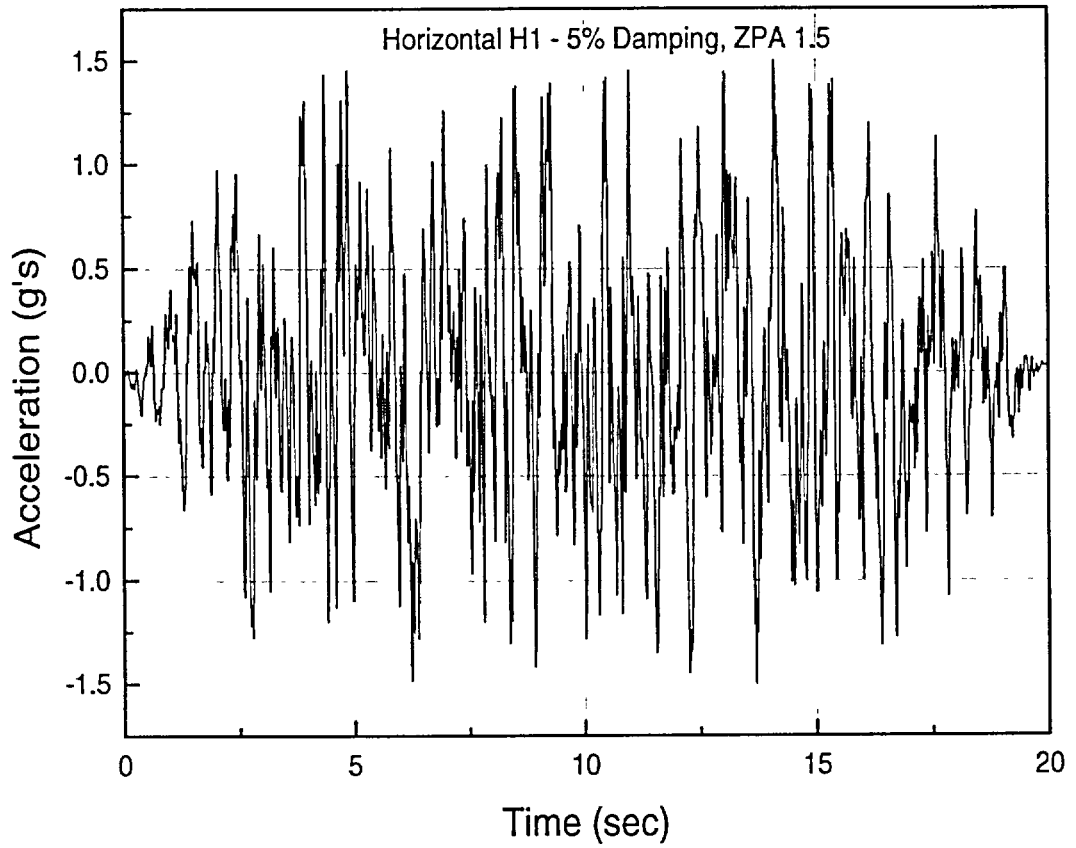


FIGURE 3.4.31 – RG 1.60 “H1”



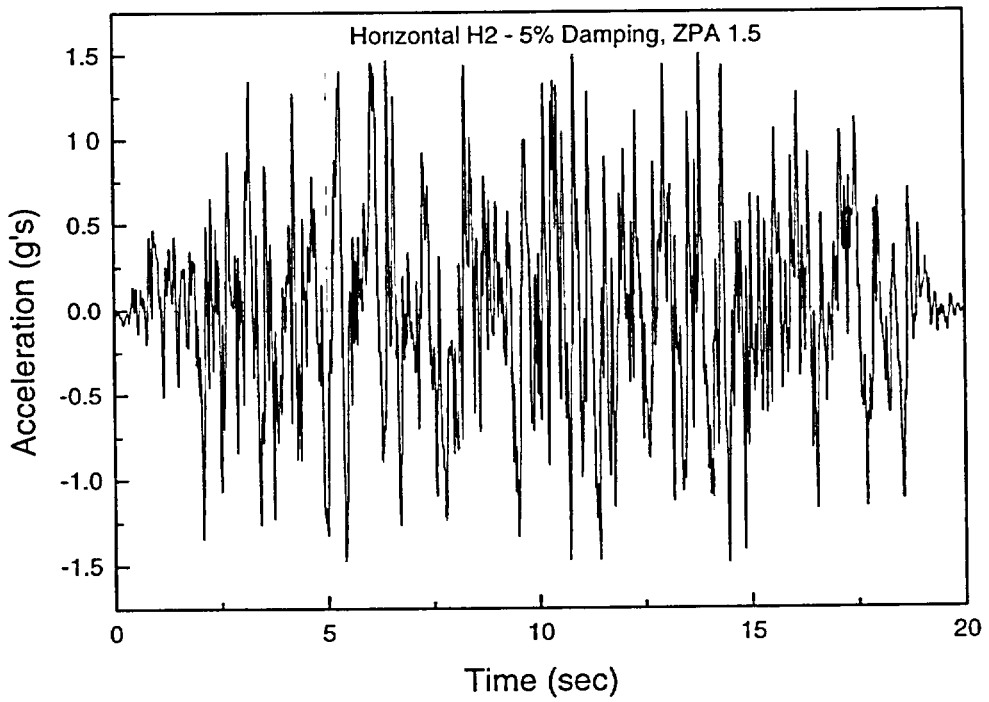


FIGURE 3.4.32 – RG 1.60 “H2”

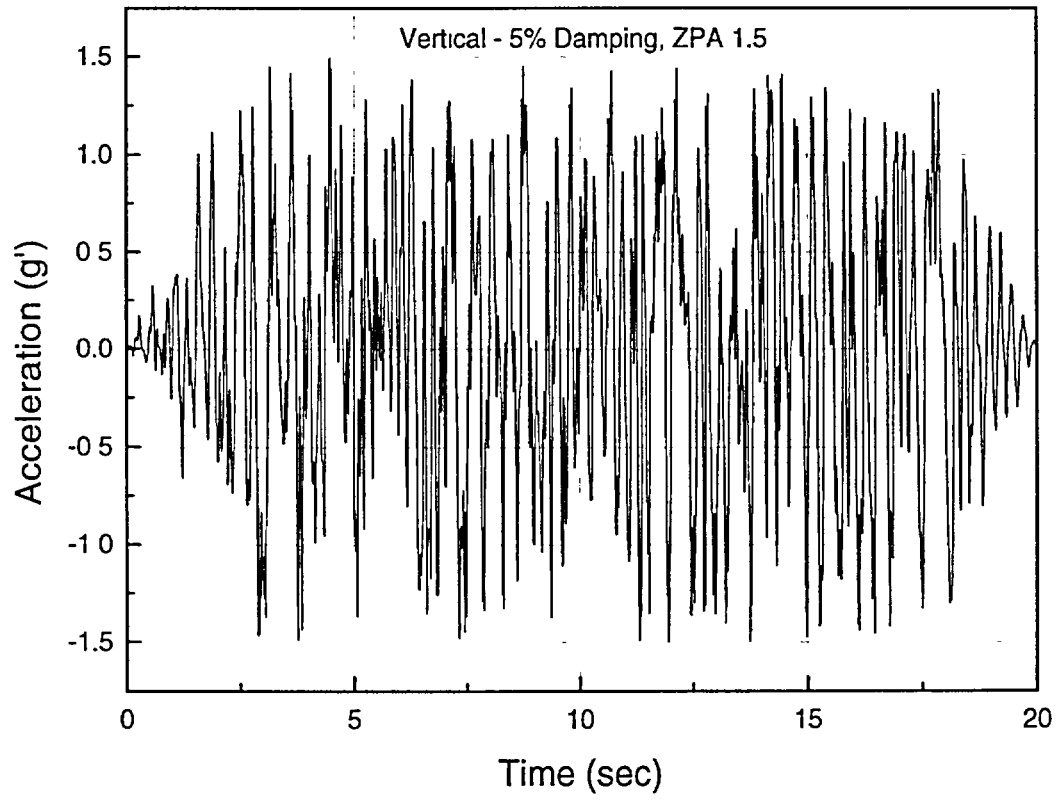


FIGURE 3.4.33 – RG 1.60 “VT”

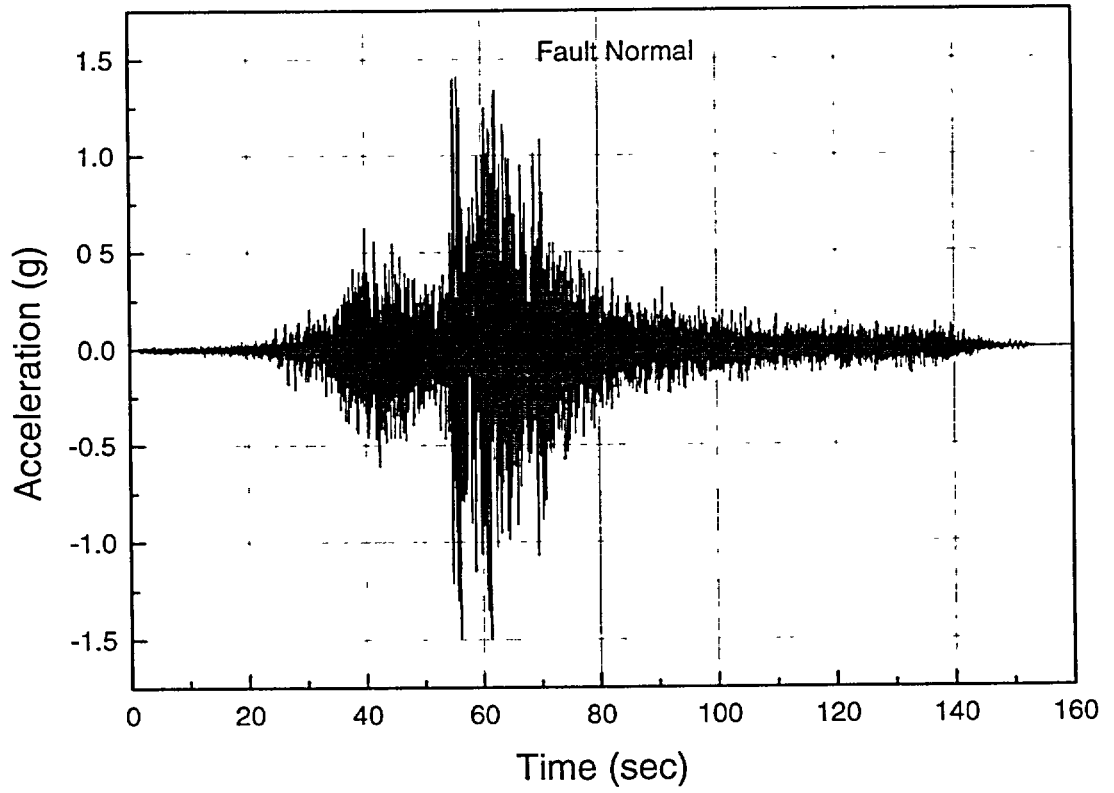


FIGURE 3.4.34 Horizontal Acceleration Time history "FN"

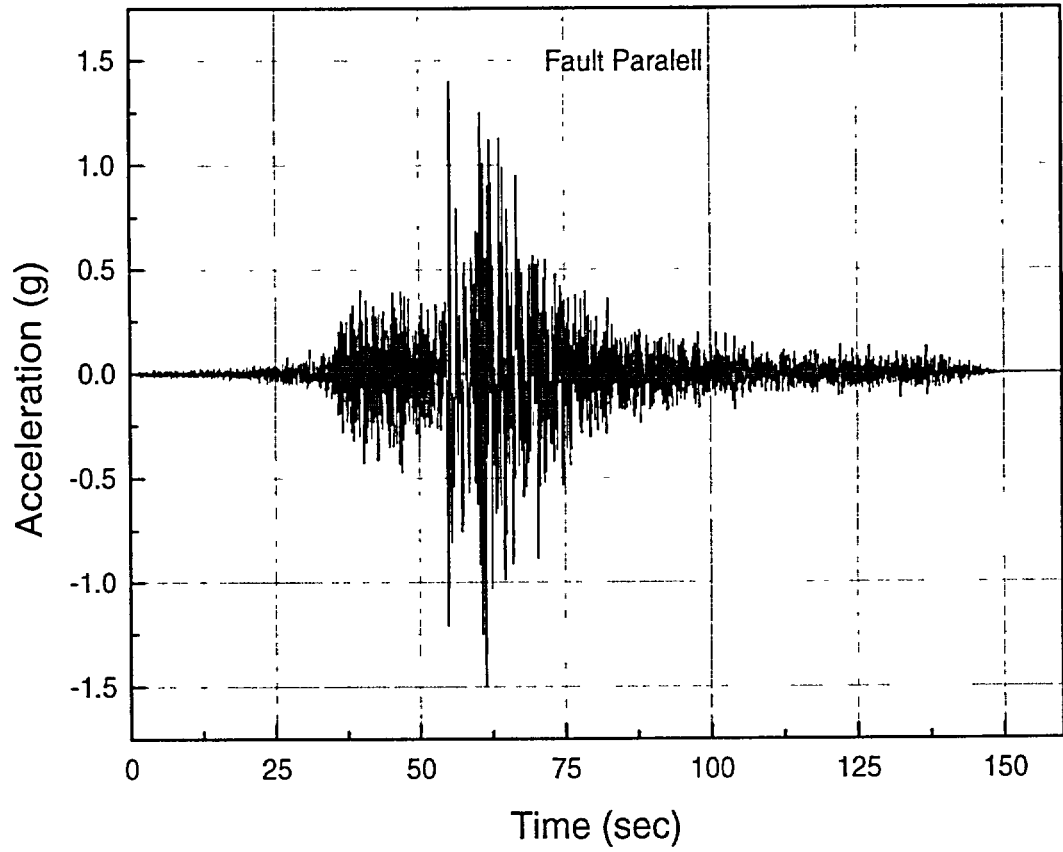


FIGURE 3.4.35 Horizontal Acceleration Time history "FP"

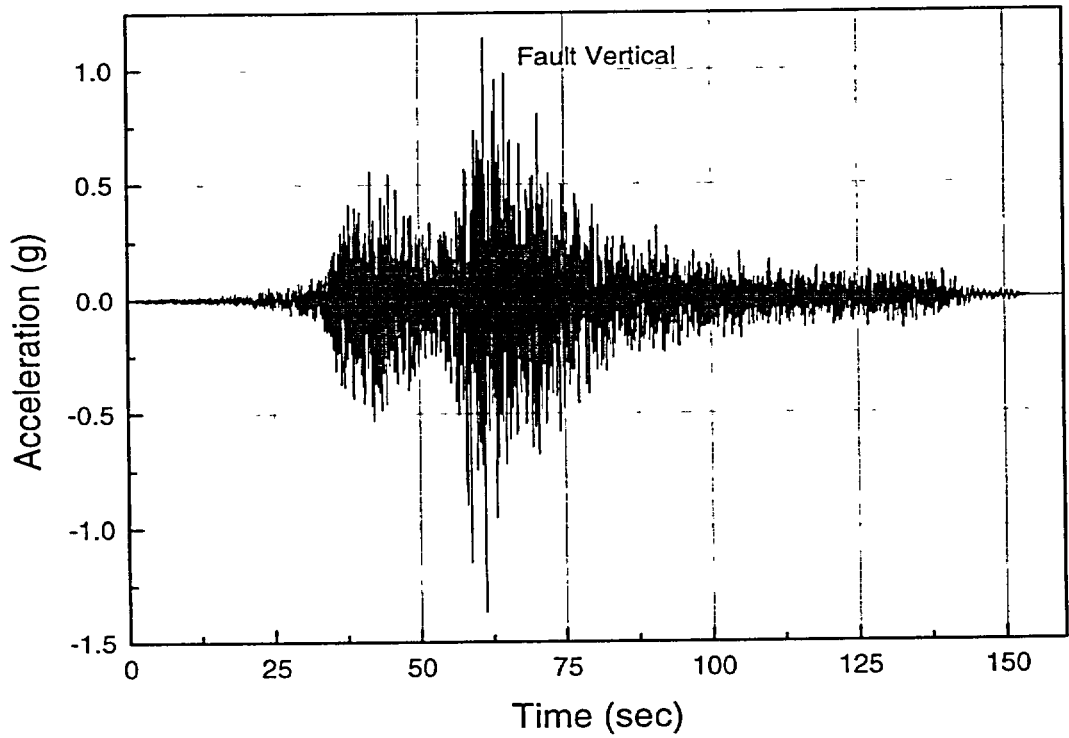


FIGURE 3.4.36 Vertical Acceleration Time history "FV"

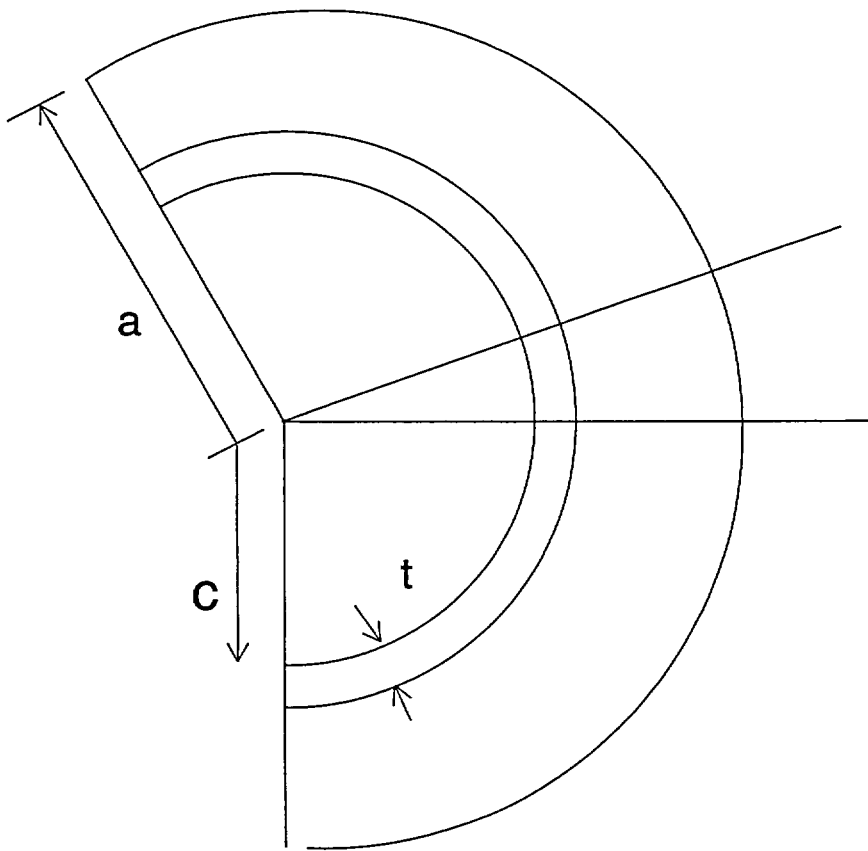


FIGURE 3.4.37 GEOMETRY FOR QUASI-STATIC ANALYSIS

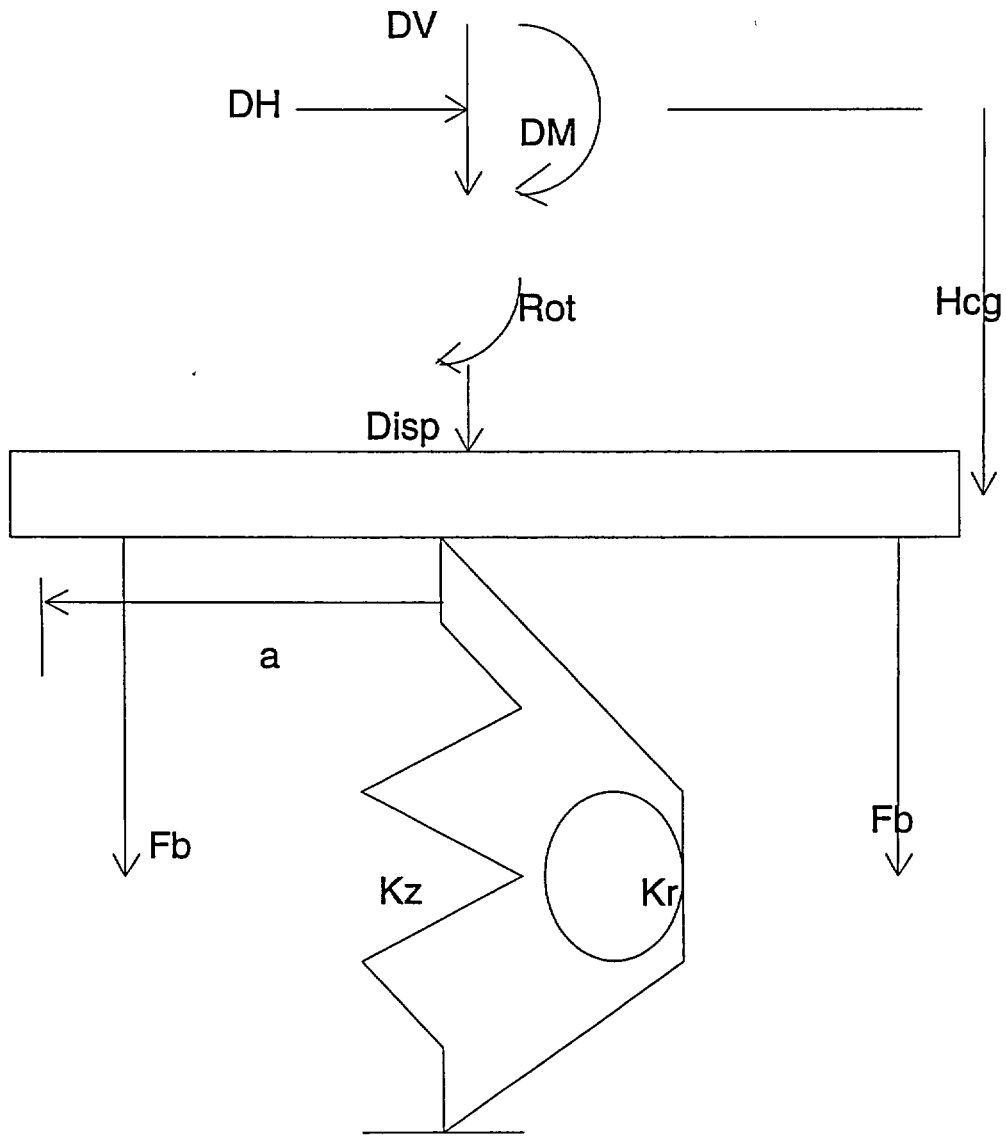


FIGURE 3.4.38 FREE BODY FOR QUASI-STATIC ANALYSIS



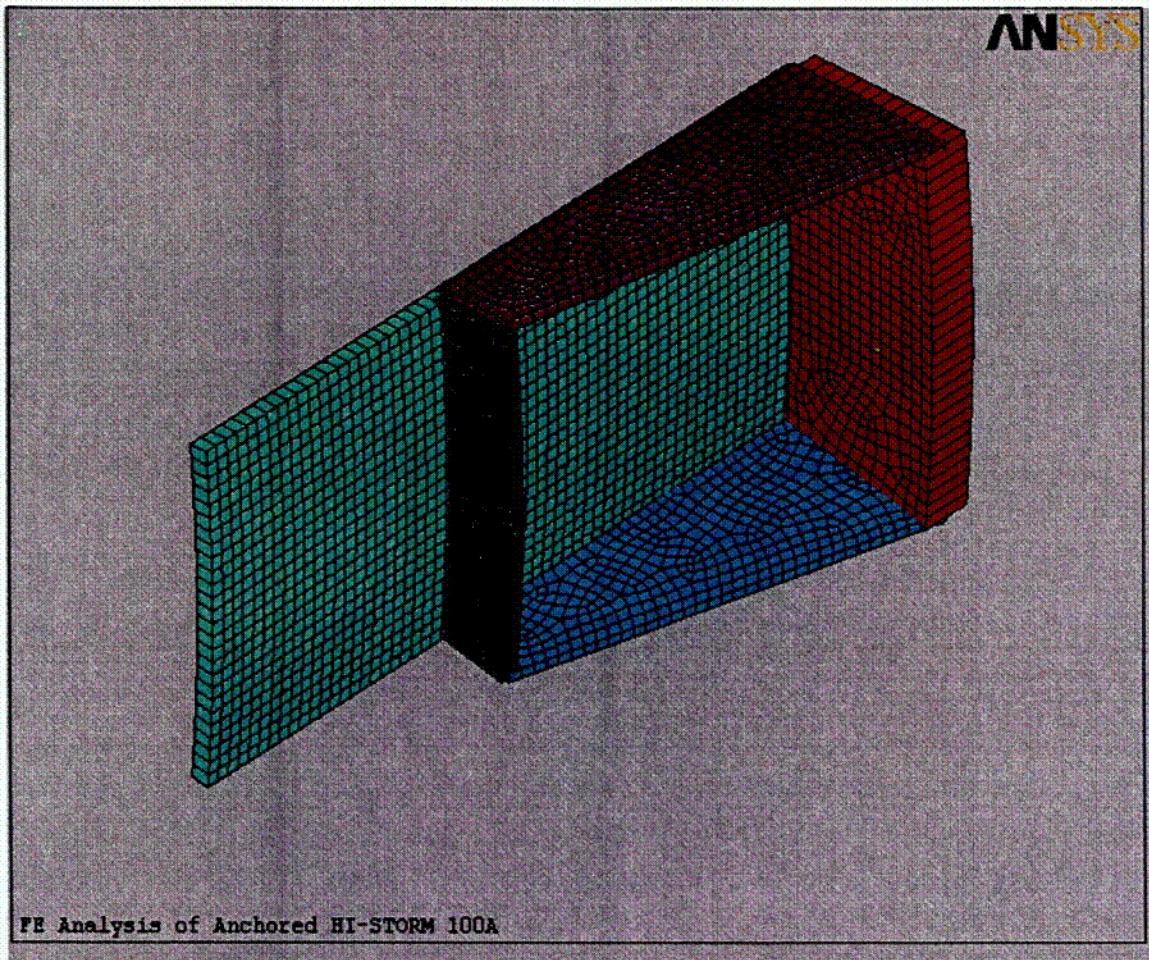


FIGURE 3.4.39 Sector Lug Finite Element Mesh



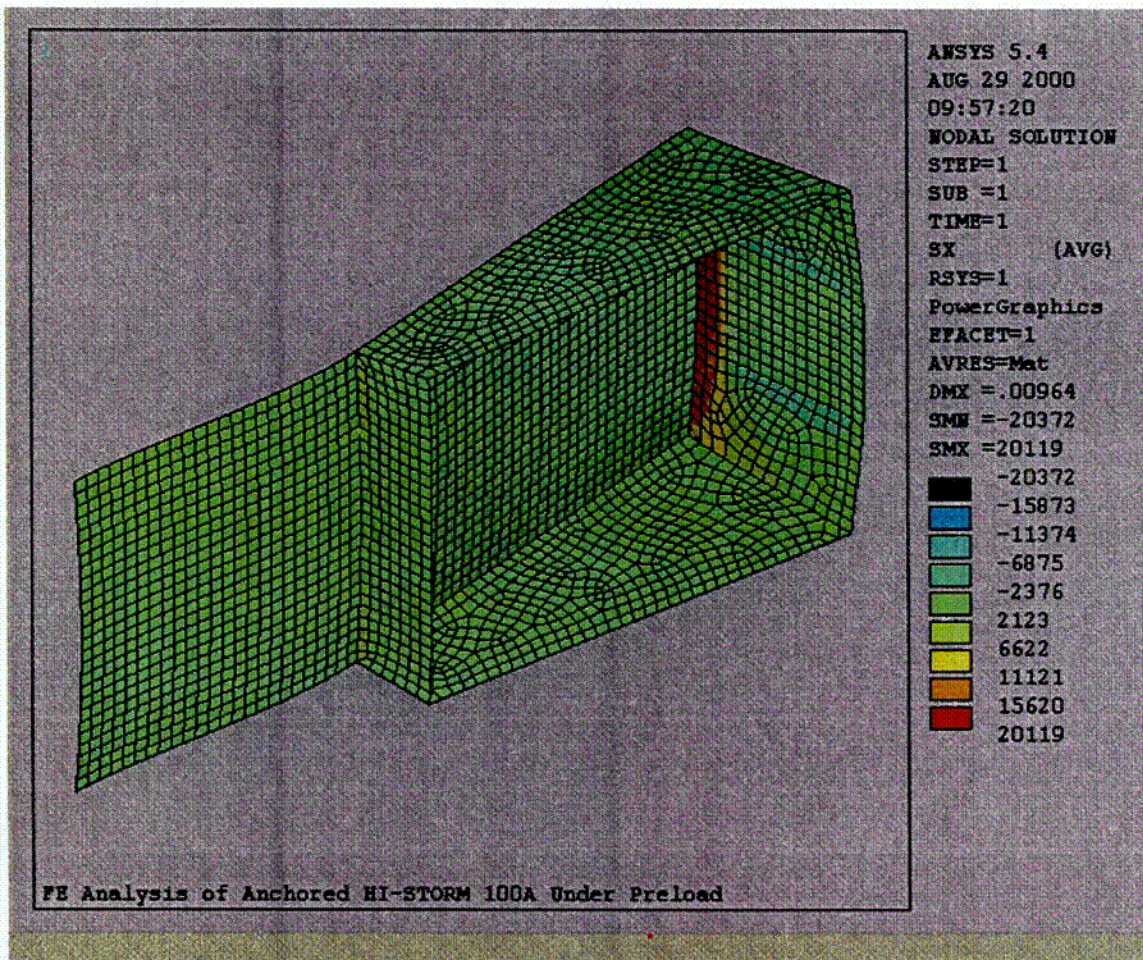


FIGURE 3.4.40 Sector Lug Stress – Case 1 Preload



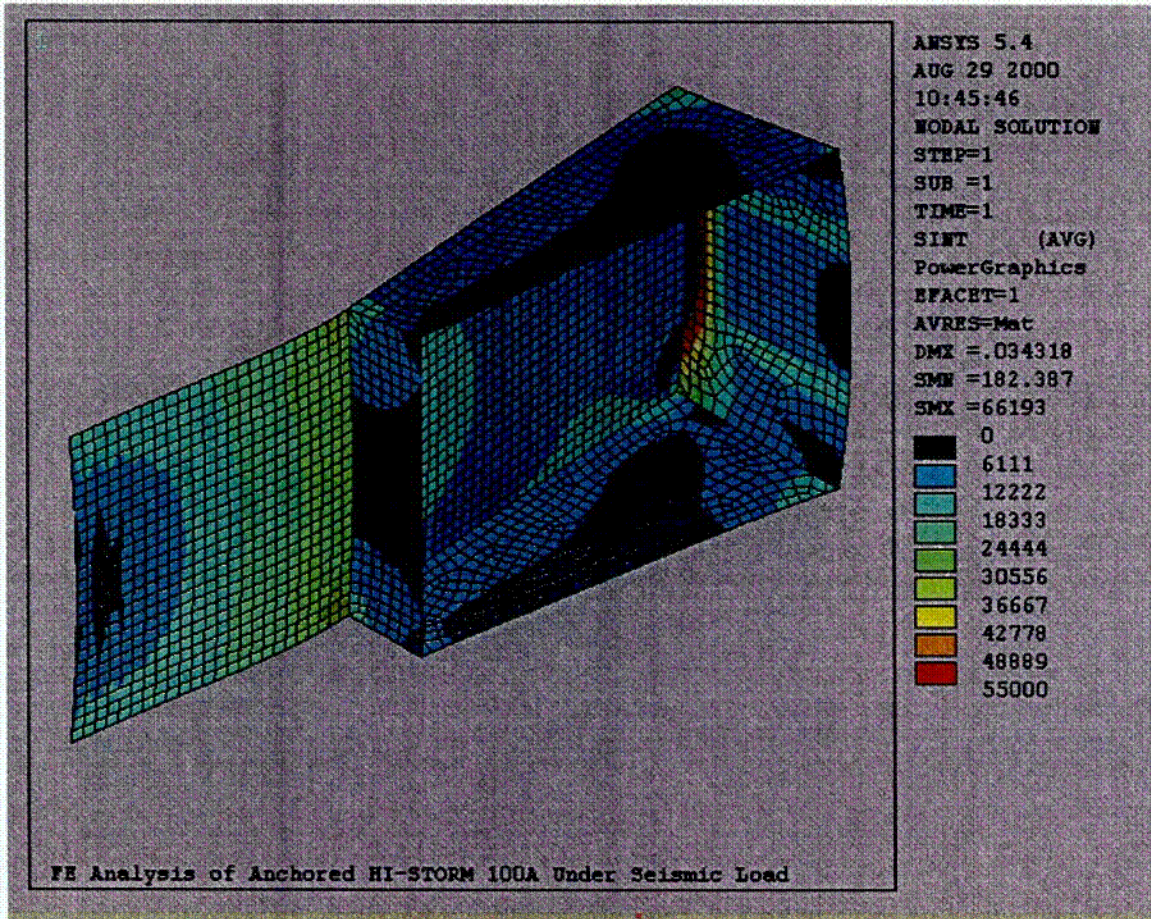


FIGURE 3.4.41 Sector Lug Stress Intensity – Case 2 Preload + Seismic



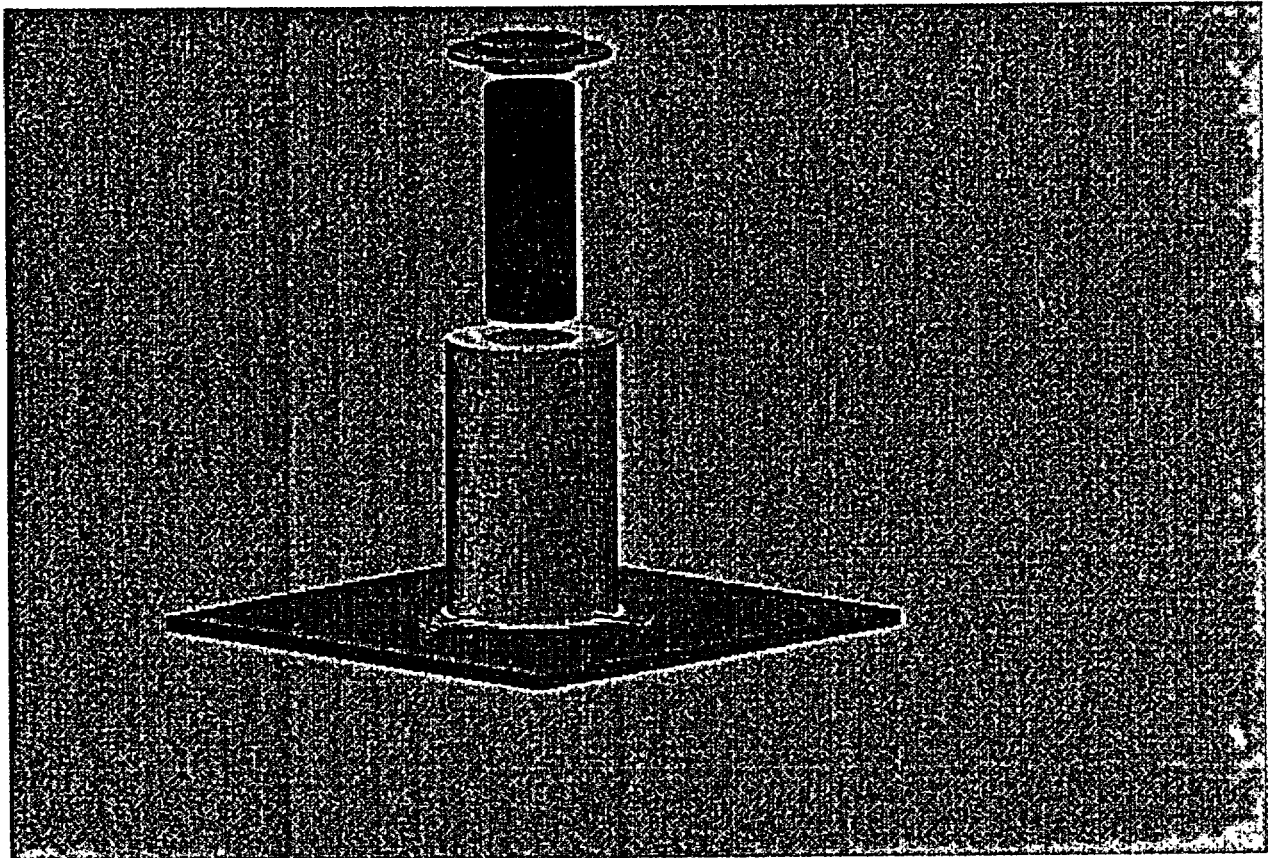


FIGURE 3.4.42: EXPLODED VIEW SHOWING GROUND PLANE, OVERPACK, MPC, AND OVERPACK TOP LID

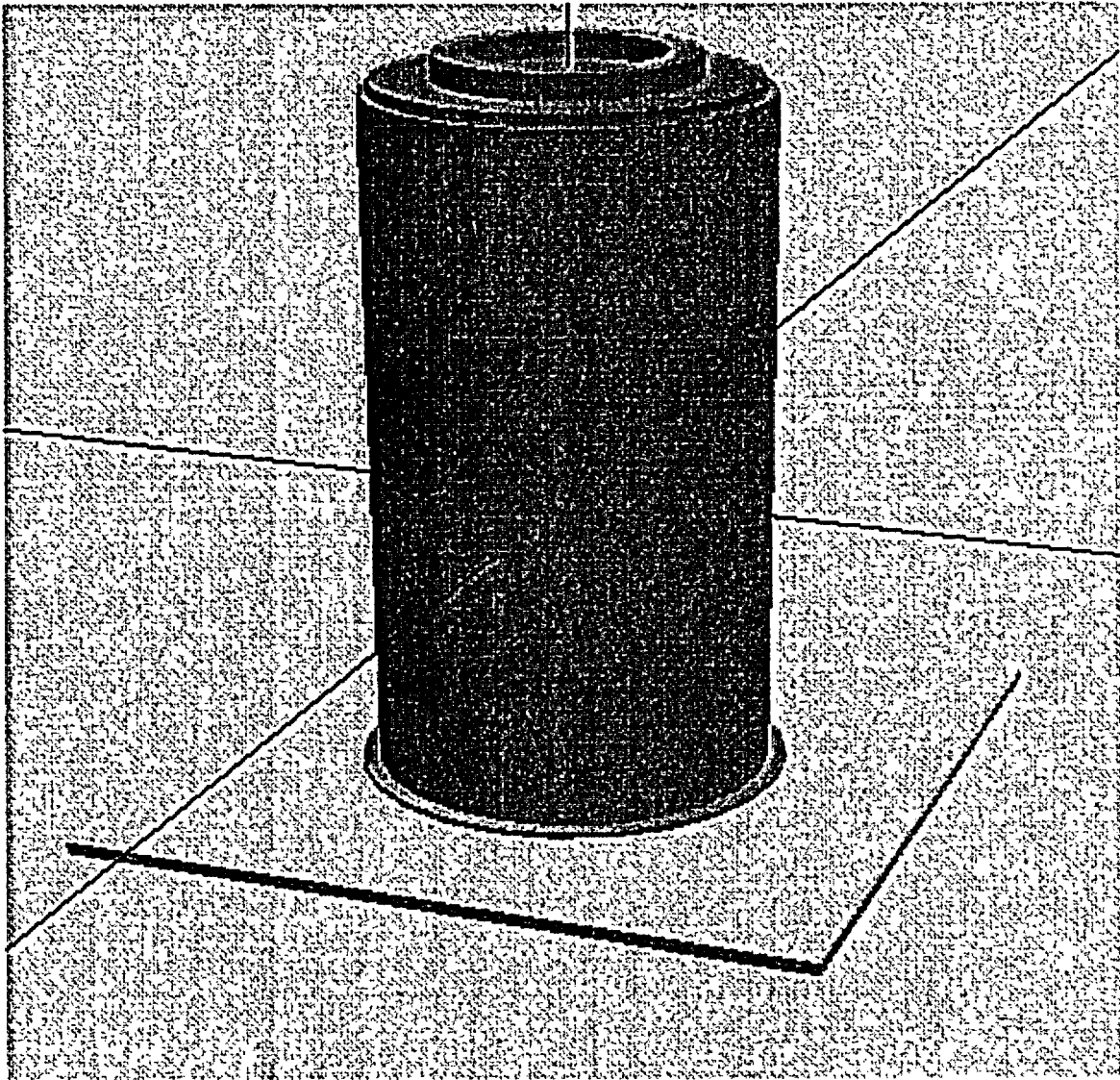


FIGURE 3.4.43: VIEW OF ASSEMBLED HI-STORM ON PAD-MPC INSIDE AND TOP LID ATTACHED (Note Extended Baseplate for Anchor Connections)



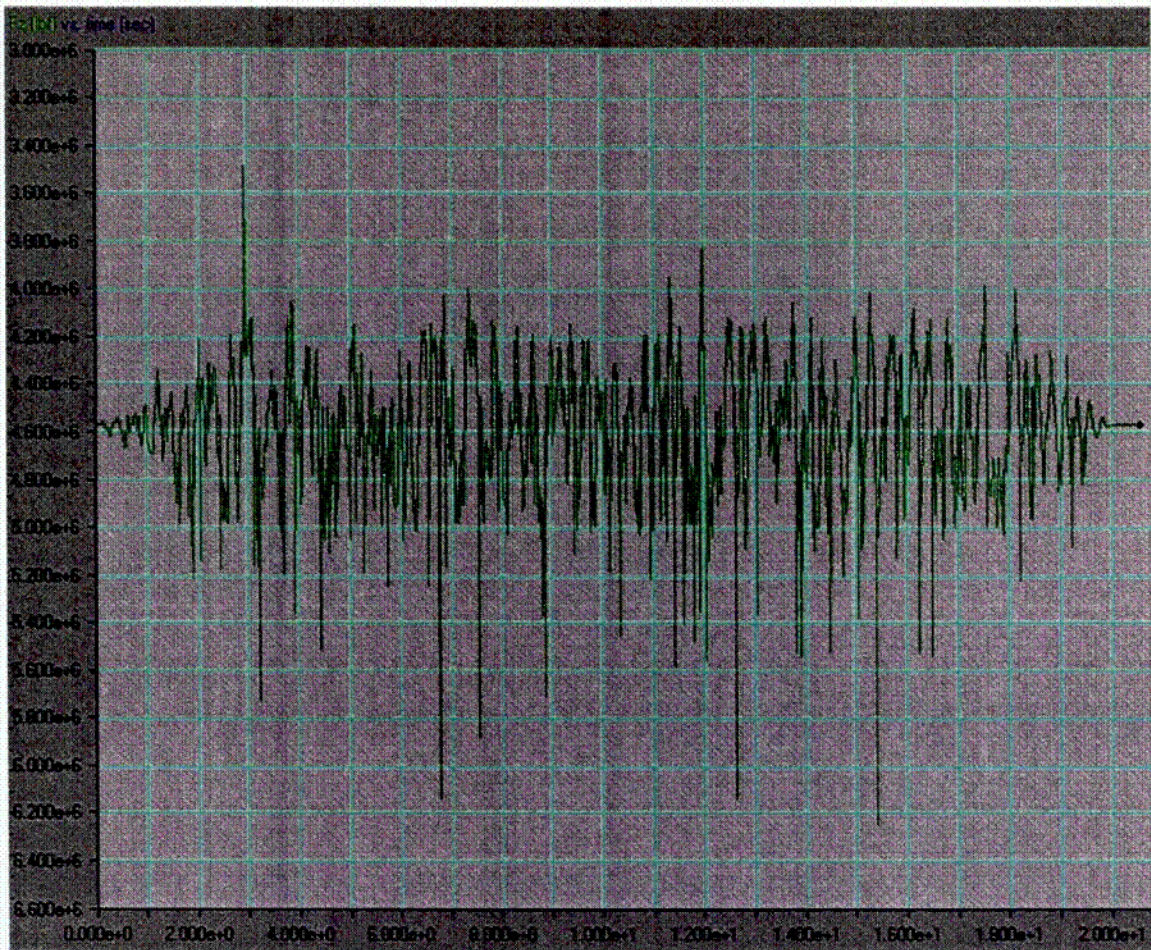


FIGURE 3.4.44 Variation of Foundation Resistance Force vs. Time for Reg. Guide 1.60 Seismic Input



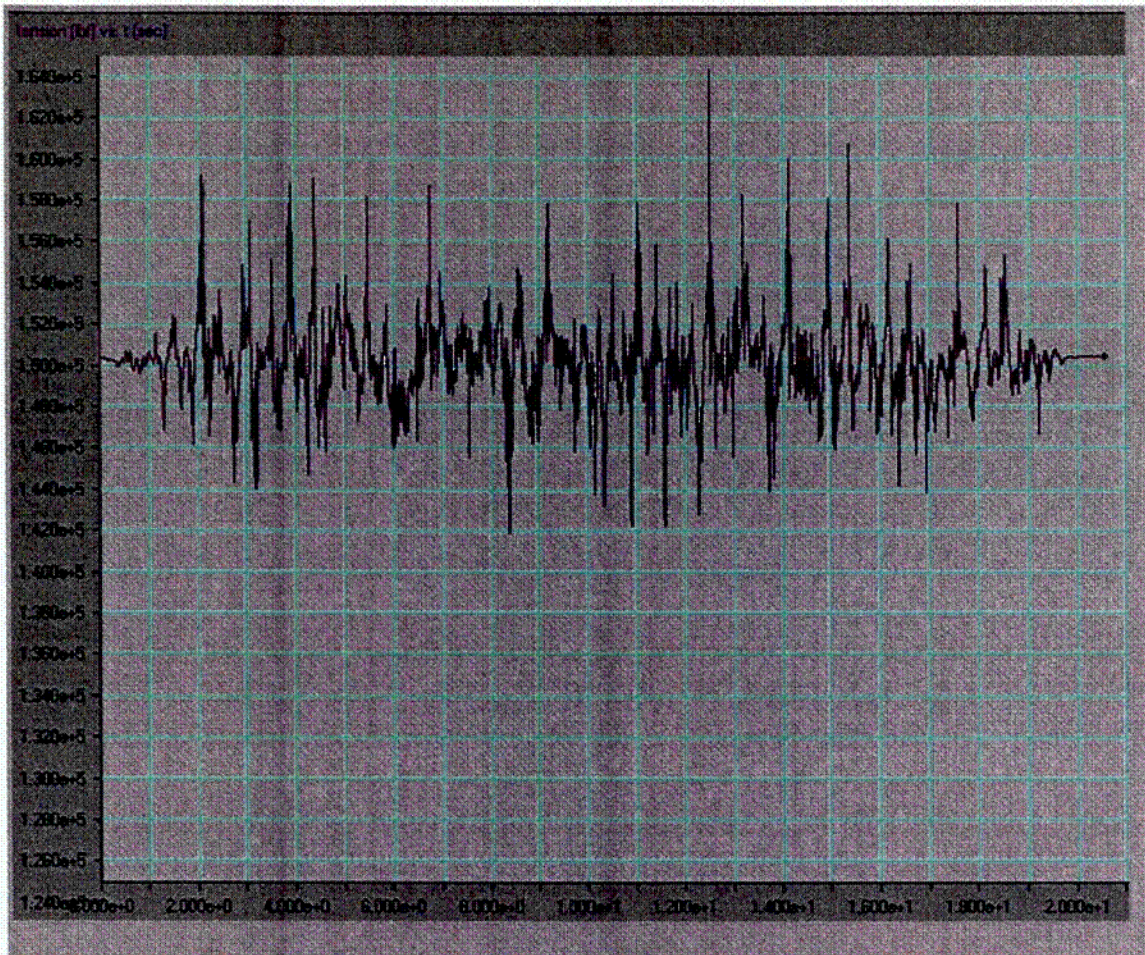


FIGURE 3.4.45 Variation of Representative Stud Tensile Force vs. Time for Reg. Guide 1.60 Seismic Input



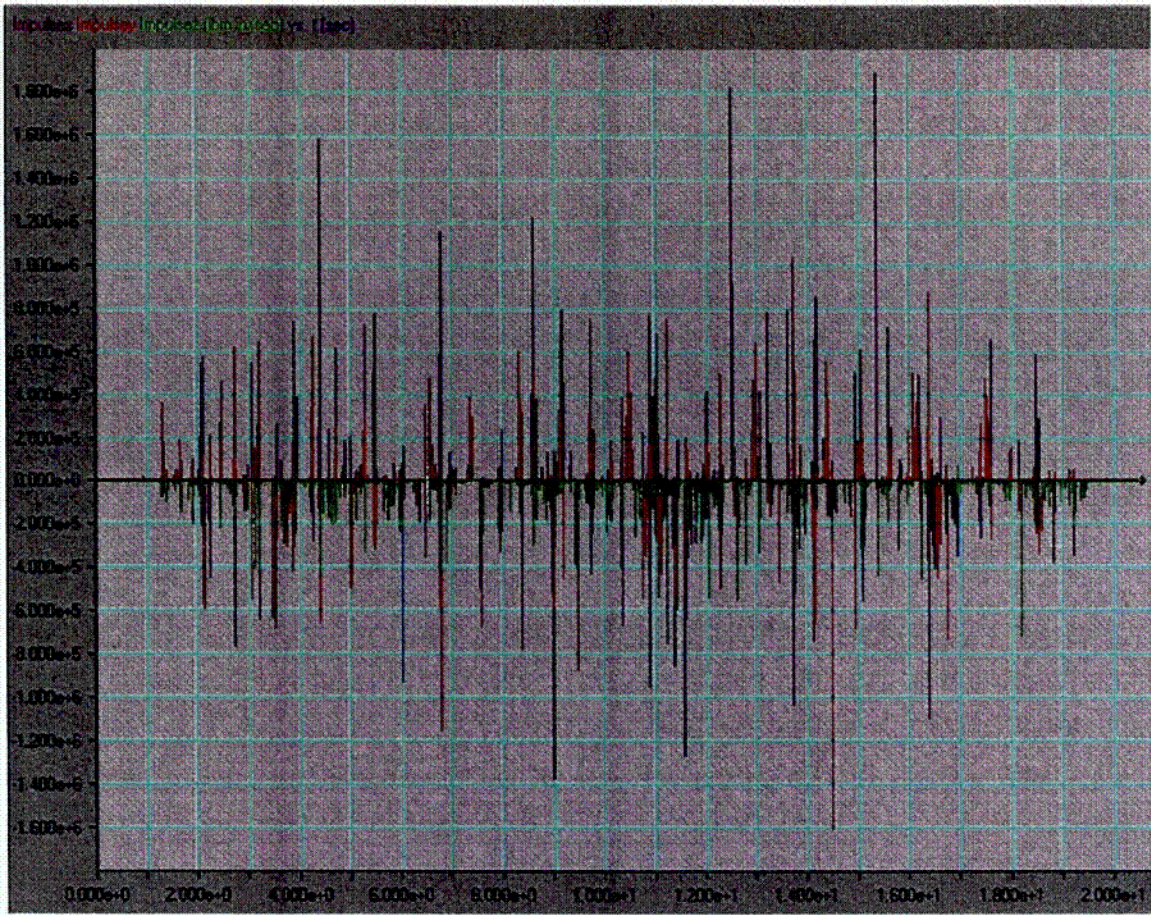


FIGURE 3.4.46 MPC/HI-STORM 100A Impulse vs. Time – Reg. Guide 1.60 Event



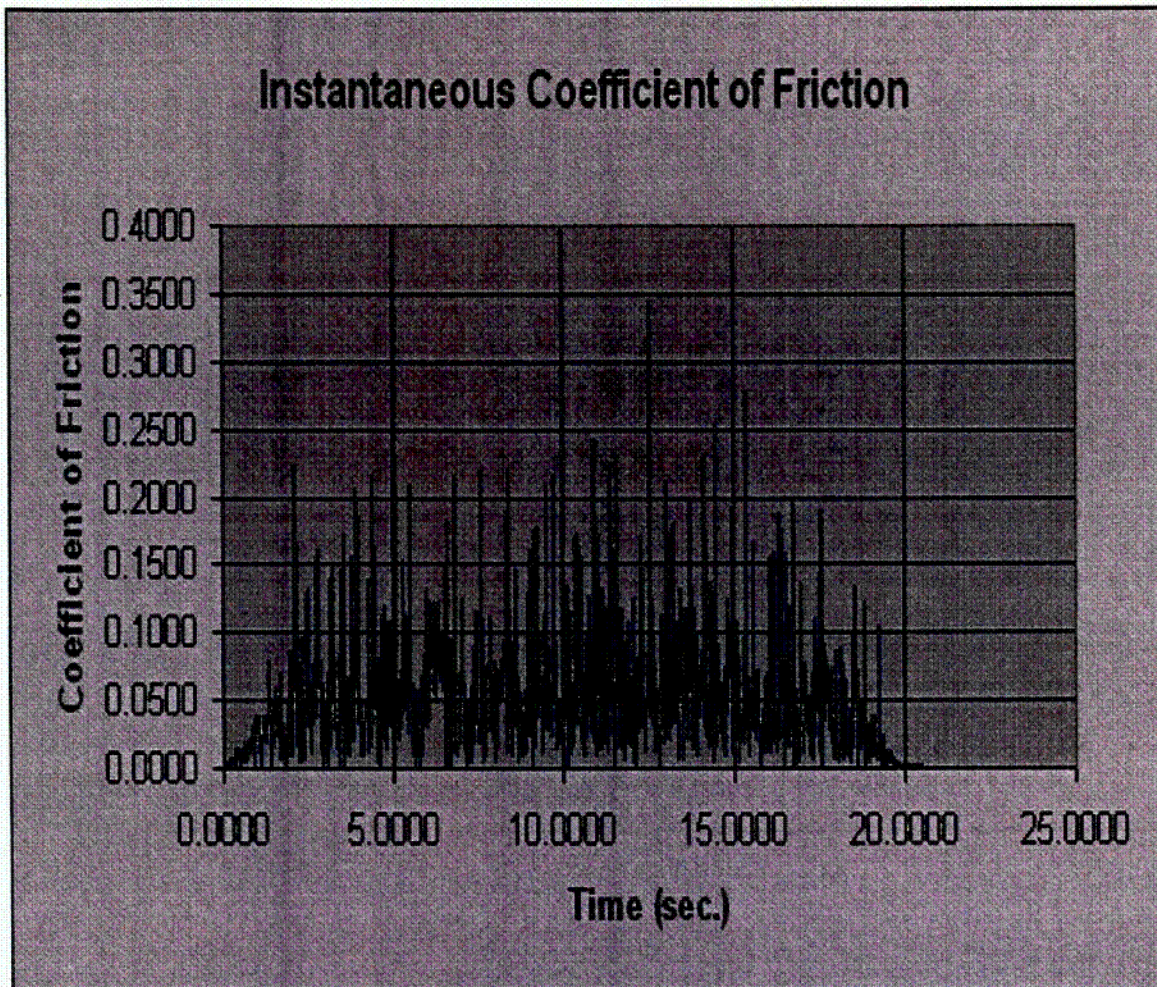
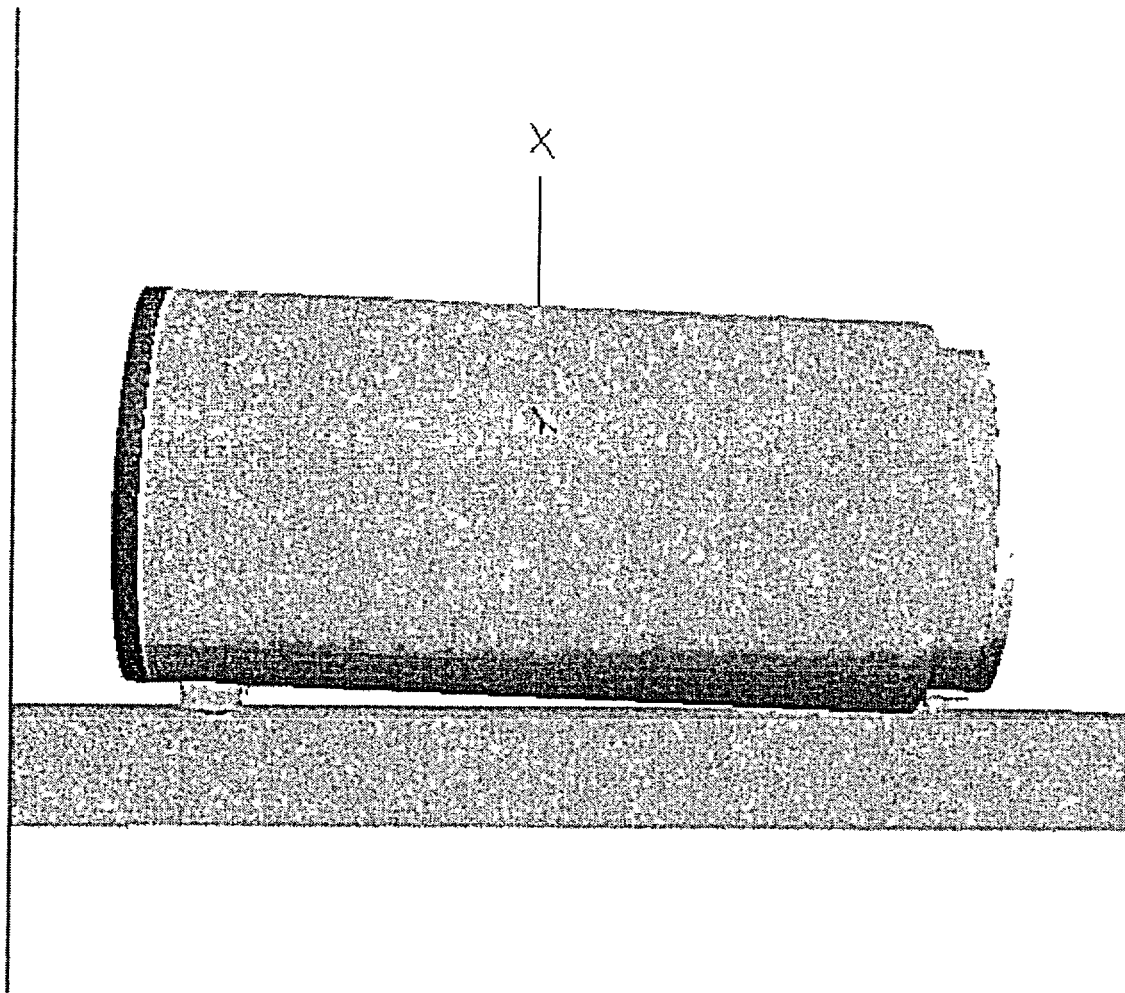
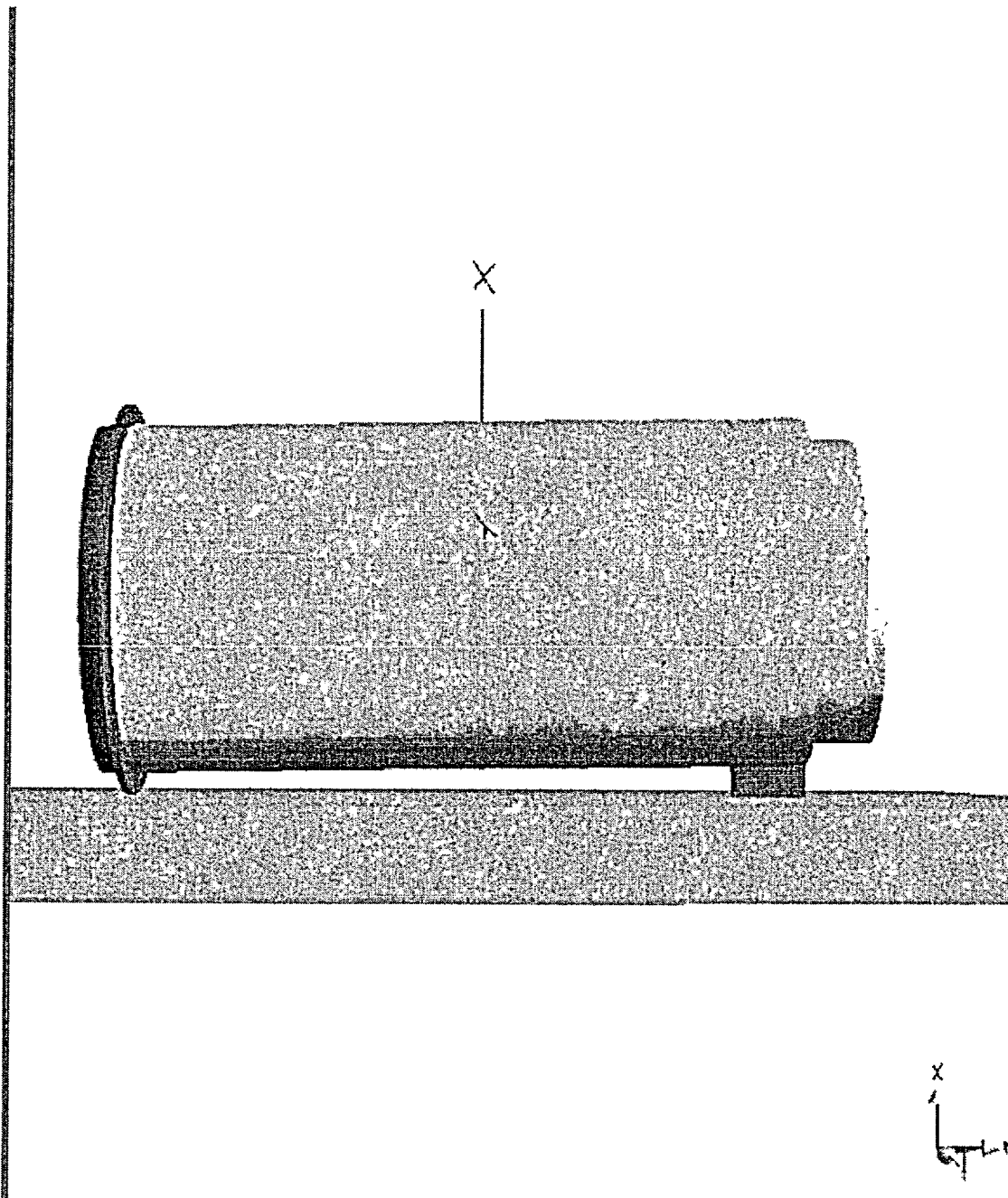


FIGURE 3.4.47 Instantaneous Calculated Coefficient of Friction – Reg. Guide 1.60 Event





**FIGURE 3.4.48; HI-TRAC 125 BENCHMARK SIMULATION OF DROP SCENARIO A**



**FIGURE 3.4.49; SIMULATION OF HI-TRAC 125D 42" HORIZONTAL DROP WITH PRIMARY IMPACT AT TOP END RADIAL SUPPORT TAB**



### 3.5 FUEL RODS

The cladding of the fuel rods is the initial confinement boundary in the HI-STORM 100 System. Analyses have been performed in Chapter 3 to ensure that the maximum temperature of the fuel cladding is below the Pacific Northwest Laboratory's threshold values for various cooling times. These temperature limits ensure that the fuel cladding will not degrade in an inert helium environment. Additional details on the fuel rod cladding temperature analyses for the spent fuel to be loaded into the HI-STORM 100 System are provided in Chapter 3.

The dimensions of the storage cell openings in the MPC are equal to or greater than those used in spent fuel racks supplied by Holtec International. Thousands of fuel assemblies have been shuffled in and out of these cells over the years without a single instance of cladding failure. The vast body of physical evidence from prior spent fuel handling operations provides confirmation that the fuel handling and loading operations with the HI-STORM 100 MPC will not endanger or compromise the integrity of the cladding or the structural integrity of the assembly.

The HI-STORM 100 System is designed and evaluated for a maximum deceleration of 45g's. Studies of the capability of spent fuel rods to resist impact loads [3.5.1] indicate that the most vulnerable fuel can withstand 63 g's in the side impact orientation. Therefore, limiting the HI-STORM 100 System to a maximum deceleration of 45 g's (perpendicular to the longitudinal axis of the overpack during all normal and hypothetical accident conditions) ensures that fuel rod cladding integrity is maintained. In [3.5.1], it is assumed that the fuel rod cladding provides the only structural resistance to bending and buckling of the rod. For accidents where the predominate deceleration is directed along the longitudinal axis of the overpack, [3.5.1] also demonstrates that no elastic instability or yielding of the cladding will occur until the deceleration level is well above the HI-STORM 100 limit of 45g's. The solutions presented in [3.5.1], however, assume that the fuel pellets are not intimately attached to the cladding when subjected to an axial deceleration load that may cause an elastic instability of the fuel rod cladding.

The limit based on classical Euler buckling analyses performed by Lawrence Livermore National Laboratory in [3.5.1] is 82 g's. In the LLNL report, the limiting axial load to ensure fuel rod stability is obtained by modeling the fuel rod as a simply supported beam with unsupported length equal to the grid strap spacing. The limit load under this condition is:

$$F = \pi^2 EI/L^2$$

In the preceding formula, E = Young's Modulus of the cladding, I = area moment of inertia of the cladding, and L = spacing of the grid straps.

Assuming that  $F = WxA/g$  with W being the weight of a fuel rod, and A = the deceleration, the Euler buckling formula can be expressed as

$$A/g = \pi^2 (ER^3 t_n / W_g L^2) = \pi^2 \beta$$

In the preceding formula,  $g$  = gravity,  $n$  = number of fuel rods in the fuel assembly,  $W_a$  = the total weight of the fuel assembly,  $t$  = cladding wall thickness, and  $R$  = cladding mean radius.

Using the preceding formula, a survey of a large variety of fuel assembly types in [3.5.1] concluded that a 17 x 17 PWR assembly resulted in the minimum value for deceleration and results in the lower bound limit of:

$$A/g = 82$$

The fuel pellet weight was omitted from the analysis in [3.5.1] by virtue of the assumption that under axial load, the cladding did not support the fuel pellet mass. Since the results may not be conservative because of the assumption concerning the behavior of the fuel pellet mass, a new analysis of the structural response of the fuel cladding is presented here. It is demonstrated that the maximum axially oriented deceleration that can be applied to the fuel cladding is in excess of the design basis deceleration specified in this FSAR. Therefore, the initial confinement boundary remains intact during a hypothetical accident of transport where large axially directed decelerations are experienced by the HI-STORM 100 package.

The analysis reported in this section of the FSAR considers the most limiting fuel rod in the fuel assembly. Most limiting is defined as the fuel rod that may undergo the largest bending (lateral) deformations in the event of a loss of elastic stability. The fuel rod is modeled as a thin-walled elastic tube capable of undergoing large lateral displacements in the event that high axial loads cause a loss of stability (i.e., the non-linear interaction of axial and bending behavior of the elastic tube is included in the problem formulation). The fuel rod and the fuel pellet mass is included in the analysis with the fuel pellet mass assumed to contribute only its mass to the analysis. In the HI-STORM 100 spent fuel basket, continuous support to limit lateral movement is provided to the fuel assembly along its entire length. The extent of lateral movement of any fuel rod in a fuel assembly is limited to: (1) the clearance gap between the grid straps and the fuel basket cell wall at the grid strap locations; and, (2) the maximum available gap between the fuel basket cell wall and the fuel rod in the region between the grid straps. Note that the grid straps act as fuel rod spacers at the strap locations; away from the grid straps, however, there is no restraint against fuel rod-to-rod contact under a loading giving rise to large lateral motion of the individual rods. Under the incremental application of axial deceleration to the fuel rod, the fuel rod compresses and displaces from the axially oriented inertial loads experienced. The non-linear numerical analysis proceeds to track the behavior of the fuel rod up to and beyond contact with the rigid confining walls of the HI-STORM 100 fuel basket.

The analysis is carried out for the "most limiting" spent fuel assembly. The "most limiting" criteria used herein is based on the simple elastic stability formula assuming buckling occurs only between grid straps. This is identical to the methodology employed in [3.5.1] to identify the fuel assembly that limits design basis axial deceleration loading. Table 3.5.1 presents tabular data for a wide variety of fuel assemblies. Considerable data was obtained using the tables in [3.5.2]. The configuration with the lowest value of "Beta" is the most limiting for simple elastic Euler buckling between grid straps; the Westinghouse 14x14 Vantage, "W14V", PWR configuration is used to obtain results.

The material properties used in the non-linear analysis are those for irradiated Zircalloy and are obtained from [3.5.1]. The Young's Modulus and the cladding dynamic yield stress are set as:

$$E = 10,400,000 \text{ psi}$$

$$\sigma_y = 80,500 \text{ psi}$$

The fuel cladding material is assumed to have no tensile or compressive stress capacity beyond the material yield strength.

Calculations are performed for two limiting assumptions on the magnitude of resisting moment at the grid straps. Figures 3.5.1 through 3.5.9 aid in understanding the calculation. It is shown in the detailed calculations that the maximum stress in the fuel rod cladding occurs subsequent to the cladding deflecting and contacting the fuel basket cell wall. Two limiting analyses are carried out. The initial analysis assumes that the large deflection of the cladding between two grid straps occurs without any resisting moment at the grid strap supports. This maximizes the stress in the free span of the cladding, but eliminates all cladding stress at the grid strap supports. It is shown that this analysis provides a conservative lower bound on the limiting deceleration. The second analysis assumes a reasonable level of moment resistance to develop at the grid straps; the level developed is based on an assumed deflection shape for the cladding spans adjacent to the span subject to detailed analysis. For this second analysis, the limiting decelerations are much larger with the limit stress level occurring in the free span and at the grid strap support locations.

It is concluded that the most conservative set of assumptions on structural response still lead to the conclusion that the fuel rod cladding remains intact under the design basis deceleration levels set for the HI-STORM 100.

Table 3.5.1 FUEL ASSEMBLY DIMENSIONAL DATA

Array ID	Array Name	Rod O.D. (in.)	Clad Thk. (in.)	$R_{mean}$ (in.)	# of Rods PWR	Assy Wt. (lb.)	Rod Length (in.)	# of Spans	Average Span (in.)	Material Modulus	BETA
14x14A01	W14OFA	0.4000	0.0243	0.20608	179	1177	151.85	6	25.30833	10400000	0.525127806
14x14A02	W14OFA	0.4000	0.0243	0.20608	179	1177	151.85	6	25.30833	10400000	0.525127806
14x14A03	W14V	0.4000	0.0243	0.20608	179	1177	151.85	6	25.30833	10400000	0.525127806
14x14B01	W14STD	0.4220	0.0243	0.21708	179	1302	152.4	6	25.4	10400000	0.550863067
14x14B02	XX14TR	0.4170	0.0295	0.21588	179	1215	152	6	25.33333	10400000	0.708523868
14x14B03	XX14STD	0.4240	0.0300	0.21950	179	1271.2	149.1	8	18.6375	10400000	1.337586884
14x14C01	CE14	0.4400	0.0280	0.22700	176	1270	147	8	18.375	10400000	1.398051576
14x14C02	CE14	0.4400	0.0280	0.22700	176	1220	137	8	17.125	10400000	1.67556245
14x14D01	W14SS	0.4220	0.0165	0.21513	180	1247	126.68	6	21.11333	24700000	1.31385062
15x15A01	CE15P	0.4180	0.0260	0.21550	204	1360	140	9	15.55556	10400000	1.677523904
15x15B01	W15OFA	0.4220	0.0245	0.21713	204	1459	151.85	6	25.30833	10400000	0.569346561
15x15B02	W15V5H	0.4220	0.0245	0.21713	204	1459	151.85	6	25.30833	10400000	0.569346561
15x15B03	W15	0.4220	0.0243	0.21708	204	1440	151.83	6	25.305	10400000	0.571905185
15x15B04	W15	0.4220	0.0243	0.21708	204	1443	151.83	6	25.305	10400000	0.570716193
15x15B05	15(2a-319)	0.4220	0.0242	0.21705	204	1472	151.88	6	25.31333	10400000	0.556610964
15x15C01	SPC15	0.4240	0.0300	0.21950	204	1425	152	6	25.33333	10400000	0.73601861
15x15C02	SPC15	0.4240	0.0300	0.21950	204	1425	152	6	25.33333	10400000	0.73601861
15x15C03	XX15	0.4240	0.0300	0.21950	204	1432.8	152.065	6	25.34417	10400000	0.731386148
15x15C04	XX15	0.4170	0.0300	0.21600	204	1338.6	139.423	9	15.49144	10400000	1.996693327
15x15D01	BW15	0.4300	0.0265	0.22163	208	1515	153.68	7	21.95429	10400000	0.854569793
15x15D02	BW15	0.4300	0.0265	0.22163	208	1515	153.68	7	21.95429	10400000	0.854569793
15x15D03	BW15	0.4300	0.0265	0.22163	208	1515	153.68	7	21.95429	10400000	0.854569793
15x15G01	HN15SS	0.4220	0.0165	0.21513	204	1421	126.72	6	21.12	24700000	1.305875606
16x16A01	CE16	0.3820	0.0250	0.19725	236	1430	161	10	16.1	10400000	1.270423729

Table 3.5.1 FUEL ASSEMBLY DIMENSIONAL DATA (continued)

Array ID	Array Name	Rod O.D. (in.)	Clad Thk. (in.)	R <sub>mean</sub> (in.)	# of Rods	Assy Wt. (lb)	Rod Length (in.)	# of Spans	Average Span (in.)	Material Modulus	BETA
16x16A02	CE16	0.3820	0.0250	0.19725	236	1300	146.499	9	16.27767	10400000	1.367126598
17x17A01	W17OFA	0.3600	0.0225	0.18563	264	1373	151.635	7	21.66214	10400000	0.613275783
17x17A02	W17OFA	0.3600	0.0225	0.18563	264	1365	152.3	7	21.75714	10400000	0.611494853
17x17B01	W17STD	0.3740	0.0225	0.19263	264	1482	151.635	7	21.66214	10400000	0.634902014
17x17B02	W17P+	0.3740	0.0225	0.19263	264	1482	151.635	7	21.66214	10400000	0.634902014
17x17C01	BW17	0.3790	0.0240	0.19550	264	1505	152.688	7	21.81257	10400000	0.687604262
BWR											
6x6A02	XX/ANF6	0.5645	0.0360	0.29125	36	328.4	116.65	4	29.1625	10400000	1.192294364
6x6C01	HB6	0.5630	0.0320	0.28950	36	270	83	3	20.75	10400000	2.500527046
7x7A01	HB7	0.4860	0.0330	0.25125	49	276	83.2	3	20.8	10400000	2.233705011
7x7B01	GE-7	0.5630	0.0320	0.28950	49	682.5	159	7	19.875	10400000	1.467601583
7x7B02	GE-7	0.5630	0.0370	0.29075	49	681	164	7	20.5	10400000	1.619330439
7x7B03	GE-7	0.5630	0.0370	0.29075	49	674.4	164	7	20.5	10400000	1.635177979
7x7B04	GE-7	0.5700	0.0355	0.29388	49	600	161.1	7	20.1375	10400000	1.887049713
7x7B05	GE-7	0.5630	0.0340	0.29000	49	600	161.1	7	20.1375	10400000	1.736760659
8x8B03	GE-8	0.4930	0.0340	0.25500	63	681	164	7	20.5	10400000	1.2906798
8x8C02	GE-8R	0.4830	0.0320	0.24950	62	600	159	7	19.875	10400000	1.352138354
8x8C03	GE-8R	0.4830	0.0320	0.24950	62	600	163.71	7	20.46375	10400000	1.27545448
9x9D01	XX/ANF9	0.4240	0.0300	0.21950	79	575.3	163.84	8	18.20444	10400000	1.367212516
10x10E01	XX10SS	0.3940	0.0220	0.20250	96	376.6	89.98	4	17.996	24700000	3.551678654

Array ID, Rod OD, Clad Thk and # of Rods from Tables 6.2.1 and 6.2.2

R<sub>mean</sub>, Average Span and THETA are Calculated.

Zircaloy Modulus from LLNL Report [2.9.1]

Stainless Steel (348H) Modulus from ASME Code, Section III, Part D



Table 3.5.1 FUEL ASSEMBLY DIMENSIONAL DATA (continued)

PWR Assy. Wt., Rod Len and # of Spans (exc as noted below) from DOE/RW-0184, Vol 3, UC-70, -71 and -85, Dec. 1987

Assy. Wt., Rod Len and # of Spans for 15x15B03, 15x15B04, 15x15C01 and 15x15C02 from ORNL/TM-9591/V1-R1

BWR Assy Wt., Rod Len. and # of Spans (exc. as noted below) from ORNL/TM-10902.

Assy Wt., Rod Len. and # of Spans for 6x6A02, 9x9D01 and 10x10E01 from DOE/RW-0184, Vol. 3, UC-70, -71 and -85, Dec 1987

Assy. Wt., Rod Len and # of Spans for 7x7B04 and 7x7B05 from ORNL/TM-9591/V1-R1.

Assy Wt. for 8x8C02 and 8x8C03 from ORNL/TM-9591/V1 -R1.

In the following, a physical description of the structural instability problem is provided with the aid of Figures 3.5.1 to 3.5.9. A stored fuel assembly consists of a square grid of fuel rods. Each fuel rod consists of a thin-walled cylinder surrounding and containing the fuel pellets. The majority of the total weight of a fuel rod is in the fuel pellets; however, the entire structural resistance of the fuel rod to lateral and longitudinal loads is provided by the cladding. Hereinafter, the use of the words "fuel rod", "fuel rod cladding", or just "cladding" means the structural thin cylinder. The weight of the fuel pellets is conservatively assumed to be attached to the cladding for all discussions and evaluations.

Figure 3.5.1 shows a typical fuel rod in a fuel assembly. Also shown in Figure 3.5.1 are the grid straps and the surrounding walls of the spent fuel basket cell walls. The grid straps serve to maintain the fuel rods in a square array at a certain number of locations along the length of the fuel assembly. When the fuel rod is subject to a loading causing a lateral deformation, the grid strap locations are the first locations along the length of the rod where contact with the fuel basket cell walls occurs. The fuel basket cell walls are assumed to be rigid surfaces. The fuel rod is assumed subject to some axial load and most likely has some slight initially deformed shape. For the purposes of the analysis, it is assumed that displacement under load occurs in a 2-D plane and that the ends of the fuel rod cladding have a specified boundary condition to restrain lateral deflection. The ends of the fuel rod cladding are assumed to be simply supported and the grid straps along the length of the fuel assembly are assumed to have gap " $g_1$ " relative to the cell walls of the fuel basket. The figure shows a typical fuel rod in the assembly that is located by gaps " $g_2$ " and " $g_3$ " with respect to the fuel basket walls. Because the individual fuel rod is long and slender and is not perfectly straight, it will deform under a small axial load into the position shown in Figure 3.5.2. The actual axial load is due to the distributed weight subject to a deceleration from a hypothetical accident of transport. For the purposes of this discussion, it is assumed that some equivalent axial load is applied to one end of the fuel rod cladding. Because of the distributed weight and the fact that a deceleration load is not likely to be exactly axially oriented, the predominately axial load will induce a lateral displacement of the fuel rod cladding between the two end supports. The displacement will not be symmetric but will be larger toward the end of the cladding where support against the axial deceleration is provided. Depending on the number of grid straps, either one or two grid straps will initially make contact with the fuel basket cell wall and the contact will not be exactly centered along the length of the cell. Figure 3.5.3 illustrates the position of the fuel rod after the axial load has increased beyond the value when initial contact occurred and additional grid straps are now in contact with the cell wall. The maximum stress in the fuel rod will occur at the location of maximum curvature and will be a function of the bending moment ( $F_2 \times (g_2 - g_1)$ ).

At some load  $F_3 > F_2$ , either the limit stress in the fuel rod cladding is achieved or the rod begins to experience large lateral movements between grid plates because of the coupling between axial and lateral load and deformation. Figure 3.5.4 shows the deformation mode experienced by the fuel rod cladding caused by the onset of an instability between two grid straps that are in contact with the fuel basket cell wall.

Once the lateral displacement initiates, the rod displaces until contact with the cell wall occurs at the mid point "A" ( see Figure 3.5.5) or the cladding stress exceeds the cladding material yield strength. Depending on the particular location of the fuel rod in the fuel assembly, the highest stressed portion of the fuel rod will occur in the segment with the larger of the two gaps " $g_2$ " and " $g_3$ ". For the discussion to follow, assume that  $g_2 > g_3$ . The boundary condition at the grid strap is conservatively assumed as simply-supported so that the analysis need not consider what happens in adjacent spans between grid straps. At this point in the loading process, the maximum bending moment occurs at the contact point and has the value  $F_4 \times (g_2 - g_1)$ . Figure 3.5.5 shows the displaced configuration at the load level where initial contact occurs with the fuel cell wall. If the maximum fuel rod stress (from the bending moment and from the axial load) equals the yield stress of the fuel rod cladding, it is assumed that  $F_3 = F_4$  is the maximum axial load that can be supported. The maximum stress in the fuel rod cladding occurs at point "A" in Figure 3.5.5 since that location has the maximum bending moment. If the cladding stress is still below yield, additional load can be supported. As the load is further increased, the bending moment is decreased and replaced by reaction loads, "V", at the grid strap and the contact point. These reaction loads V are shown in Figure 3.5.7 and are normal to the cell wall surface. Figure 3.5.6 shows the configuration after the load has been further increased from the value at initial contact. There are two distinct regions that need to be considered subsequent to initial contact with the fuel basket cell wall. During the additional loading phase, the point "A" becomes two "traveling" points, A, and A'. Since the bending moment at A' and A is zero, the moment  $F_5 \times (g_2 - g_1)$  is balanced by forces V at the grid strap and at point A or A'. This is shown in Figure 3.5.7 where the unsupported length current "a" is shown with the balancing load. At this point in the process, two "failure" modes are possible for the fuel rod cladding.

The axial load that develops in the unsupported region between the grid strap and point A' causes increased deformation and stress in that segment, or,

The straight region of the rod, between A and A', begins to experience a lateral deformation away from the cell wall.

Note that in this latter scenario, the slope at A or A' remains zero so this should never govern unless the flat region becomes large. The final limit load occurs when the maximum stress in either portion of the rod exceeds the yield stress of the tube. In what follows, the most limiting fuel assembly from the array of fuel types considered is subject to detailed analysis and the limit load established. This limit axial load is considered as the product of the fuel rod weight times the deceleration. Therefore, establishing the limit load to reach cladding material yield establishes the limiting axial deceleration that can be imposed.

The preceding discussion has assumed end conditions of simple support for conservatism. The location of the fuel rod determines the actual free gap between grid straps. For example, a fuel rod furthest from the cell wall that resists lateral movement of the assembly moves to close up all of the clearances that exist between it and the resisting cell wall. The clearance between rods is the rod pitch minus the rod diameter. In a 14 x 14 assembly, there are 13 clearance gaps plus an additional clearance  $g_3$  between the nearest rod and the cell wall. Therefore, the gap  $g_2$  is given as

$$g_2 = 13(\text{pitch-diameter}) + g_3$$

Figure 3.5.9 provides an illustration of the fuel rod deformation for a case of 5 fuel rods in a column. Clearly for this case, the available lateral movement can be considerable for the "furthest" fuel rod. On the other hand, for this fuel rod, there will be considerable moment resistance at the grid strap from the adjacent section of the fuel rod. The situation is different when the rod being analyzed is assumed to be the closest to the cell wall. In this case, the clearance gap is much smaller, but the moment resistance provided by adjacent sections of the rod is reduced. For calculation purposes, we assume that a moment resistance is provided as  $M = f \times K\theta$  for the fuel rod under analysis where

$K = 3EI/L$ ,  $L =$  span between grid straps, and "f" is an assumed fraction of K

The preceding result for the rotational spring constant assumes a simple support at each end of the span with an end moment "M" applied. Classical strength of materials gives the result for the spring constant. The arbitrary assumption of a constant reduction in the spring constant is to account for undetermined interactions between axial force in the rod and the calculated spring constant. As the compressive force in the adjacent members increases, the spring constant will be reduced. On the other hand, as the adjacent span contacts its near cell wall, the spring constant increases. On balance, it should be conservative to assume a considerable reduction in the spring constant available to the span being analyzed in detail. As a further conservatism, we also use the angle  $\theta$  defined by the geometry and not include any additional elastic displacement shape. This will further reduce the value of the resisting moment at any stage of the solution. In the detailed calculations, two limiting cases are examined. To limit the analysis to a single rod, it is assumed that after "stack-up" of the rods (see Figure 3.5.9), the lateral support provided by the cell wall supports all of the rods. That is, the rods are considered to have non-deforming cross-section.

Numerical Analysis - Based on the tabular results in Table 3.5.1, the fuel assembly with the smallest value for the deceleration based on the classical Euler buckling formula is analyzed in detail. The following input data is specified for the limiting 14 x 14 assembly [3.5.2]:

Inside dimension of a HI-STORM 100 fuel basket cell	$s := 8.75 \cdot \text{in}$
Outside envelope dimension of grid plate	$gp := 7.763 \cdot \text{in}$
Outer diameter of fuel rod cladding	$D := .4 \cdot \text{in}$
Wall thickness of cladding	$t := .0243 \cdot \text{in}$
Weight of fuel assembly(including end fittings)	$W := 1177 \cdot \text{lb}$
Number of fuel rods + guide/instrument tubes in a column or row	$n := 14$
Overall length of fuel rod between assumed end support	$L_t := 151 \cdot \text{in}$
Length of fuel rod between grid straps	$L_s := 25.3 \cdot \text{in}$
Average clearance to cell wall at a grid strap location assuming a straight and centered fuel assembly	$g_1 := .5 \cdot (s - gp)$ $g_1 = 0.494 \text{ in}$
Rod pitch	$\text{pitch} := 0.556 \cdot \text{in}$
Clearance := $(n - 1) \cdot (\text{pitch} - D)$	Clearance = 2.028 in
Minimum available clearance for lateral movement of a fuel rod between grid straps	$g_3 := g_1 + .5 \cdot [gp - (n \cdot D + \text{Clearance})]$ $g_3 = 0.561 \text{ in}$
Maximum available clearances for lateral movement of a fuel rod between grid straps	$g_2 := g_3 + \text{Clearance}$ $g_2 = 2.589 \text{ in}$



Young's Modulus of Zircalloy [3.5.1]

$$E := 10400000 \cdot \text{psi}$$

Dynamic Yield Strength of Zircalloy [3.5.1]

$$\sigma_y := 80500 \cdot \text{psi}$$

Geometry Calculations:

Compute the metal cross section area  $A$ , the metal area moment of inertia  $I$ , and the total weight of a single fuel rod (conservatively assume that end fittings are only supported by fuel rods in the loading scenario of interest).

$$A := \frac{\pi}{4} \cdot [D^2 - (D - 2 \cdot t)^2]$$

$$I := \frac{\pi}{64} \cdot [D^4 - (D - 2 \cdot t)^4]$$

$$A = 0.029 \text{ in}^2$$

$$I = 5.082 \times 10^{-4} \text{ in}^4$$

$$W_r := \frac{W}{n^2}$$

$$W_r = 6.005 \text{ lbf}$$

As an initial lower bound calculation, assume no rotational support from adjacent spans and define a multiplying factor

$$f := 0.0$$

Compute the rotational spring constant available from adjacent sections of the rod.

$$K := 3 \cdot E \cdot \frac{I}{L_s} \cdot f$$

$$K = 0 \text{ lbf} \cdot \text{in}$$

Now compute the limit load, if applied at one end of the fuel rod cladding, that causes an overall elastic instability and contact with the cell wall. Assume buckling in a symmetric mode for a conservatively low result. The purpose of this calculation is solely to demonstrate the flexibility of the single fuel rod. No resisting moment capacity is assumed to be present at the fittings.

$$P_0 := \pi^2 \cdot E \cdot \frac{I}{L_t^2}$$

$$P_0 = 2.288 \text{ lbf}$$

Note that this is less than the weight of the rod itself. This demonstrates that in the absence of any additional axial support, the fuel rod will bow and be supported by the cell walls under a very small axial load. In reality, however, there is additional axial support that would increase this initial buckling load. The stress induced in the rod by this overall deflected shape is small.

$$\text{Stress}_1 := \frac{P_0 \cdot g_1 \cdot D}{2 \cdot I} \quad \text{Stress}_1 = 444.32 \text{ psi}$$

$$\text{Stress}_d := \frac{P_0}{A} \quad \text{Stress}_d = 79.76 \text{ psi}$$

The conclusion of this initial calculation is that grid straps come in contact and we need only consider what happens between a grid strap. We first calculate the classical Euler buckling load based on a pin-ended rod and assuming conservatively that the entire weight of the rod is providing the axial driving force. This gives a conservatively low estimate of the limiting deceleration that can be resisted before a perfectly straight rod buckles.

$$a_{\text{lim1}} := \pi^2 \cdot E \cdot \frac{I}{L_s^2 \cdot W_r} \quad a_{\text{lim1}} = 13.57$$

The rigid body angle of rotation at the grid strap under this load that causes contact is:

$$\theta_1 := \text{atan} \left[ 2 \cdot \frac{(g_2 - g_1)}{L_s} \right] \quad \theta_1 = 9.406 \text{ deg}$$

Conservatively assume resisting moment at the grid is proportional to this "rigid body" angle:

$$M_r := K \cdot \theta_1 \quad M_r = 0 \text{ in}\cdot\text{lbf} \quad (\text{in this first analysis, no resisting moment is assumed})$$

The total stress at the grid strap due to the axial force and the resisting moment is

$$\sigma_{\text{gs}} := \frac{W_r \cdot a_{\text{lim1}}}{A} + \frac{M_r \cdot D}{2 \cdot I} \quad \sigma_{\text{gs}} = 2841.172 \text{ psi}$$

The total stress at the contact location is

$$\text{Stress}_2 := \frac{[W_r \cdot a_{lim1} \cdot (g_2 - g_1) - M_r] \cdot D}{2 \cdot I} \quad \text{Stress}_2 = 6.721 \times 10^4 \text{ psi}$$

$$\text{Stress}_{2d} := \frac{W_r \cdot a_{lim1}}{A} \quad \text{Stress}_{2d} = 2841.172 \text{ psi}$$

$$\text{Stress}_{2t} := \text{Stress}_2 + \text{Stress}_{2d} \quad \text{Stress}_{2t} = 7.005 \times 10^4 \text{ psi}$$

This is the maximum value of the stress at this location since, for further increase in axial load, the moment will decrease with consequent large decrease in the total stress.

The safety factor is

$$\frac{\sigma_y}{\text{Stress}_{2t}} = 1.149$$

The axial load in the unsupported portion of the beam at this instant is

$$P_{ax} := \frac{(W_r \cdot a_{lim1})}{\cos(\theta_1)} \quad P_{ax} = 82.599 \text{ lbf}$$

At this point in the load process, a certain axial load exists in the unsupported span on either side of the contact point. However, since the unsupported span is approximately 50% of the original span, the allowable deceleration limit is larger. As the axial load is incrementally increased, the moment at the contact point is reduced to zero with consequent increases in the lateral force V at the grid strap and at the contact points A and A'. Figure 3.5.8 provides the necessary information to determine the elastic deformation that occurs in the unsupported span as the axial load increases and the contact points separate (and, therefore, decreasing the free span).

From geometry, coupled with the assumption that the deflected shape is a half "sin" function with peak value "δ", the following relations are developed:

Assume "a" is a fraction of 50% of the span (the following calculations show only the final iterated assumption for the fraction

$$\epsilon := .9 \quad a := \epsilon \cdot \left( \frac{L_s}{2} \right) \quad a = 11.385 \text{ in}$$

Calculate "b" in Figure 3.5.8

$$b := \left[ (a)^2 + (g_2 - g_1)^2 \right]^{.5} \quad b = 11.576 \text{ in}$$

an equation for  $\delta$  can be developed from the geometric relation

$$\frac{(g_2 - g_1)}{a} := \frac{b}{2(R - \delta)}$$

The inverse of the radius of curvature, R, at the point of peak elastic deflection of the free span, is computed as the second derivative of the assumed sin wave deflection shape. Based on the geometry in Figure 3.5.8, the peak deflection is:

$$\delta := .5 \cdot \left[ \left[ a \frac{b}{2 \cdot (g_2 - g_1)} \right]^2 + 4 \cdot \left( \frac{b}{\pi} \right)^2 \right]^{.5} - a \cdot \frac{b}{4 \cdot (g_2 - g_1)}$$

$$\delta = 0.426 \text{ in}$$

For the assumed "a", the limiting axial load capacity in the unsupported region is conservatively estimated as:

$$a_{\text{lim2}} := \pi^2 \cdot E \cdot \frac{I}{(b)^2 \cdot W_r} \quad a_{\text{lim2}} = 64.816$$

The corresponding rigid body angle is:

$$\theta_2 := \text{atan} \left[ 1 \cdot \frac{(g_2 - g_1)}{a} \right] \quad \theta_2 = 10.429 \text{ deg}$$

The axial load in the unsupported portion of the beam at this instant is

$$P_{ax} := \frac{(W_r \cdot a_{lim2})}{\cos(\theta_2)} \quad P_{ax} = 395.763 \text{ lbf}$$

The resisting moment is

$$M_r := K \cdot \theta_2 \quad M_r = 0 \text{ in}\cdot\text{lbf}$$

The total stress in the middle of the unsupported section of free span "b" is

$$\text{stress}_3 := \frac{(P_{ax} \cdot \delta - M_r) \cdot D}{2 \cdot I} \quad \text{stress}_3 = 6.635 \times 10^4 \text{ psi}$$

$$\text{stress}_{3d} := \frac{P_{ax}}{A} \quad \text{stress}_{3d} = 1.38 \times 10^4 \text{ psi}$$

$$\text{stress}_{3t} := \text{stress}_3 + \text{stress}_{3d} \quad \text{stress}_{3t} = 8.015 \times 10^4 \text{ psi}$$

The safety factor is

$$\frac{\sigma_y}{\text{stress}_{3t}} = 1.004$$

The total stress at the grid strap due to the axial force and any the resisting moment is

$$\sigma_{gs} := \frac{W_r \cdot a_{lim2}}{A} + \frac{M_r \cdot D}{2 \cdot I} \quad \sigma_{gs} = 1.357 \times 10^4 \text{ psi}$$

The safety factor is

$$\frac{\sigma_y}{\sigma_{gs}} = 5.932$$

For this set of assumptions, the stress capacity of the rod cladding has been achieved, so that the limit deceleration is:

$$A_{limit} := a_{lim2} \quad A_{limit} = 64.816$$

This exceeds the design basis for the HI-STORM 100 package.



If there is any restraining moment from the adjacent span, there is a possibility of exceeding the rod structural limits at that location due to the induced stress. Therefore, the above calculations are repeated for an assumed moment capacity at the grid strap.

$$f := 1. \quad K := 3 \cdot E \cdot \frac{I}{L_s} \cdot f$$

The rigid body angle of rotation at the grid strap under this load that causes contact is:

$$\theta_1 := \text{atan} \left[ 2 \cdot \frac{(g_2 - g_1)}{L_s} \right] \quad \theta_1 = 9.406 \text{ deg}$$

Conservatively assume resisting moment at the grid a function of this angle, is

$$M_r := K \cdot \theta_1 \quad M_r = 102.875 \text{ in}\cdot\text{lbf}$$

The total stress at the grid strap due to the axial force and the resisting moment is

$$\sigma_{gs} := \frac{W_r \cdot a_{lim1}}{A} + \frac{M_r \cdot D}{2 \cdot I} \quad \sigma_{gs} = 4.333 \times 10^4 \text{ psi}$$

The total stress at the contact location is

$$\text{Stress}_2 := \frac{[W_r \cdot a_{lim1} \cdot (g_2 - g_1) - M_r] \cdot D}{2 \cdot I} \quad \text{Stress}_2 = 2.672 \times 10^4 \text{ psi}$$

$$\text{Stress}_{2d} := \frac{W_r \cdot a_{lim1}}{A} \quad \text{Stress}_{2d} = 2841.172 \text{ psi}$$

$$\text{Stress}_{2t} := \text{Stress}_2 + \text{Stress}_{2d} \quad \text{Stress}_{2t} = 2.956 \times 10^4 \text{ psi}$$

This is the maximum value of the stress at this location since, for further increase in axial load, the moment will decrease with consequent large decrease in the total stress.

The axial load in the unsupported portion of the beam at this instant is

$$P_{ax} := \frac{(W_r \cdot a_{lim1})}{\cos(\theta_1)} \quad P_{ax} = 82.599 \text{ lbf}$$

At this point in the load process, a certain axial load exists in the unsupported span on either side of the contact point. However, since the unsupported span is approximately 50% of the original span, the allowable deceleration limit is larger. As the axial load is incrementally increased, the moment at the contact point is reduced to zero with consequent increases in the lateral force V at the grid strap and at the contact points A and A'. Figure 3.5.8 provides the necessary information to determine the elastic deformation that occurs in the unsupported span as the axial load increases and the contact points separate (and, therefore, decreasing the free span).

From geometry, coupled with the assumption that the deflected shape is a half "sin" function with peak value "δ", the following relations are developed:

Assume "a" is a fraction of 50% of the span (the following calculations show only the final iterated assumption for the fraction

$$\varepsilon := .7 \quad a := \varepsilon \cdot \left( \frac{L_s}{2} \right) \quad a = 8.855 \text{ in}$$

Calculate "b" in Figure 3.5.8

$$b := \left[ (a)^2 + (g_2 - g_1)^2 \right]^{.5} \quad b = 9.1 \text{ in}$$

The inverse of the radius of curvature, R, at the point of peak elastic deflection of the free span, is computed as the second derivative of the assumed sin wave deflection shape. Based on the geometry in Figure 3.5.8, the peak deflection is:

$$\delta := .5 \cdot \left[ \left[ a \cdot \frac{b}{2 \cdot (g_2 - g_1)} \right]^2 + 4 \cdot \left( \frac{b}{\pi} \right)^2 \right]^{.5} - a \cdot \frac{b}{4 \cdot (g_2 - g_1)}$$

$$\delta = 0.427 \text{ in}$$

For the assumed "a", the limiting axial load capacity in the unsupported region is conservatively estimated as:

$$a_{lim2} := \pi^2 \cdot E \cdot \frac{I}{(b)^2 \cdot W_r} \quad a_{lim2} = 104.9$$

The corresponding rigid body angle is:

$$\theta_2 := \text{atan} \left[ 1 \cdot \frac{(g_2 - g_1)}{a} \right] \quad \theta_2 = 13.314 \text{ deg}$$

The axial load in the unsupported portion of the beam at this instant is

$$P_{ax} := \frac{(W_r \cdot a_{lim2})}{\cos(\theta_2)} \quad P_{ax} = 647.331 \text{ lbf}$$

The resisting moment is

$$M_r := K \theta_2 \quad M_r = 145.619 \text{ in-lbf}$$

The total stress in the middle of the unsupported section of free span "b" is

$$\text{stress}_3 := \frac{(P_{ax} \cdot \delta - M_r) \cdot D}{2 \cdot I} \quad \text{stress}_3 = 5.145 \times 10^4 \text{ psi}$$

$$\text{stress}_{3d} := \frac{P_{ax}}{A} \quad \text{stress}_{3d} = 2.257 \times 10^4 \text{ psi}$$

$$\text{stress}_{3t} := \text{stress}_3 + \text{stress}_{3d} \quad \text{stress}_{3t} = 7.402 \times 10^4 \text{ psi}$$

The safety factor is

$$\frac{\sigma_y}{\text{stress}_{3t}} = 1.088$$

The total stress at the grid strap due to the axial force and any the resisting moment is

$$\sigma_{gs} := \frac{W_r \cdot a_{lim2}}{A} + \frac{M_r \cdot D}{2 \cdot I} \quad \sigma_{gs} = 7.928 \times 10^4 \text{ psi}$$

The safety factor is  $\frac{\sigma_y}{\sigma_{gs}} = 1.015$

For this set of assumptions, the stress capacity of the rod cladding has been achieved, so that the limit deceleration is:

$$A_{limit} := a_{lim2} \quad A_{limit} = 104.9$$

### Conclusions

An analysis has demonstrated that for the most limiting PWR fuel assembly stored in the HI-STORM 100 fuel basket, a conservative lower bound limit on acceptable axial decelerations exceeds the 45g design basis of the cask. For a reasonable assumption of moment resisting capacity at the grid straps, the axial deceleration limit exceeds the design basis by a large margin.

It is concluded that fuel rod integrity is maintained in the event of a hypothetical accident condition leading to a 45g design basis deceleration in the direction normal to the target.



### FUEL ROD DEFORMATION PHASES

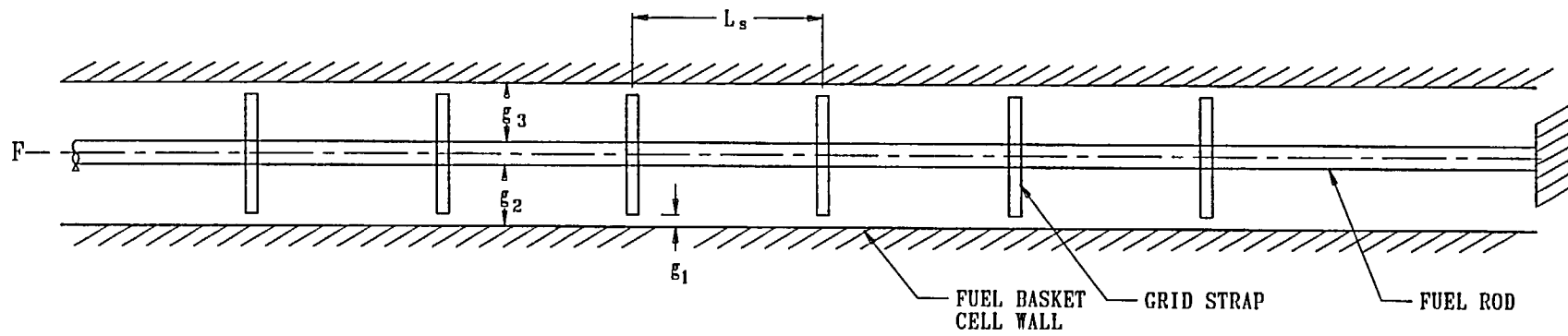


FIGURE 3.5.1;  $g_1 > 0$

FUEL ROD DEFORMATION PHASES

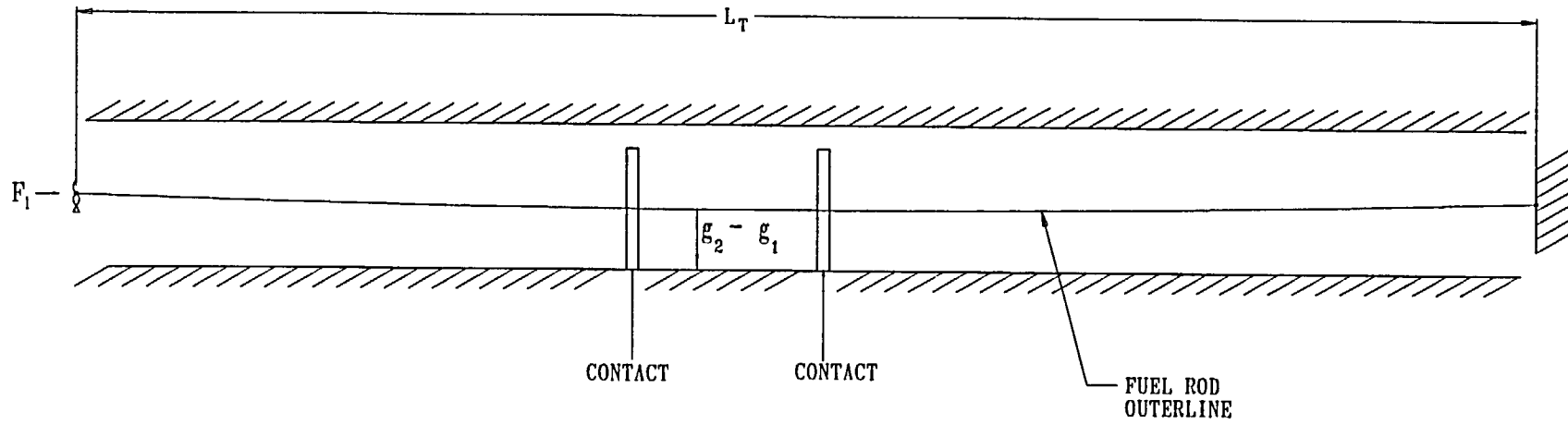


FIGURE 3.5.2;  $g_1 = 0$

FUEL ROD DEFORMATION PHASES

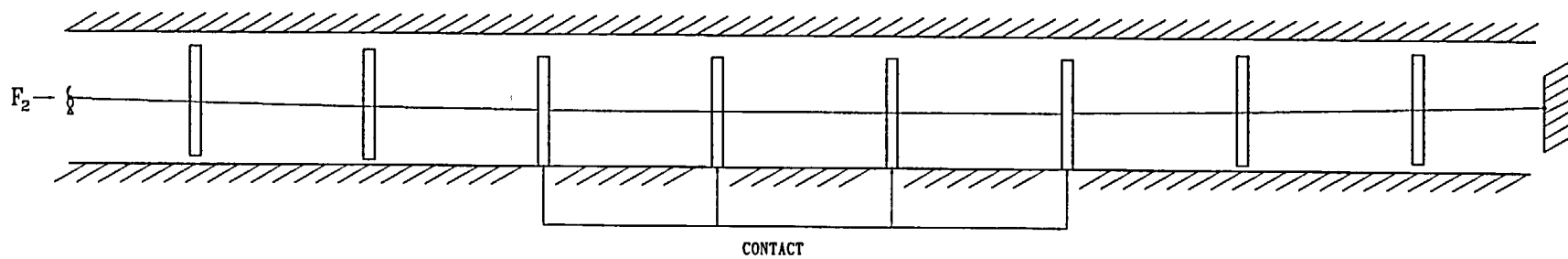


FIGURE 3.5.3;  $g_1 = 0, F_2 > F_1$

FUEL ROD DEFORMATION PHASES

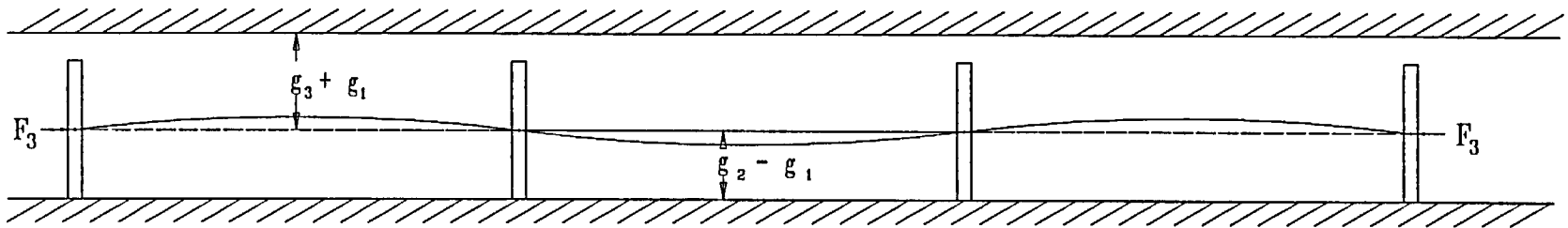


FIGURE 3.5.4; INTER-GRID STRAP DEFORMATION  $F_3 > F_2$



### FUEL ROD DEFORMATION PHASES

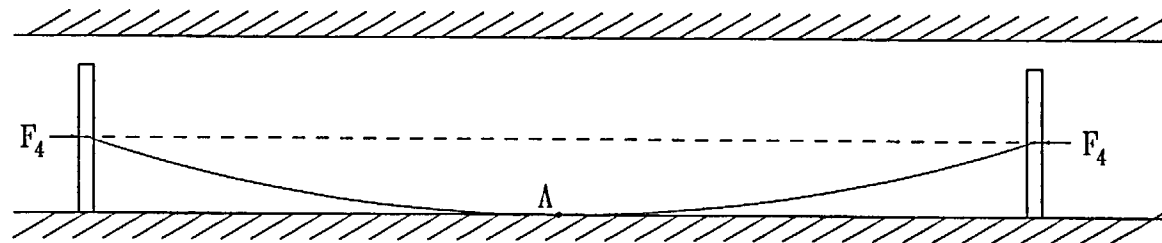


FIGURE 3.5.5; POINT CONTACT AT LOAD  $F_4$   
MAXIMUM BENDING MOMENT AT  $A$

### FUEL ROD DEFORMATION PHASES

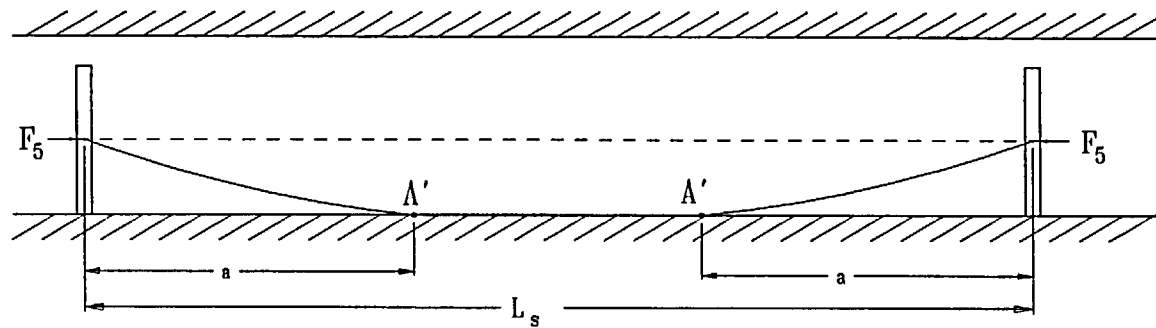


FIGURE 3.5.6; EXTENDED REGION OF CONTACT  
 $F_5 > F_4$  , ZERO BENDING MOMENT AT  $A'$

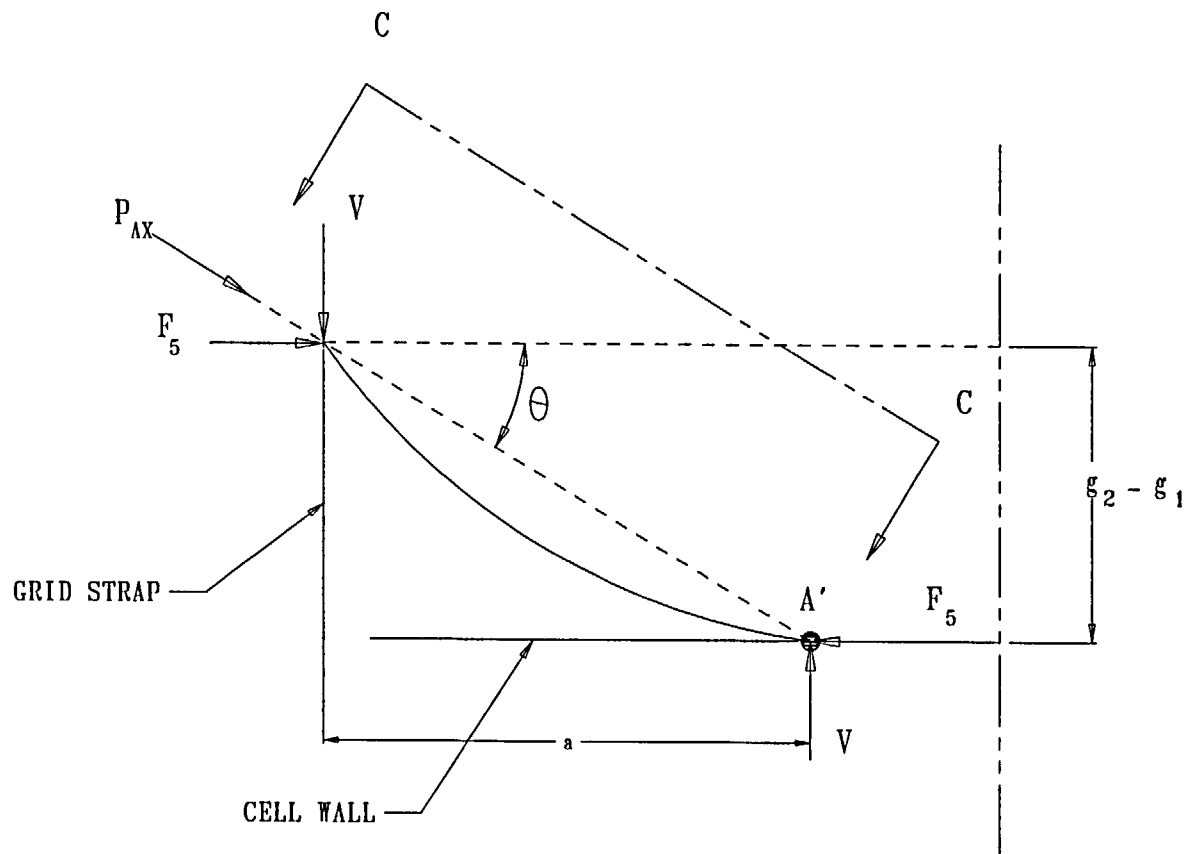
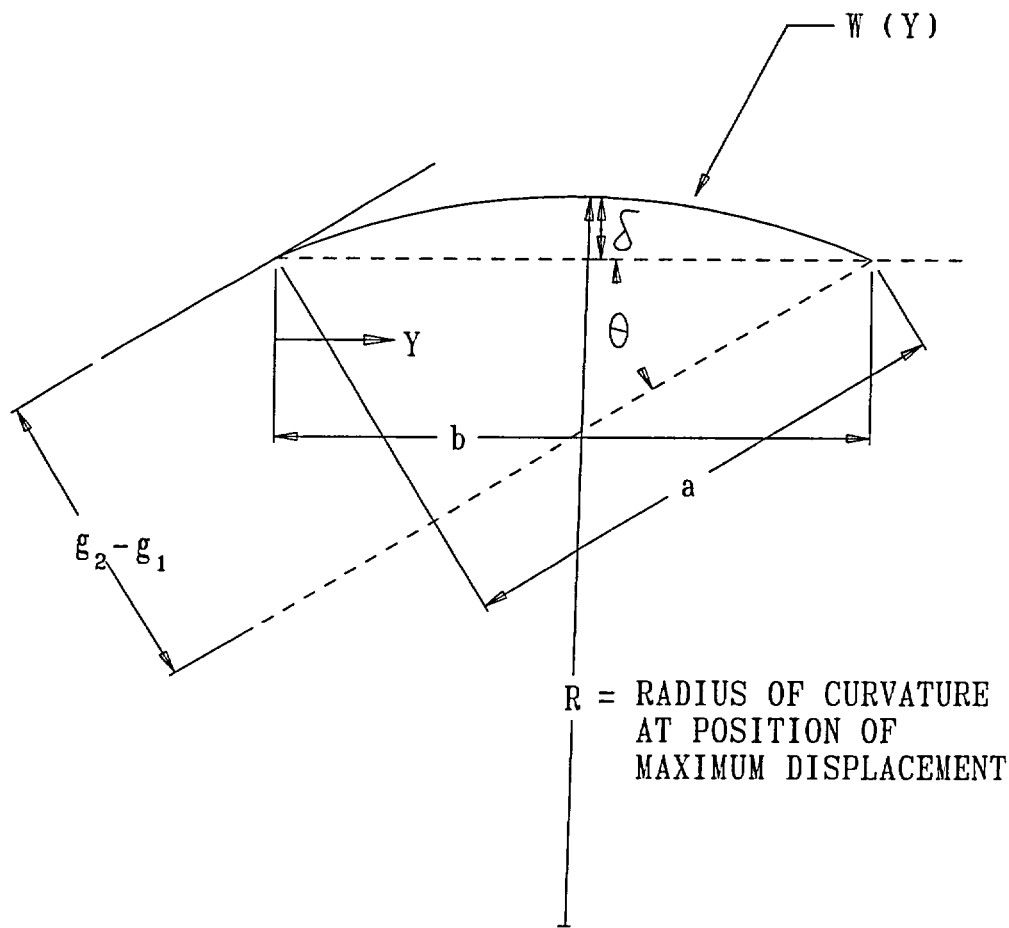


FIGURE 3.5.7; FREE BODY DIAGRAM WHEN MOMENT AT  $A' = 0$   
 $P_{AX} = F_5 / \cos(\theta)$ . RESISTING MOMENT  $M_R$   
 AT GRID STRAP NOT SHOWN



$$Z = R - \delta$$

$$W(Y) = \delta \text{SIN}(\pi Y/b)$$

FIGURE 3.5.8; VIEW C - C



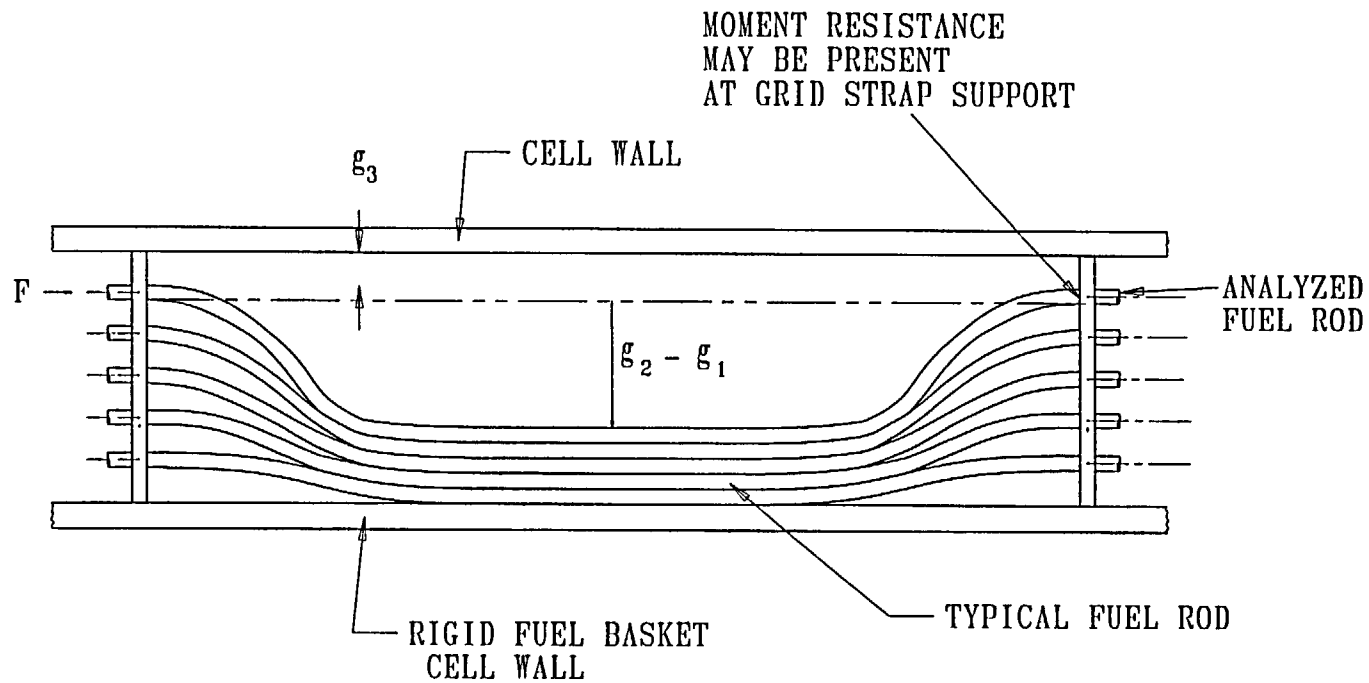


FIGURE 3.5.9; EXAGGERATED DETAIL SHOWING MULTIPLE FUEL RODS SUBJECT TO LATERAL DEFLECTION WITH FINAL STACKING OF ROD COLUMN